DOCTORAL DISSERTATION

Morphological Approach for Motor-sensory Compensation of Soft Body with Structural Damages: Case of Soft Whisker

NGUYEN Huu Nhan

Supervisor: HO Anh Van

Graduate School of Advanced Science and Tehcnology

Japan Advanced Institute of Science and Technology

Information Science

March, 2022

JAPAN ADVANCED INSTITUTE OF SCIENCE AND TECHNOLOGY

Abstract

Graduate School of Advanced Science and Technology

Doctoral Dissertation

Morphological Approach for Motor-sensory Compensation of Soft Body with Structural Damages: Case of Soft Whisker

by NGUYEN Huu Nhan

After decades of intensive research and creative innovation, modern autonomous machines (robots) now have the capabilities to accomplish pre-programmed tasks with an incredible precision repeatably in multi-thousands (or even millions) cycles. A study of 46 countries and 800 occupations by McKinsey Global Institute [1] has reported that, by 2030, there would be at least 800 million global employees lost their jobs to high-functional robotic systems. Although the process of industrial robot development is still growing fast and strong, as a roboticist, I personally think it is time to bring robotic systems out of their "cozy home" in factory workplaces to more challenging, unstable environments (*ex*, near humans) where adaptability, robustness, and resilience against all kinds of uncertainties are vitally required. For the last decade, there is a nascent class of robots called *soft robots* that offer flexibility to a few components or even the whole robot's body similar to living organisms. These machines are built with many intriguing abilities of locomotive behaviors, perceptions, and cognition that we have seen a lot from natural species, whilst pretty rare or none existed in rigid robots before. With this spirit, resilience in response to structural changes to the body due to critical damages is an instance.

Researchers in the field have been struggling to develop a new clan of regenerative robots by integrating flexibly adaptable controllers. However, such approaches

have never, so far, proved themselves as efficient methods in actual scenarios mostly because the processor can not afford in terms of time for a massive computational burden as they usually assign. Not to mention the expensive cost to build up supportive systems does not ensure successful resilience. Meanwhile, biological counterparts such as rodents [2] or spiders [3], through millions years of evolution, learn how to couple their variable body's morphology with the brain to facilitate their interaction with the surrounding and enable intelligent functionalities including resilience. Such fascinating intelligence are widely known with the name *embodied intelligence* - or embodiment. This thesis attempts to clarify the use of embodied intelligence for the development of a new generation of resilient robots with a particular focus on soft tactile sensory systems. This work is achieved by summarizing all investigations (which are reported in top-ranked conference proceeding [4] and journals [5][6] in robotic field) that I have done on an soft whisker-like tactile sensor with variable morphology.

As an inhabitant in unstructured, lack-of-vision environments, rodents such as rats rely much on the sensibility of their vibrissal system for various tactile exploration tasks. However, high frequency of physical impacts to the surroundings poses a critical challenge in maintenance of the sensing function in response to injured whiskers (e.g eroded, broken), so-called resilience process. To successfully mimic such exquisite ability into an artificial whisker, I introduced a novel design of whisker sensor that is able to actively change its morphology (*i.e.*, equivalent to tactile perception) in order to regain the original sensitivity despite being broken. Experimental results shown in this thesis demonstrate the feasibility of the idea of resilience based on adaptive morphology and its possibility to aid in tactile perception in more complex scenarios. It is also expect to reset our common sense in creating intelligent autonomous machines.

Keywords: Soft tactile sensor, Swarm robotic system, Local minima problem

Acknowledgements

Foremost, my sincere appreciation and thankful gratitude go to my kind, wise supervisor ***Assoc. Prof. Ho Anh Van*** who gave me a wonderful opportunity to be a part of his lab and has always been extremely patient throughout all thick and thin of mine. For the past years, your mentoring, encouragement and inspiration have pushed me beyond all kinds of boundaries not only in top-level academics (that sometimes I feel I would not have been able to go this far) but also in many aspects of life. Last but not least, It is not often to have a Ph.D advisor that brings me the feel of a dearest friend, just a couple of months after the day I arrived, who is willing to help and suffer with me. It was a great privilege and honor to me.

I would also thank all committee members ***Assoc. Prof. Okada Shogo***, ***Prof. Unoki Masashi*** and ***Prof. Perla Maiolino*** for participating in my Ph.D defense session and helping me strengthen my thesis. My special appreciation also goes for ***Prof. Chong Nak Young*** as my second supervisor for keeping my research in the right direction within a bigger picture of robotics science, and ***Prof. Nguyen Le Minh*** for his excellent advice for my minor research project.

My sincere thanks also extend to all colleagues who I got chances to work with, to my labmates who have been very supportive, friendly, and always ready to give me a hand whenever I need. I always feel fortunate to work in such an active and encouraging environment.

I can not sum up all debt that I owe to my parents ***Mr. Nguyen Duy Khanh*** and ***Mrs. Nguyen Do Minh Trang*** who unconditionally spent half of their life exhaustively working to raise me and my younger brother, to teach me how to be a good person, to always be behind my back with love and care, and to always be proud of their sons. I love you from the bottom of my heart.

I owe a deep sense of gratitude and apology to my wife ***Mrs. Nguyen Thi Hoang Linh*** for her unlimited support and sacrifice, for her patience with my darkest frustration times, for filling my life with her pure love, happiness and goofiness, and most importantly, for grating me an extraordinary favor of being a dad of a cutest,

most handsome, precious boy ***Nin***. I still have the rest of my life to make you two happy and I love you two so badly.

Contents

List of Tables

List of Figures

List of Abbreviations

DoF	**D**egrees **o**f **F**redoom
MorphCom	**Morph**ological **Com**pensation
TacMorph	**T**actile **Com**pensation by Variable **Morph**ology
FEM	**F**inite **E**lement **M**ethod
GA	**G**enetic **A**lgorithm
LC-DoF	**L**ocally **C**ontrollable **D**egrees **o**f **F**redoom
RL	**R**einforcement **L**earning

1 Introduction

1.1 Embodied Intelligence: From Nature to Robotics

Throughout the history of nature development, living creatures across a wide range of scales have been thriving through hazardous and constant-changing environments thanks to an exquisite style of intelligence which is known by the name: *Embodied Cognition* [7]. This can be simply understood as specific biological behaviors emerging from imitating coupling between agent's physical body from cell-level lifeforms to higher-level artifacts such as legs, central system (*i.e.,* brain) and their living environment [8]. By this definition, my interest in intelligence, therefore, only ascribes to physical systems whose biological mechanisms offer intelligent behaviors that can be seen from their intimate interaction with the environment. So, in this thesis, I particularly play around with two following questions: 1) How does a wild animal take advantage of his body to overcome harsh situations (*e.g* injured)? 2) Could artificial agents like robotic systems exploit this strategy to be able to get unforeseen benefits which normally cost an extreme amount of effort in terms of computation or control?.

To begin with, it is crucial to clarify why the body is necessary for intelligence. Figure 1.1 decomposes neural incorporation between physical body and brain (controller) and environments where the embodiment is negotiating information and energy through physical interactions. This scheme indicates the outcome behaviors of the agent against its surroundings have emerged through continuous and dynamic processes of physical and information exchange between the body and the brain. Such landscape is somehow against the famous quote "I think, therefore I am" from Rene Descartes - a French philosopher in the seventeenth-century quoted

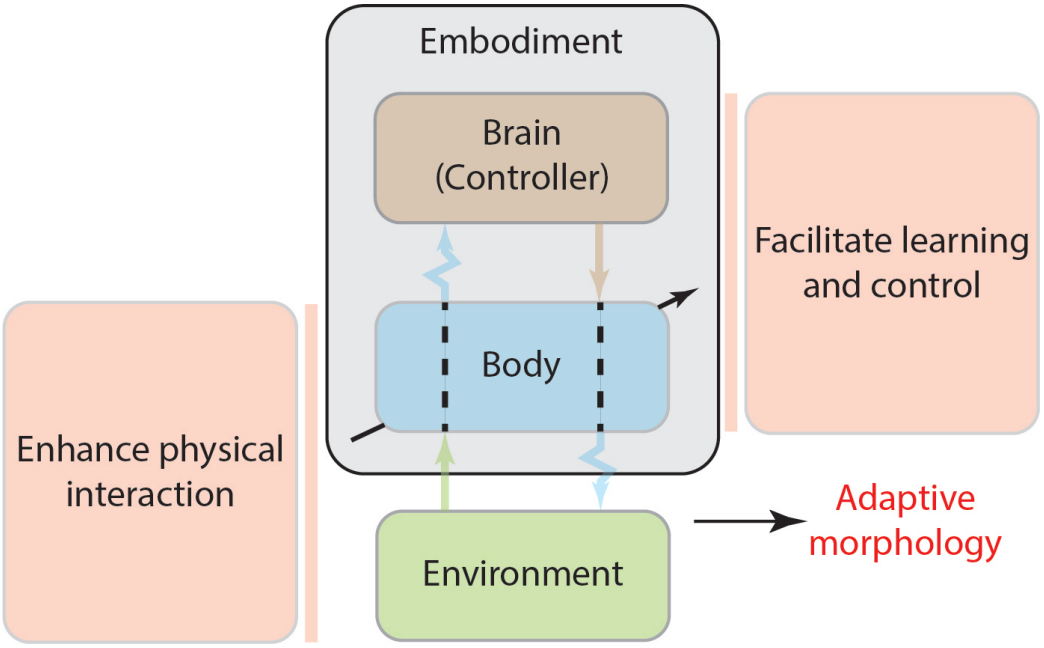

FIGURE 1.1: Implications of embodiment to achieve intelligent behaviors via adaptive morphology

in his *Discourse on the Method, 1637* [9] that indicates the body is separated from the brain during executing daily activities. It means that the body is just a problem domain whereby the brain needs to *itself "compute and decide"* how the body is going to react to a specific interacting situation. However, many examples in nature (even with humans) declare the opposite. For instance, we use our hands, or more specifically, fingers to grasp, manipulate objects with an enormous variety of physical properties [10]. Hence, finger's movements, in order to specialize to the object properly, are not only the consequences of a complex network of motors (*i.e,* finger joints) and sensory feedback (acquired from receptors underneath the skin) but also their geometrical and material characteristics [11]. For example, it would not be a big deal when we try to lift up a box in a normal environment, but in a wet environment, our fingertips usually form wrinkle patterns (see Fig. 1.2(A)) so as to most likely ensure the box not falling out of our hands [12]. Even though the underlying mechanic of wrinkled fingertips is not verified yet, it is feasible to assume that an adaptive change of morphology (as illustrated in Fig. 1.1) could improve tribological contact condition [13] . Another example is observed from four-legged animals such as dogs whose muscle-tendon system (Fig. 1.2(B)) in their legs are elastic (this is also true for human legs), thereby, the knee (*i.e.*, leg's joint), during running or

walking sections, can perform smoothly adaptive movements over uneven ground without significant control from the brain [14].

From above examples, complete and successful embodied (biological or not) intelligent agents must adopt the following attributes:

- As physical systems, hence, they must obey laws of physics (friction, gravity, and energy dissipation) in order to achieve desired performance. When we walk or run, the soft arch of our feet must comply with friction and gravity
- They generate sensory data during the interaction phase with the open world. These sensations can be categorized into two classes: *"exteroceptive"* and *"proprioceptive"*. The first term implies sensory feedback obtained from in-contact relation with the environment such as visual, auditory and tactile perception. Whereas, the latter encapsulates those produced and perceived by internal self-stimulating within their own body. For example, we feel pressure patterns on our feet (exteroceptive) as well as stretching and contracting of muscles as the legs move. Experiments have shown that sensory-motor coordination can be adapted so as to self-modulate their forthcoming sensory feedback.
- Finally, a certain amount of processes or computation, which would have to be done by the central system (*i.e.*, brain), are assigned to the physical body. The use of dynamics of the physical properties (including morphological and material) to facilitate control can be referred to the term: *"Morphological Computation"*.

The emergence of the topic of embodied intelligence is closely matched with the development in robotics with the focus on morphological computation and sensory-motor coordination. Over the last couple of decades, automatic machines like robots play an important role in enhancement of not only the productivity of the manufacturing industry but also the quality of our society in many aspects thanks to their precision, repeatability and controllability [15]. More recently, there has been an increasing interest in adaptivity, learning and autonomy which is reflected by a vast of researches, scientific reports on developing artificial intelligence (AI) for

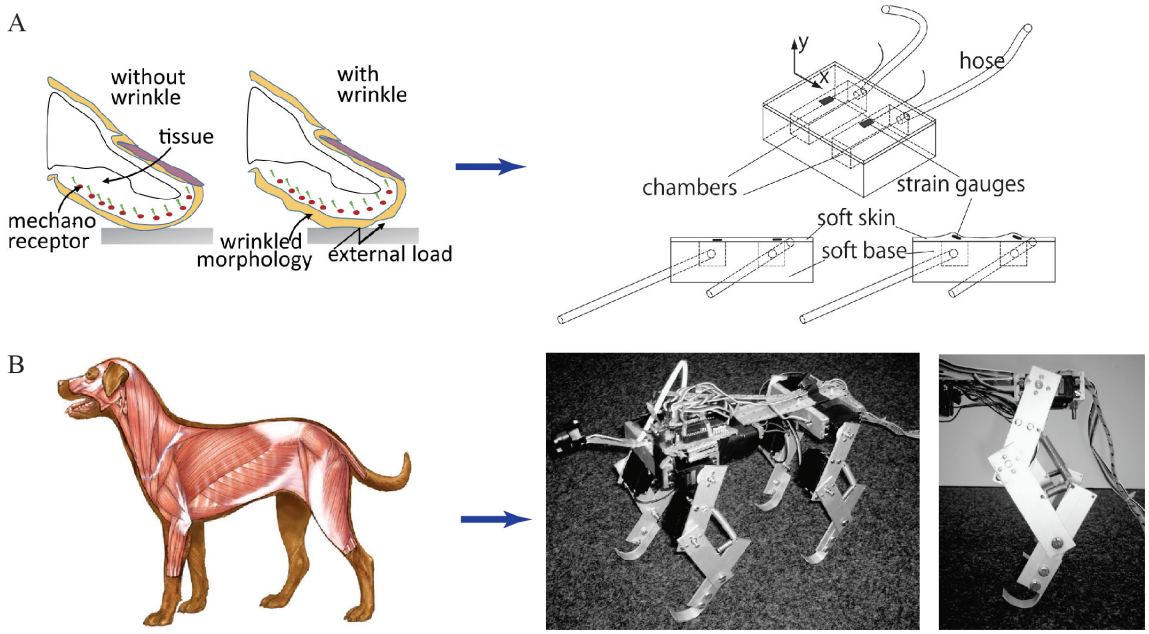

FIGURE 1.2: Illustration of how artificial systems exploit bio-inspired morphology to enable embodied intelligence in (A) tactile sensing (adapted from [19]) and (B) locomotion (adapted from [20] and [21])

robotic systems [16]. The reasons for this trend are manifold, but the most important one is the intention to reduce the gap (in its literal sense) between robots and the human community at an individual scale. In considering embodied biological agents, we might concern about physical actions and neural processing between body and brain which would be equivalent to the relation of robot's actuation and its controller [17]. In fact, there has been much evidence up to date proving that if the robot's morphology (*i.e*, shape or structure, stiffness) are taken into account of learning, development and the generation of proper in-contact actions with the environment (including humans), many tasks are much easier to accomplish with simple control policies [18].

The wrinkle formation on our fingertips which appear after soaking in water (see Fig. 1.2(A)) would be a good example of how a biological phenomenon could be useful in artificial systems. Authors in [19] took this inspiration to establish a novel design of a soft tactile sensor that is able to actively change the texture of the sensing pad at will from flat to an undulating surface. By doing that, the sensor is more sensitive with dynamic shear variation from sliding objects on its surface in comparison with initial morphology. This result means that, depending on the

task, sensing modalities can be easily switched from one (static measurement) to another (dynamic measurement) and vice versa, by changing morphology only. Fumiya Iida and Rolf Pfeifer [22] introduced a very simple design of a quadruped robot that employs a three-segment model of animal legs. Additionally, there are two springs connecting the lower and upper parts of each leg to intuitively replicate muscle tendon in animals (see Fig. 1.2(B)). This robot, with a simple control program, can achieve this relatively complicated rapid locomotion by exploiting the correlation between oscillation movement of each leg, robot's morphology (*i.e.*, its configuration and spring stiffness), and other attributes such as friction or gravity. These comparable examples at first answer the question raised at the beginning of this section that a robotic system could be beneficial from their own physical body. Secondly, they highlight the concept of embodied intelligence through its principles, *i.e.* morphological computation and sensory-motor coordination, to allocate tasks among the controller (brain), the morphology and the environment. If this interplay can be well characterized, this could upgrade our decades-old mindset on building and operating intelligent machines.

Despite its appeal, its mechanism and application method remain elusive and unpopular. Therefore, it is of great worth demonstrating the power of embodied intelligence as a new approach to designing robots that would probably help us to understand the natural world. This is also one of the main motivation of my thesis which will be clarified more clearly in the next section.

1.2 Motivations: Resilience via adaptive morphology

Nowadays, modern robots have no longer been limited to repetitive tasks in a predefined environment, but are increasingly involved in uncertain workplaces to accomplish complex missions [23]. Furthermore, the idea of bringing automated machines close to human society through physical interaction and communication is no longer a sort of daydreams but becoming a realistic goal for scientists and engineers. However, to confidently deploy robots in complex real-world scenarios,

where are not perfectly measured like factory, the adaptation is the key for them to survival. Nowadays, in the context of close Human-robot interaction (HRI), modern rigid robots have been integrated with perception, cognition skills and *"smart"* decision-maker based on AI to support robot's controller in more challenging tasks. Despite many inspiring success stories of these machines, there are still some critical aspects that they have not efficiently carried out, in which, *fragility* is of the most interest of mine. Since the maintenance is not always available especially in isolated scenes [24] or public areas, therefore, the necessity of a self-recovery function to tackle such situations of unexpected physical damages in robot's structure is widely recognized by roboticists as a desirable attribute for the next generation of adaptable robots. Indeed, much work has sought methods to recover a robot's operation from structural damages in an automatic manner. The most common solution is to first diagnose the failure, then try to update the control parameters to bypass it [25]. Such approaches seems to work fine with rigid robots whose broken parts are as fixed in shape or reconfigured by spare components. However, they, without a doubt, put more computational burden on the centralized controller, not to mention a considerable probability that our robots can not afford in term of time, energy, money, or even fail to recover.

On the side, the biological systems are remarkably resilient. Specifically, unlike conventional robotic systems, natural systems do not compromise with injured body by merely searching for new control policies that perfectly works with the impaired body, but adaptively deforming their body's morphology (even the broken parts) to manifest adaptation (*i.e.*, self-recovery function). Wild animals execute this in many different styles which can be summarized into two strategies: the body can 1) theoretically re-grow [26] or 2) re-shape lost parts and embrace an entirely new morphology in the manner of remaining the functioning of this body part [27]. The first strategy is more likely relevant to the body growth or evolutionary process that organisms (whether in robotic or synthetic systems) go through slowly over their lifetimes to promote long-term viability. While the second strategy might be referred to as the short-term solution for a specific adaptation goal.

Although, in certain designs [28] [29], rigid robots could change their structural arrangement, however, the searching space of possible configurations those robots can achieve are limited at best. Fortunately, recent advances in material science and 3D printing technologies have allowed us to fabricate soft bodies, machines capable of largely deforming their rest structure in infinite degrees of freedom (DoF). Nevertheless, similar to above examples of rigid robots, *invariable* soft bodies only allow to conform the dynamical variation of external environments at a low level, mostly thanks to their compliant structure. Inspired by the idea presented in Fig. 1.1, if the soft body could be selectively adapted through bending, twisting, compressing, or expanding compliant structures (*i.e.,* varying internal stimulation), theoretically, there will be infinite solutions for morphology to attain. In other words, we might expect a higher level of adaptability in comparison with other cases (see Fig. 1.3(A)). Such devices, in one hand, facilitate investigation of embodied artificial intelligence in modern robotic devices, but in the other hand, emphasize the inadequacy of current development on novel actuators for shape-changing. Firstly, under the perspectives of mechanical systems, a soft body can not undergo an exceeding deformation due to the allowable range of tensile strain. One can envisage future advanced soft materials capable of "self-synthesizing" their lost parts, but that day seem far off. Whereas, soft robots capable of locally deforming their body within a transformability range to enable adaptive behaviors such as resilience, are already becoming more realistic.

There exist early attempts conducted in simulation environment proving that allowing the body's morphology to vary could remain (or even improve) locomotion function despite structural damages. In this thesis, I pay attention on how adaptive morphology could ensure the sensing performance of a soft tactile sensor (see Fig. 1.3). In particular, I am impressively stunned with the way rodents can adaptively deal with situations when their sensing organs - whiskers, are broken. The detail of this bio-mechanism and its possibility to be converted into an artificial system will be discussed clearly in the rest of my thesis. in which novel soft tactile sensor is of my most interest [30]. To clarify the role of damage recovery function in

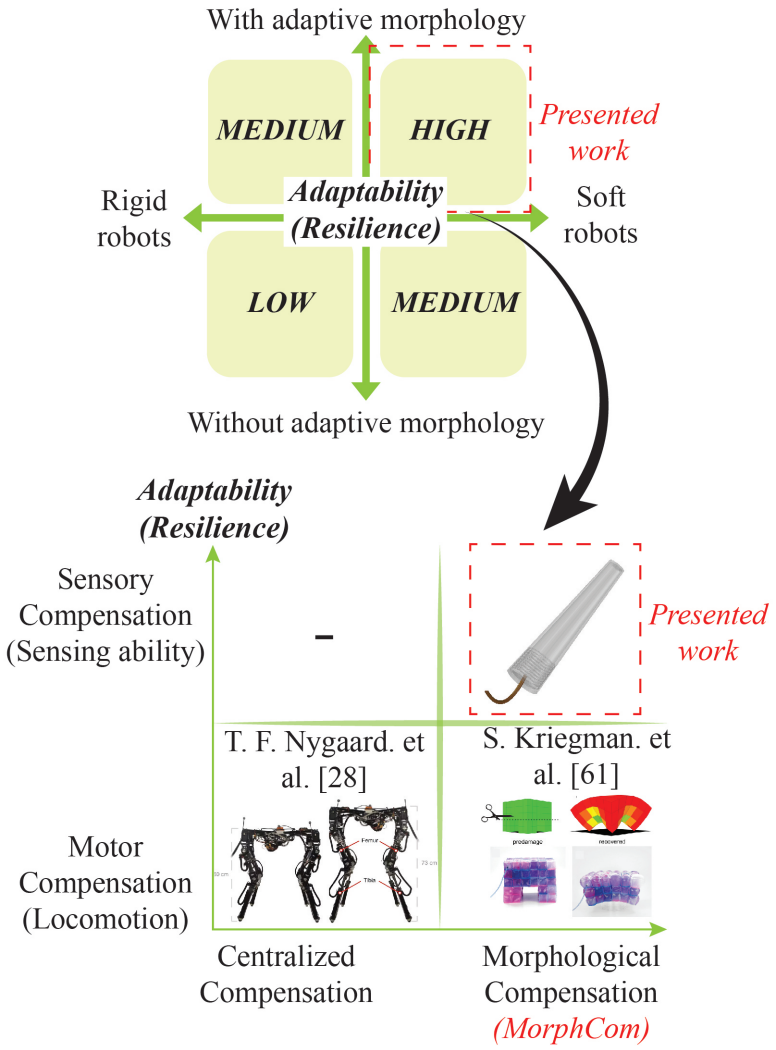

FIGURE 1.3: Position of this research in the field of Embodied Intelligence via adaptive morphology in the attempt of enhancing robot's adaptability

a soft sensory system, I hypothesize that if the morphology of the resting sensor body can be properly deformed, the sensitivity of this device (after being broken or trimmed) can be restored back to its original state even though the shape might not be regenerated completely. Since this idea exploits body's morphology, I refer it as *Morphological Compensation (MorphCom)* strategy [5]. The scope of this thesis lies around two following questions:

1. What is the role of adaptive morphology in the resilience of a soft mechanism?

2. How can we derive a proper compensation strategy based on morphological change?. In other words, how can we determine the proper morphology that should be achieved to accomplish a specific compensation task?

1.3 Objectives and contributions

The main objective of this thesis is to pave a way for implementing embodied intelligence via adaptive morphology to enhance robustness and adaptability of soft robotic devices against physical damages. In more details, a showcase of soft tactile whisker sensor will be tested its tactile compensation ability enabled by adaptively variable morphology to maintain the sensor's sensitivity with the same contact conditions. Furthermore, changing morphology would require additional actuation modules to access the deformation of the body. Hence, it is unclear how we can build flexible connection mechanisms among each "cell" module and the body and how these module works to various mechanical properties (*e.g* more elastic, stiffer or softer) in the right manner so that simple model of control is sufficient. To tackle these challenges, a suitable pipeline of designing, fabricating and modeling for a tested prototype (here is a soft whisker sensor) will be considered.

Based on these above objectives, the expected contributions of the study presented in this thesis are shown below:

1. The proposed idea contributes to early investigation of embodied intelligence in enhancement of robustness and adaptability against uncertainties (e.g, physical damages) for various robotic tasks (not only tactile sensing) and devices which will be discussed in the section for future works (see Chapter 7.2).

2. This work highlights the importance of adaptive morphology for generating unprecedented diversity and behavioral characteristics for the next generation of soft robots

3. This study is expected to shed a light on the contribution of the dynamic change of the soft body's morphology to active tactile perception with novel, computationally cheaper strategy, so-called morphological adaptation which allows a body plan to *self-select* their forthcoming sensory experiences.

1.4 Overview of the thesis

This thesis comprehensively synthesizes the contents of 3 peer-reviewed scientific papers which are published in the leading journals in the robotic field (2 papers) and the proceeding of relevant conferences. The general structure is organized as followed:

- Chapter 1 highlights the concept of *Embodied Intelligence* in addition to motivations, objectives and expected contributions of presented works.

- Chapter 2 presents state of art on soft robotics in general taking soft tactile sensory system as the core of concentration and current progress on the development of artificial systems with resilience in both practical scenarios and virtual simulations. This section again discusses the advantages of the controller and motor-sensory coupling, which is mainly inspired by biological systems, under the context of morphological computation for unforeseen action and perception. This aims to demonstrate how such idea can reduce the gap between robots and living creatures in terms of adaptive behaviors. The general idea of morphological computation and its applicability will be discussed from broader scenes rather than limited to re-silience in sensory systems.

- Chapter 3 briefly reviews the existing artificial whisker designs that have been reported with inspiration from biological whiskers. More importantly, the mechanism to transfer tactile data from the vibrissae system to *"information processor"* inside the rat's brain will be introduced. More importantly, the mechanic of neural processing that rats use to compensate for broken whiskers and my hypothesis under a roboticist's point of view will be introduced. Based on the above discussion, the proposal of *TaCMorph: Tactile Compensation by Variable Morphology* (see Fig. 3.3) which is taken as a guide for building up the proposed whisker design as illustrated in Fig. 3.5. The fabrication process and general working principle are also included.

- Chapter 4 shows in detail the analytical model for studying mechanical behaviors of the whisker under the light of a quasi-static analysis in two modes: 1) Normal mode for the original state of whisker morphology and 2) Compensation mode for the compensated state of the broken whisker. An experiment set up to verify the above analytical models and compensation strategies are designed. Experimental results will be evaluated by comparing them with those calculated from the numerical models.

- Chapter 5 introduces two distinct compensation strategies as summarized in section. 5.2.4 applicable for two potential configurations of the proposed whisker sensor (see Fig. 5.10). Whereby, one configuration hopefully is suitable to serves as a platform for testing biological hypotheses of the rodent vibrissae system. Whereas, the other is more practical for robotic applications. Their efficiency will be experimentally assessed with different cases of structural damages. Relevant discussions revealing the feasibility of the tactile resilience based on adaptive morphology will also be conducted.

- Chapter 6 tries to improve compensation capacity and clarify the contribution of geometrical factors on such attribute. The optimization framework (as summarized in Fig. 6.5) for interested geometrical parameters as mentioned in this section. A list of optimization objectives and their effect on the adaptive range of the proposed whisker are discussed. I will particularly pay attention on clarifying the conflict among objectives and propose a solution for this circumstance. Based on that, an appropriate fitness function considers all factors upon their contribution to the compensation performance. The optimized design for a specific demand on compensation capacity and its performance will be compared with the previous design as used in Chapter 4.

- Finally, chapter 6 summarizes all the findings and contributions presented in this thesis and discusses potential applications and future research directions to extend the existing work are also presented.

1.5 Contributed Publications

Journal publications:

- ***N. H. Nguyen*** and V. A. Ho, "Tactile Compensation for Artificial Whiskered Sensor System Under Critical Change in Morphology," IEEE Robotics and Automation Letters, vol. 6, no. 2, pp. 3381–3388, 2021, (DOI: 10.1109/LRA.2021.3064460)
- ***N. H. Nguyen*** and V. A. Ho, "Mechanics and Morphological Compensation Strategy for Trimmed Soft Whisker Sensor," Soft Robotics, (DOI: 10.1089/soro.2020.0056).

Conference proceedings:

- ***N. H. Nguyen***, T. D. Ngo, D. Q. Nguyen and V. A. Ho, "Contact Distance Estimation by a Soft Active Whisker Sensor Based on Morphological Computation," 2020 8th IEEE RAS/EMBS International Conference for Biomedical Robotics and Biomechatronics (BioRob), pp. 322-327, 2020.
- N. M. D. Le, ***N. H. Nguyen***, T. D. Ngo and V. A. Ho, "Vision-based Sensory System for UAVs: Fabrication, Calibration, and Measurement," 2022 IEEE/SICE International Symposium on System Integration (SII2022), Norway, 2022. (Accepted)

2 Background and Related Works

2.1 Why Soft Robotics?

Going through the third industrial revolution, automated machines those we often call by the name "Robots" have taken places of human forces in industrial production lines thanks to the convergence and synergy of larger information and communication technology (ICT), advanced manufacturing systems, 3D printing, nanotechnology and more recently, artificial intelligence (AI). Conventionally, industrial robots are a collection of rigid links made of stiff materials, connected to each other through joints. These rigid bodies, on one side, help robots to accomplish tasks in well-structured environments with a high level of load capability, repeatability, reliability, and precision [31], but on the other side, forbid them from other applications which require more adaptively controlled actions in the open world [32]. On the opposite side, rigid components in biological systems occupy a minority of their bodies, but natural species generally make good use of flexible, elastic body parts (*e.g* tendon, muscles, or skin) in order to resiliently accommodate environmental variation and actively or passively conform to spatial constraints [33]. To reduce such salient differences in constituent materials of artificial and natural systems, robots either fully or partially composed of soft materials open an emerging field that leverages *softness* to explore flexibility to achieve multiple missions with the same mechanism, adaptability to uncertainties or unstable environments, finally, compliant properties needed for safe physical interaction with humans [34]. It should be noted that soft robotic technologies do not technically outperform their counterparts in many regards of industrial manufacturing tasks or even the features

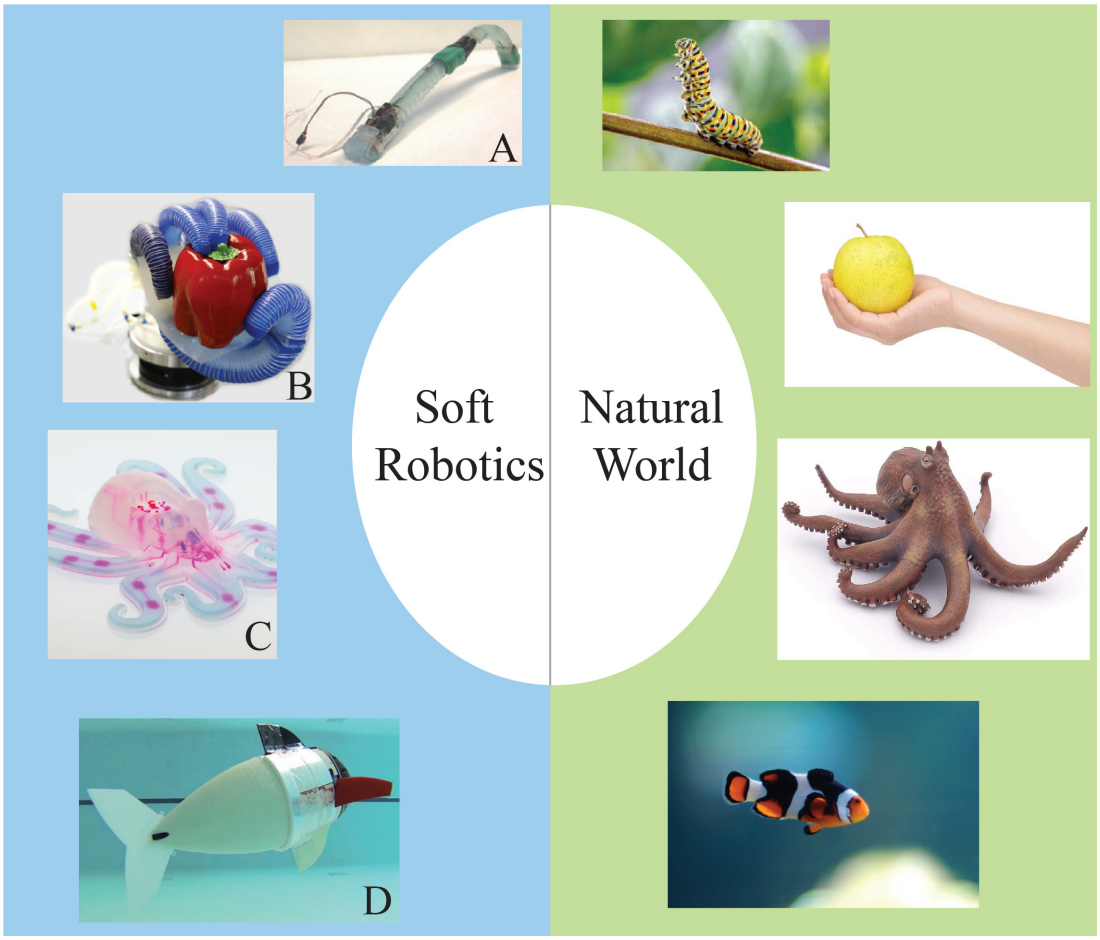

FIGURE 2.1: Soft robotic systems inspired by a range of biological systems: (A) Caterpillar-inspired robot (adapted from [35]), (B) soft human-like robot hand (adapted from [36]), (C) octopus-inspired robot (adapted from [37]) and (D) an underwater fish-like robot (adapted from [38])

we hope soft robots will comparatively excel at such as higher flexibility for manipulation, grasping, etc. The reason encompasses a wide range of technical and physical aspects, however, here I only pay attention to the relationship between the controller and the body. In most rigid robots with finite DoF that usually are kept as low as possible, controllers often only deal with minimized negative effects from the robot's structure or morphology (*i.e.*, physical noises) since they are made from rigid links. As a result, full states of the robot can be determined sufficiently with limited and measurable parameters facilitating accurate control for a specific task. On contrary, soft robots possess continuum topology with closely infinite DoF for higher behaviors diversity, although they tolerate low accuracy, load capacity, energy-efficient and speed [39]. Instead, compliant bodies provide innovative approaches to function robots with novel capabilities that are hard or impossible to

achieve with rigid bodies, whilst very common in our natural world. As a matter of fact, living organisms have been inspiring researches on soft robotics from many different perspectives as shortly illustrated in Fig. 2.1, in which, the implementation of embodied intelligence principles is of the main benefit [8]. This direction mainly investigates the collaboration of the brain and nervous system (controller) with the compliant body to permanently compromise with external perturbances using experienced memories obtained from the dynamic of the body's morphology as a lifelong evolution. This has not only been explored among biologists but also in the roboticists community under the concept of morphological computation (see section 2.3).

Many implementations have been reported in the literature to date exploiting morphology for novel devices aiming to enhance the quality and safety of physical interaction with surrounding including humans. Haptic sensing devices constituted from soft materials are, in the author's belief, the most beneficial [40]. Inspired by the concept of embodied intelligence, I hypothesize that if the morphology of the functional components, which either join a contact with the environment or not but have an effect on overall sensing performance, are adaptively changeable, then, more advanced and lifelike functions for tactile sensors that were not possible before (*resilience*) will be activated. Since this thesis mainly studies a showcase of a bio-inspired soft tactile sensor, thus, next sub-section will deliver a direct gateway toward the current state of the art in terms of soft sensor structures, sensing abilities.

2.1.1 A background on soft tactile sensor

Typically, the more difficult robotic tasks, the more information not only associated with the robot's dynamic states but also the dynamical variation of the operation ground would be required [41]. Hence, we have seen recently a growing need for hybrid sensory systems that can feed as many physical properties from the surroundings as possible particularly to learning-based adaptive controllers which are always data-hungry [42]. In this regard, compliant haptic interaction, which is one of the richest sources of physical information available, has invited a lot of attention

from robot inventors/researchers on the development of soft tactile sensors [43]. Tactile sensors are basically able to emulate the *"touch"* perception through measures resulting from the contact between the object and the sensing element such as force, strain, vibration, so on and so forth.

The transduction principles are varied from piezo-resistive, piezo-capacitive, piezo-electric whose general designs for such types will consist of a soft substrate which is utilized to encapsulate the sensing elements [44]. This design prevents the object from over-penetrating into the sensor body causing damages to active elements thanks to compliant materials for transferring contact force evenly distributed over a large contact area (which is impossible for stiff tactile sensor). The tactile feedback will be converted from the mechanical responses mostly generated from the contact consequences reflected by body deformation, thus, due to high flexibility, the large measurement area, rich sensory information, and high sensitivity against physical impacts are realized in soft tactile sensors. Besides, a vast of reports on optical-based tactile sensor have been established [45]. This type of sensor relies on optical sensor in cameras to capture movement of the visual cues (*e.g* markers) which represents for the touchpad deformation. These devices are even more robust since the sensing element is isolated from contact areas and high spatial resolution is available.

In addition to being highly sensitive and stretchable, to fulfill the demands of robotic systems for tactile perception, tactile sensing devices must be widely scalable allowing them to cover the whole robot's body with different surfaces. For example, P. Maiolino *et. al.* [46] proposed a large-scale capacitive-based tactile skin for humanoid robots. Their sensor was constructed as a matrix of sensing elements (taxels) where each small scale tactile unit is stretchable, bendable, and sensitive with contact pressure. Nevertheless, single-point tactile sensory systems always face the critical challenge of bulking wires as well as analog-to-digital converters, etc., serving a large number of taxels. Not to mention the significant cost, necessary equipment, technologies required for fabrication have constraint ther popularity. L. V. Duong and V. A. Ho in [47] introduced an optical tactile sensor particular for robot link. The design is simple, less wiring and very low cost compared to above

systems. Many similar devices (in small scale) with the same principle are widely known. Generally, most of existing tactile sensor attempts to emulate human perception through skin, finger tip, etc., into robotic system, while little similar efforts have been made on wild animals except rodent's whisker (review on whisker-like robotic sensor in literature will be presented in section 3.1). Tactile sensory organs would rather be test cases for studying dynamic of neural system corresponding to biological sensing behaviors, for example, when the sensing organ's structure is critically damaged.

It is also the fact that, due to routinely wearing out with physical impacts, The possibility that the tactile sensor body can be lost to injury, is notable. Furthermore, there have been increasingly recognized proofs for a coupling relation between the morphology of the sensor body and sensing ability (tactile perception or sensation modalities [19],[48]-[49]). Herein, the author intentionally seeks an approach to leverage the inherent softness of the tactile sensor body to enhance the robustness and adaptability against structural damages. Next sections present the state of the art of resilient robots and relevant technical features regarding the geometrical architecture, control systems and physical interfaces to potentially support the development of the self-recovery abilities.

2.2 Resilient Robots: Inspiration, Concept and State of the Arts

Current robotic systems lack the resilience that we can widely observe in natural creatures. Biological systems equip themselves with regenerative and adaptive capabilities allowing them to adjust the geometry of their organs toward complex anatomy to compromise with the constant change of environment and external as well as internal perturbations during their lifetimes [50]. In which, many organisms have capabilities to self-recover from serious injuries by regenerating or reconfiguring morphology of broken parts in response to the new critical condition. For example, salamanders are able to regrow their limbs when they are accidentally

amputated [51]. In similar scenarios, there are species, although their bodies are significantly reshaped or completely replaced after regeneration process, are able to preserve prior features such as memories, learned behaviors, intelligence for regeneration processes. Planaria flatworms are capable to use their memories of shape for rebuilding their body on a new scale to completely recover no matter where the injury occurs [52]. However, it is not true for every species. For instance, spiders legs, which are used for locomotion, building web, and sensing abilities, can not be completely regenerated. Instead, an organ called *Lyriform*, that plays the role as a mechanoreceptor to perceive all external mechanical stimulation, will change its morphology (equivalent to its sensitivity) so as to facilitate the normal operation of the neural system (*i.e*, brain) to justify imperfect leg's functioning compared to the original state [3]. This particular adaptation mechanism is quite analogous to the way rodent's brain update their neural circuitry continuously to adapt to dramatic changes of the whisker body. Chapter 3 will discuss this inspiring phenomenon in more details. In general, it is reasonable to say the adaptation procedure of animals to a new body (either fully or partially regenerated) is a learning algorithm with a behavior-performance space constructed from previous experience to ensure the organism can succeed in its ecological niche throughout life cycle [53].

Taking these intriguing stories in biology as a proof-of-concept, roboticists have realized the importance of resilience in modern robotic systems. So far, while some approaches have been proposed, the majority of them obey two purely algorithmic approaches to deal with damages: 1) embracing the new structure by self-identifying new control rules [25] or choosing an alternative pre-programmed contingency plan in response to prior-detected errors [54] for failure compensation, 2) Changing the configuration of the robot by rearranging or replacing its components [55][56][57].

Robots applying the first strategy are theoretically expensive (for damage detectors system) and difficult to design. Moreover, there maybe circumstances that can be anticipated, hence, searching for new compensatory behaviors often fails due to incorrect damage identification or unavailable suitable contingency plan. Bongard

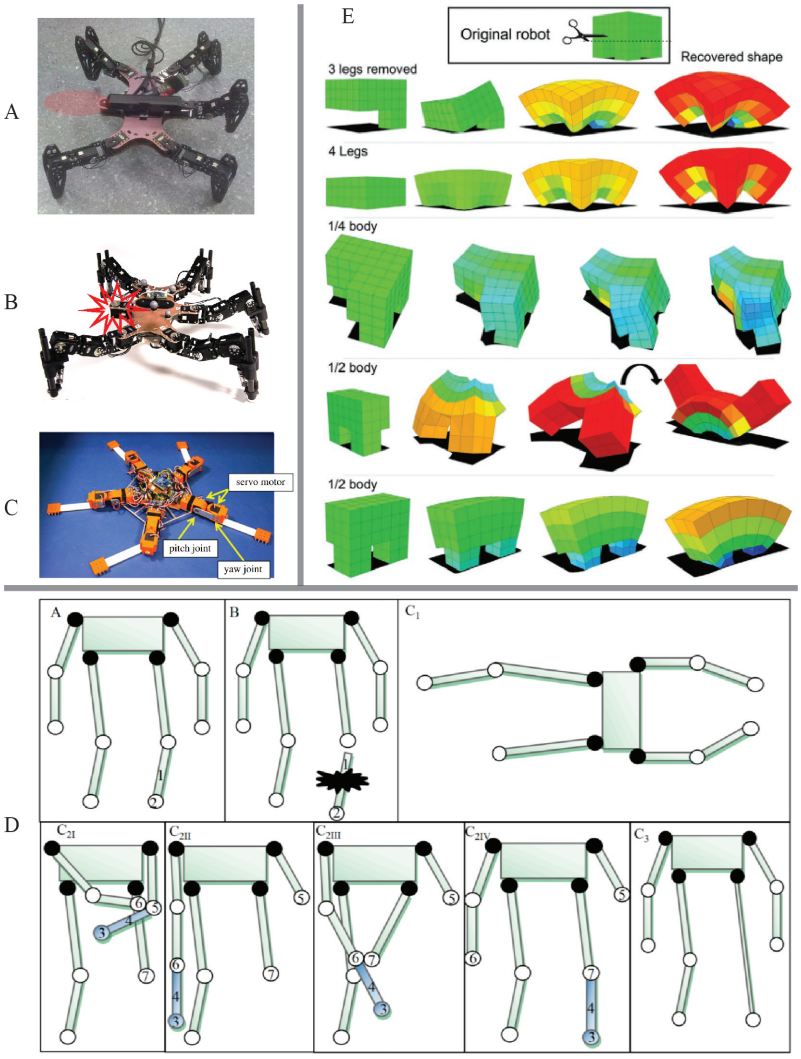

FIGURE 2.2: (A)(B) Hexapod robots (adapted from [58], [54] and [59]) (C) brittle star-like robot can enable resilience by searching a new control policy (adapted from [60]), while (D) shows an example of resilient robot based on re-configurable structure (adapted from [55]) and finally a simulated voxel-based robot (E) demonstrates the self-recovery process for its locomotion by optimizing its morphology through selective inflation and deflation of the voxels (adapted from [61])

et al. [25] propose a method to continuously search appropriate behaviors upon the newest dynamics model to adapt to unexpected damages without the requirement of fault diagnosis. Similar method can be found in [58]. However, the main disadvantage of this solution is that the processor will incur a major computational burden to seek and testify the newest model by attempting them in actual scenarios . Thus, in some cases, the final compensatory model is not feasible in terms of time, stability and accuracy. Authors in [60] introduced a brittle star-like robot that can regain its locomotion ability when a leg is amputated in a few seconds by self-coordinating the other intact legs. G. Ren *et al.* [62] treat artificial regeneration

algorithm as a "Trial-and-Error" process (analogous to how injured animals gradually get familiar with their new body) to recover its performance regardless of being damaged. Similarly, authors in [54][59] introduced another efficient "Trial-and-Error" methods that could find a compensatory control policy with an acceptable number of trials. Generally speaking, these algorithms worked well with complex robotic systems as long as they are as data-efficient as possible, otherwise, searching through so many trials would probably make the damage conditions worse. Thus, learning-based and self-model approaches are often limited to a certain set of damage types and specified functionalities, or in other words, I would say they perform a low-efficiency resilience [63]. The second strategy could be applied to a class of robots called *self-configurable* robots which consist of many homogeneous or heterogeneous modules that can actively change the connectivity among them. Thanks to this special ability, they could overcome damage suffering situations by replacing disabled modules [57] or re-configuring their body to remain overall performance without making use of the broken parts. Despite its potential, a majority of the current self-configurable robots have not equipped themselves with explicit resilient capabilities because of difficulties in autonomously controlling the recovery process (*i.e.*, reconfiguration process) and designing mechanical modules appropriate for such tasks [63]. A more feasible trail for this strategy is related to the newest innovations in the development of novel advanced composite materials that are able to self-heal cracks or punctures across the soft body, while still remain the mechanical characteristic of the material, thanks to complex chemical reactions. These materials are suitable for various applications in robotics [64] and prosthetics [65]. Unfortunately, they require a substantial amount of time to completely heal [66], and seem to work well with small cracks and punctures while they could be useless when a body part is completely disassembled from its agents [67].

As a matter of fact, the above recovery mechanisms work based on the fact that the impaired body parts are still unchanged or only configured, while flexibly deforming the whole body or constituent components to re-grow or adapt has not been seriously considered. In this regard, robots whose components are made of

soft, elastic materials such as silicon rubber shed a light on making use of active shape-changing and its underlying physical properties to enable many compelling capabilities like resilience. Such theory has been previously mentioned as *Embodied Intelligence* or *Morphological Computation* [7][8][19][24] which will be reviewed in the next section. Regenerative spider's leg [3] shows a unique demonstration of how morphology change can be used to recover from damages similar to what happen in rodent's brain. Nevertheless, similar systems pose challenges to engineers in the robotic community to create a novel design paradigm and robust computational medium to continually and properly drive robot's morphology to the desired state. Simulations would be a solution to weed out unsuccessful designs and strategies for morphological transformation before attempting them in reality. A work by S. Kriegman *et al.* [61] proved that functional recovery can be accomplished by simply shifting the rest-structure from the original state to another without any change in the controller. They expressed this idea through a voxel-based robot simulator where each cuboid voxel is actuated periodically by using optimized phase-shifted signals to achieve desired locomotion. By applying the evolutionary algorithm, an optimal shape is established prior to operation start to maximize the performance of the robot (evaluated by how far it can locomote within a given time) even when different degrees of damage ranging from cutting one leg to all legs or even halving the body occur.

Although shape-changing could benefit robot's operation in many unanticipated aspects, it remains many unclear concerns to really transfer this kind of robot to practical scenarios. This achievement depends on the development of advanced smart materials, fast shape-sensing techniques and an underpinning paradigm for designing similar systems. Here, I introduced a prototype for the whisker sensory system which can actively change its morphology in order to combat loss of sensing performance caused by serious damages such as amputated body. As far as I am aware, this is the first realistic robotic device capable to implement resilience by adapting its morphology. The underlying mechanics of this idea will be studied through a detailed analytical model, which is then used as a "*brain*" to suggest a

proper morphology for a specific compensation task. This work promises not just new robotic devices with unforeseen yet capabilities but also a new route for the science of robotics. Next section provides some examples of how adaptive morphology may enhance robot's performance in general and the haptic sensation in particular.

2.3 Morphological Computation for Intelligent Behaviours

The definition for morphological computation is rather general. At some points, morphological computation can be understood as the exploitation of the geometrical and material properties of a physical body to facilitate the controlling process [68]. In other words, It also means that some of the computational burdens, which are normally assigned to the central system, will be delegated to the body's morphology. Let revisit the example of a dog's legs, their smooth movement while running or jumping is not a consequence of the controlling signals from the brain - which is probably too slow to process all relevant dynamic aspects, but the result of elastic properties of the muscle-tendon system within a leg. That is to say, a part of the control sequence responsible for the leg's motion is taken by the morphology of the leg. As mentioned before, this idea encapsulates around the mutually interactive relation between the environment with the physical body (either biological organism or artifact) coupled with the brain [8]. Hence, within this thesis, it should be noticed that the *computation* is an analysis process for mechanical results related to geometrical and material properties from body-environment physical interaction. While this concept is very popular in biological systems, its attention among roboticists only arises along with the emerging of Soft Robotic field [21]. Because they are composed of compliant materials as observed in biological matter, soft robots potentially lead to plenty of promising functionalities thanks to their biocompatible characteristics. In this section, we will survey how biological systems make use of their morphology to support daily "computation" tasks. Then, existing robotic systems especially tactile sensory systems that employ morphological computation

to produce novel behaviors with either reduced supervision from the controller or none at all.

In biology, a particular body morphology could be a medium to achieve a specific contact condition with the environment. Tree frogs and grasshoppers have an ability to stably hold themselves on a tree thanks to an array of hexagonal cells and a network of grooves [69][70]. Thanks to such specially patterned surface, this species can inject an amount of liquid onto the surfaces between their pads and the tree to create adhesion forces. More interestingly, tree frog is able to actively activate and deactivate the pattern network on their toes respective to on-surface and off-surface states during locomotion. Thus, I argue that this mechanism is hypothetically served as an active sensory system to inform the brain whether the feet are on the ground by computing the adhesive force. In another point of view, organ morphology also regulates the information flow as well as modality so that this organ can perform for different tasks. This is common in tactile sensing organs such as wrinkled surfaces on human's fingertips as previously introduced. The shape and arrangement of either sensory receptors or organs containing them will decide what kind of signals that the brain will be acquired from stimulation sources [71]. The geometrical transformation of Lyriform organs in spider legs with implications on the feedback of leg positions, which is critically important for locomotion, web building and prey localization, is clear evidence. Biologists in [3] argue that: tuned sensor's output fed into closed-loop control facilitates normal operation of the central system (*i.e.,* the animal's brain) to converge leg's performance to the desired state. This argument can be understood that the sensory feedback obtained from the interaction with the environment (spider's web) is normally referred to as exteroceptive sensation is combined with a compensatory value resulting from the internal change of Lyriform's morphology (proprioceptive sensation) to achieve resilience.

While living creatures demonstrate that a small change in morphology could enable significant adaptation or new functionalities, the realization of morphological computation in artificial systems is still relatively elusive, especially in tactile sensing systems. A series of works [19][48][72][73] investigating a novel tactile sensory

system that can actively form a wrinkle-like surface onto the touch-pad to change the posture of the embedded sensing element (strain gauge). By switching from no-wrinkle to with-wrinkle mode and vice versa, this sensor will be able to adjust its sensing modalities among static measurement for applied indention (no-wrinkle mode) and dynamic measurement for sliding action (with-wrinkle mode). Josie Hughes *et al.* [49] attempted to envelop a tactile sensor with a jamming filter which can actively vary its own morphology in a variety shapes upon tactile tasks. For instance, their experimental results suggest that if the filter's structure is molded appropriately, the classification precision when performing tactile discrimination will be significantly increased. It should be noticed that both forming wrinkle and vary jamming filter shapes are accomplished prior to starting joining in-contact relationship with the environment. Hence, these works again illustrate the potential role of proprioceptive cues generated by internal mechanical variations (stiffness, geometry or damping parameters) while changing morphology in aiding tactile perception. However, many open challenges emerge regarding how and to what extent of proprioceptive feedback, or in another word, the change of morphology is beneficial for a specific task such as self-recovery [40]. The aim here is to tackle these challenges under the perspective of resilient tactile sensor devices based on an analytic investigation of the variations of mechanical properties and their functional influences. Thanks to this great effort, the desired morphology states, which generate compensatory sensitivity for the tactile sensory system in spite of damages, will be estimated. The remaining of this thesis will review a showcase of a bio-inspired whiskered sensory system for method verification.

3 Morphological Compensation: A case study on artificial whisker

In this chapter, the main content gathers around the inspiring sources and development of a novel artificial whisker sensor which has resilience. The reason to choose this delicate organ to assess the feasibility of TacMorph is not only because of their wide utilization in many species of terrestrial and marine mammals as primary sensing organs to sense and navigate in their gloomy living environment for daily tasks but also its fragility against frequent physical impacts. A question arises: How does a rodent such as rat cope when a whisker suffers several types of damages (*e.g* eroded, trimmed or cracked) on the body?. Interestingly, the answer for this question have amazed me of how a serious issue could be solved by solely changing morphology of a neural cell while sensing habits remain the same.

Given the vastness of the biological investigation available, in this chapter, I will show the insights on how this embodiment could and should be exploited in a tactile sensor. At first, in the following section, I will give an overview on whiskers in natural animals focusing on their inspiration to artificial whisker and their potential applications in robotics. Next, a short explanation for the compensation mechanism that rats use to pass over the situation of loss tactile perception because of injured body. With purpose of transferring this intelligent behavior to actual robotic and biomimetic devices, I hereby introduce a generalized paradigm for similar designs named ***TaCMorph***, which stands for ***Ta****ctile* ***C****ompensation by Variable* ***Morph****ology*. Based on this platform, the final section addresses a design and fabrication process for an artificial whisker sensor that obeys TaCMorph platform.

3.1 Whiskers in biology and robotics

In addition to the attraction to researchers in the field of neuroscience and biology, rapid tactile discriminatory abilities of living animals have been benefiting many active touch sensing techniques on modern robotic systems [74]. In which, long facial whiskers or vibrissae system of rodents is biologically fascinating not only due to exquisite neural responses against external stimulation at peripheral level or at higher levels [75], information transduction mechanism [76] but also mechanical behaviors while sensing of the vibrissae system [77]. Specifically, thanks to cyclic whisking motions to swing back and forth for proximal surrounding exploration [78], all mechanical information related to spatial features such as orientation and texture, which are also desirable data for robots, will be transmitted along the body length to the receptor at the base. As a result, the mechanical properties of the vibrissa and control of whisker movement (remind us to a robotic system) will specify its tactile perception. Nature has bestowed many great gifts on this animal, in which, the main distinction of rodent's whisker from other types of sensing organ is a high-density of nerve terminals and sensory receptors surrounding the follicle-sinus complex (FSC) [79]. Thus, bending moments resulting from in-contact relation between whisker body and the environment will be converted into neural signals and transmitted to the cerebral cortex for further processing [80]. Such procedure allows mammals to sense a wide range of properties such as shape, texture of the contact opponent and location of contact or substance stream (*e.g* seals can detect water flow generated by preys). It should be noted that sensing behaviors of rats require a relatively simultaneous movements of every single whisker (both macrovibrissae and microvibrissae) suggesting that morphology of the vibrissal array make an important contribution to the signal properties gained from interaction with the environment. Hence, there have been a number of studies [81] analysing in detail the morphological properties which are associated with arrangement of whisker array, the length and the structure of the whisker shafts as well as the degrees of freedom in the movement of both whisker and the mystacial pad. In which, the second

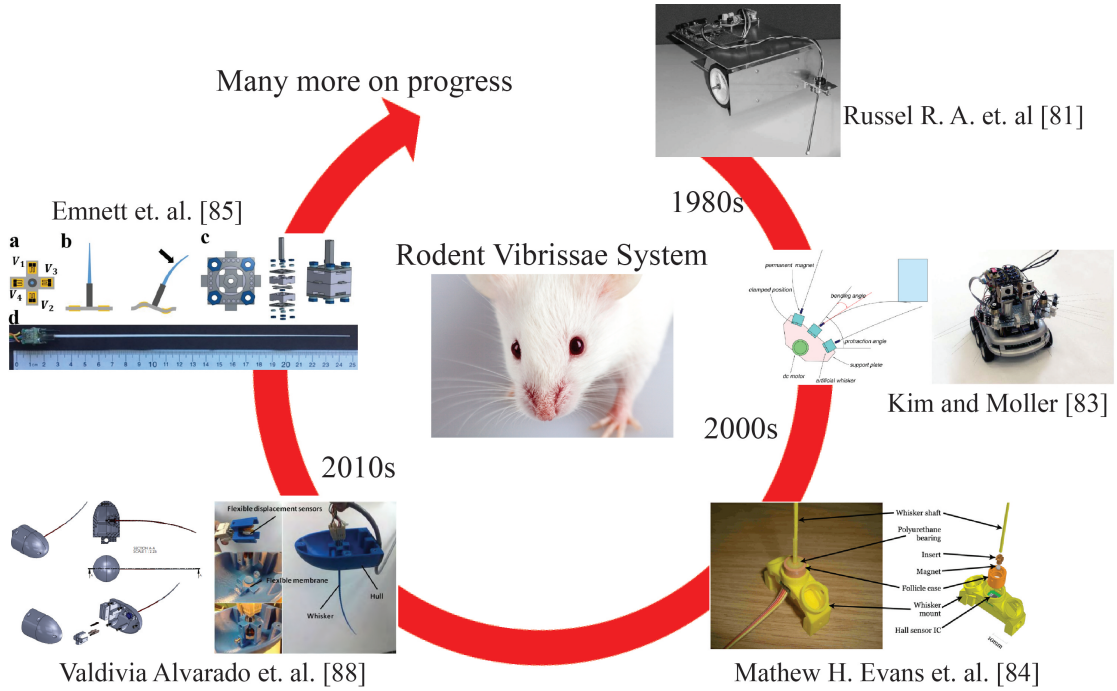

FIGURE 3.1: A brief history of development of biomimetic vibrissae system for robotic applications

and the third feature (for the first time considered in a biomimetic whisker sensor) will be studied in my whisker design and the analytical model.

Haptic sensing through *touch* offers enormous potential to robots in assessing their surrounding environment, or interaction with human beings [82]. In this context, biomimetic artificial tactile sensor based on rodent vibrissae offers to robotic implementations, especially for mobile robots, an easy and efficient solution to acquire a diversity tactile perception due to its simple structure and sensing principle. Such systems allows robots to perform tactile sensing in a distance with the surrounding obstacles in a wider area (compared to other conventional cutaneous tactile sensor) to prevent any unexpected collisions. As a matter of fact, research in this area have past a long journey ever since 1980s with works by Russell [83] who controlled a stiff cat-inspired whisker-like wire to locate and track the profile of the touched objects. For the next more than 30 years, studies on biomimetic or engineered whisker-like sensory systems mimicking active mammalian vibrissae systems have become the primary research trend for roboticists and neuroscientists. Kaneko *et al.* [84] was first to propose a flexible whisker-like shaft and a method to correlate the the curvature of the whisker and the mechanical torque at the base by

introducing the term *Rotational compliance* which denotes resistance of the whisker against protraction movement. Whisker sensor designed by Kim and Moller [85] and Mathew H. Evans et al. [86] share similar principle to produce tactile data from sensory feedback of a magnetic sensor (Hall effect sensor) located near its base. These prototypes showed good performance in radial distance detection and texture discrimination as long as noise from the measuring devices was minimized. Emnett et al. in [87] conducted a preliminary analysis of a whisker as a cantilever beam and suggested that an information set comprising three components of force/moment is sufficient to estimate contact point location in 3D space. Materials used for construction of vibrissal shalf are diverse ranging from rigid material (*e.g* steel [88]) to specially molded composites such as silicon-rubber [4] or even actual rat whiskers. Fend *et al.* presented a mobile robot platform called Khepera which is integrated with an array of real whisker glued to condenser microphone. Recently, there have been increasing studies mimicking seal's whisker ability that sense any disturbances generated from pre-contact air or water flow [89][90]. This might enable an aquatic or flying robot capable to analyze ocean currents or air streams.

While most of these whisker sensors make use of passive sensing strategy indicating the whisker sensor will stay still during making contact with the obstacle, rats instead exploit active sensing strategy by actively controlling their whisker arrays throughout contact phase with help of muscular modules beneath the snout [91]. A series of works leaded by M. J. Pearson concentrating on active sensing control observed from bio-whisker movement. Their first released whiskered robot was WhiskerBot [92] containing a bilateral array of glass fibre whiskers whose geometry resemble rat whiskers with a certain scaled rate. This robot uses shape-memory allot (SMA) combined with embedded springs as actuator to generate whisker contraction and extension motions which directly affect to sensory feedback measured by sensing element (strain gauge). To provide more degrees of freedom for vibrassae system, their next release SCRATCHbot [93] with updates on actuator for single whisker (DC motors) and sensing element (Hall effect sensors) was introduced.

The next evolution was to develop a completely modular artificial whisker (BIOTACT [94]) where each individual whisker own itself actuation mechanism and controller increasing its applicability in various applications such as navigation probe for robotic manipulator [94] or mobile robot [74].

According to [74],the investigation of biomimetic whisker sensory systems should aim for two goals: 1) an artificial whisker sensory system combined with a mobile robot could be a useful platform for neuronscientists learning and verifying unsolved yet hypothesises regarding biological vibrissae system. 2) Secondly, this gives a hint of a new approach for development of autonomous robotic system with high-performing, robust, and more importantly, high adaptability navigation system. The whisker device presented in this thesis is expected to satisfy both these targets by establishing a bio-inspired design for the whisker shaft which mimics loosely geometrical properties that have not been yet attempted before (see section 3.4.2) and flexibility. Moreover, rodent's adaptive mechanism particular for compensation of loss tactile feedback due to trimmed whisker will be emulated through TaCMorph platform and compensatory strategies in the remaining of this Chapter.

3.2 Tactile Compensation based on Structural Plasticity of Barrel Cortexes

Several properties of the vibrissal system make it stand out as an interesting model system (for either engineered and biological topics) in which to investigate theories about the adaptation in their neural system to cope with the situation of sensation lesions. In fact, there are many areas of the rat's brain that exhibit different neural activities resulting in a very sophisticated bio-neural system. Hence, to avoid going beyond the scope of this thesis, this section aims to provide readers who are not specialized in biology or neuroscience a most simple and straightforward characterization of the ascending sensory pathways and the reaction of respective cortical areas, especially those are more related towards tactile sensing modality called *somatosensory areas* [95] when whiskers are fractured.

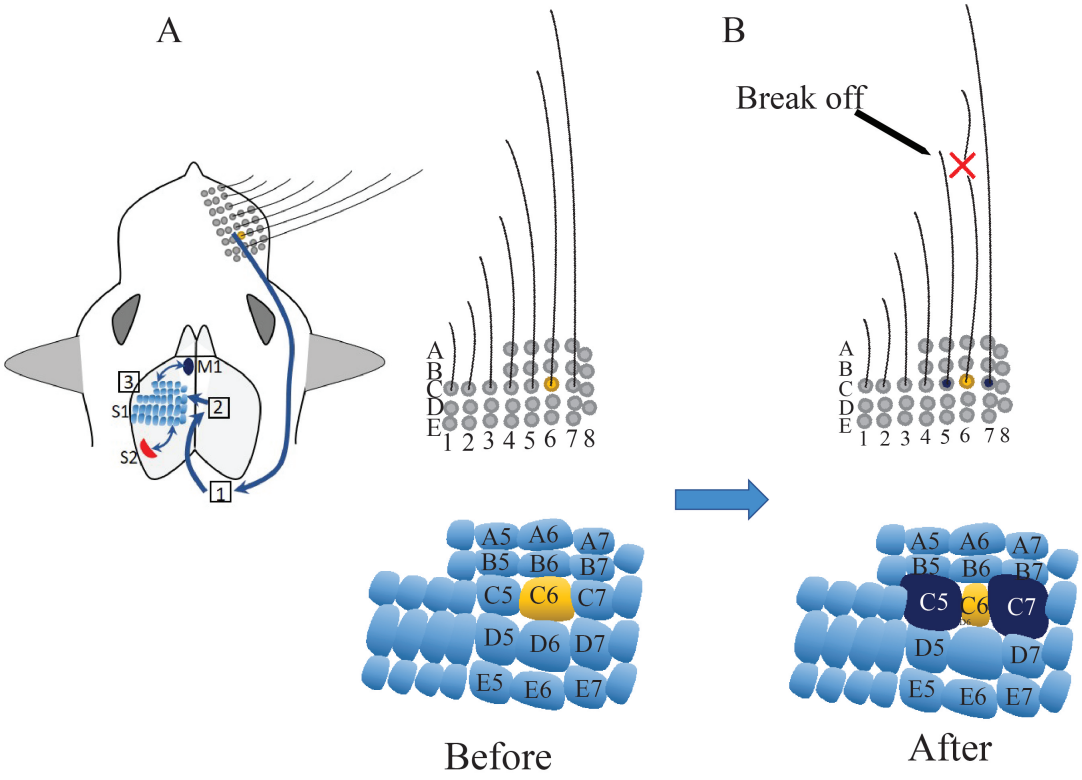

FIGURE 3.2: (A) The tactile signal transmission path begins from the whisker follicle-sinus complex, on one side of the snout, to the brain stem (1), then the thalamus (2) and ends up at primary somatosensory barrel cortex (3). (B) The configuration of the barrel cortexes corresponding to the whisker *C6* (yellow barrel) and the neighbor whiskers *C5* and *C7* (dark blue barrels) before and after C6 is broken off (Illustrations in A and B are adopted from [2]) and [96]

Ascending sensory pathways indicate the conveyors to transfer sensory signals from mechanoreceptors in the follicles at the snout to the somatosensory areas. Due to the absence of visual cues, in rats, somatosensory areas devoted to the region of the snout (where house their tactile sensing organs - whiskers) are significantly larger than others of most mammals [97]. Then a majority of mechanical signals goes to primary (S1) before collectively directing to secondary (S2) somatosensory cortexes (for recognition of object features) and M1 (motor commands for whisking movements) (see Fig. 3.2) for further processing. Notice that S1 is represented by a topological map, in which, aggregates of barrel-shape neurons (normally called barrel cortex) are patterned surprisingly similar to anatomical and functional topographic maps of whiskers [96]. There have been shreds of evidence demonstrating

that each barrel cortex, or in particular its size, in the S1 map will reflect the sensitivity of the respective whisker [79]. From this perspective, critical questions arise: What will happen to the barrel cortex of a trimmed whisker? Does S1 topological map take any role in the adaptive mechanism that we are interested in? and to what extend?.

Many studies in biology and neuroscience have characterized the contribution of whiskers to sensorimotor development by trimming collective whiskers of rats and observing behavioral adjustments [79], as well as the structural dynamics of neocortical neurons when those rats grew up [98]. Two remarkably inspiring studies [79] and [2] investigating the structural plasticity of barrel cortex show that removing follicle or trimming the whisker leads to the alterations of their cortical representation in S1 somatosensory topological map (see Fig. 3.2 for illustration). More specifically, the new S1 topological map will comply the following rule: the area of the barrel cortex allocated to a whisker reduced when the whisker was broken (*i.e.*, its sensitivity decreased), while the neighboring areas allocated to intact whiskers appeared to increase (*i.e.*, became more sensitive) as *compensation*. For instance, consider three adjacent macrovibrissae C5, C6 (the broken one) and C7 (see Fig. 3.2(B), which is adopted from [2]). It is clearly seen that the spatial area of the barrel cortex of the whisker *C6* after breaking off was occupied by the barrels of the two nearest barrel cortexes of *C5* and *C7*. It is the consequence of changing spine and synapse densities upon manipulation of sensory experience [2]. In other words, the densities of the spine and synapse (*i.e.*, the size of the corresponding barrel cortex) of a trimmed whisker appear to be decreased due to its deprivation from sensing function and vice versa. In summary, I argue that the transformation of S1 somatosensory topological map is intuitively a sort of embodied intelligence relying on morphological change of sensing organs (*i.e.*, barrel cortex) to perform compensatory behaviors for tactile perception.

The above phenomenon, once again, impressively strengthens the popularity as well as the significant role of embodied intelligence not only in resilience but also in learning, evolving in nature. The next section will introduce a platform that would

help to integrate similar abilities into artificial tactile sensors.

3.3 *TaCMorph*: Tactile Compensation by Variable Morphology

As mentioned previously, the morphological change of a barrel cortex, where directly processes tactile feedback before distributing them to other areas of the brain, is equivalent to the increase of storage capacity for sensation memory [2]. From an engineering point of view, it also means the corresponding whisker will be more sensitive to mechanical stimuli acquired from physical interactions with surroundings. In spite of the fact that the morphology-based compensatory mechanism is executed in the rat's brain rather than the whisker itself, I hypothesize the following suggestion: an adaptive tactile sensor should be able to actively adjust the sensitivity by changing its morphology. The aim is to enable such devices to maintain their sensibility as close as possible to their original state (*i.e.*, before being broken/trimmed), so-called resilience. Since this hypothesis exploits the sensor body's morphology, we refer to it as Morphological Compensation (MorphCom) strategy. To address this challenge, I hereby proposed a generalized platform of *TaCMorph* (Tactile Compensation by Variable Morphology) as described in Fig. 3.3, which follows one of the two compensation strategies offered by biological systems as presented in section 2.2:

- ***First strategy:*** A part of the soft body will be actuated in order to re-shape the original structure (see Fig. 3.3A).
- ***Second strategy:*** The morphology of the soft structure will be varied in order to relocate the sensing element in another position or posture (see Fig. 3.3B).

The idea behind TaCMorph is based on the observation of biological sensing systems when they seem to enable various tactile perceptions by changing their own morphology purposely (*e.g.* human finger's skin [19]). Whereby, the morphology can be understood as a state of a compliant body represented by a combination of

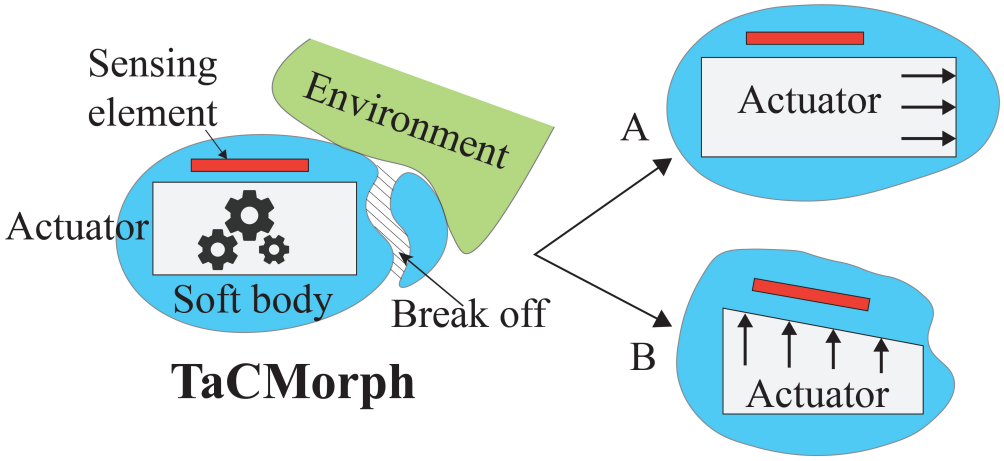

FIGURE 3.3: Scheme of *TaCMorph* platform which is divided into two mode: (A) The injured body will be re-shaped into to regain the original shape or sensitivity of the sensing element and (B) The rest structure is varied to change either location or posture of the sensing element (*i.e.*, its sensitivity)

mechanical and *geometrical* properties. Here, TaCMorph attempts to mimic the bio-layout of natural tactile sensing organs when sensing elements (*i.e.* mechanoreceptors) are normally "*hidden*" beneath a thick soft tissue layer to avoid disassembling or damage due to excessive contact force (see Fig. 1). Furthermore, inside the soft body, an integrated actuating system is utilized to change selectively geometrical variables to obtain the desired morphology. Thereby, the sensitivity of the sensing element will be varied accordingly to maintain the tactile perception with the same stimuli source despite the broken structure. Along with strain gauges and compressed air, other employable options might be accelerometers for the sensing element and a gear system for the actuator.

In this research, my device adopted the First strategy by modulating the air chamber morphology (analogous to medulla layer) inside the whisker body in order to vary sensory output of the sensing element. The fundamental differences between the compensation mechanism in rodent's brain and morphological compensation concept are shown graphically in Fig. 3.4. The design, fabrication process, sensory transducer and principle of tactile compensation applied for the proposed whisker sensor will be introduced in the next section.

3.4 Artificial Whisker Sensor with Variable Morphology

3.4.1 Design of biologically-inspired variable morphology whisker sensor

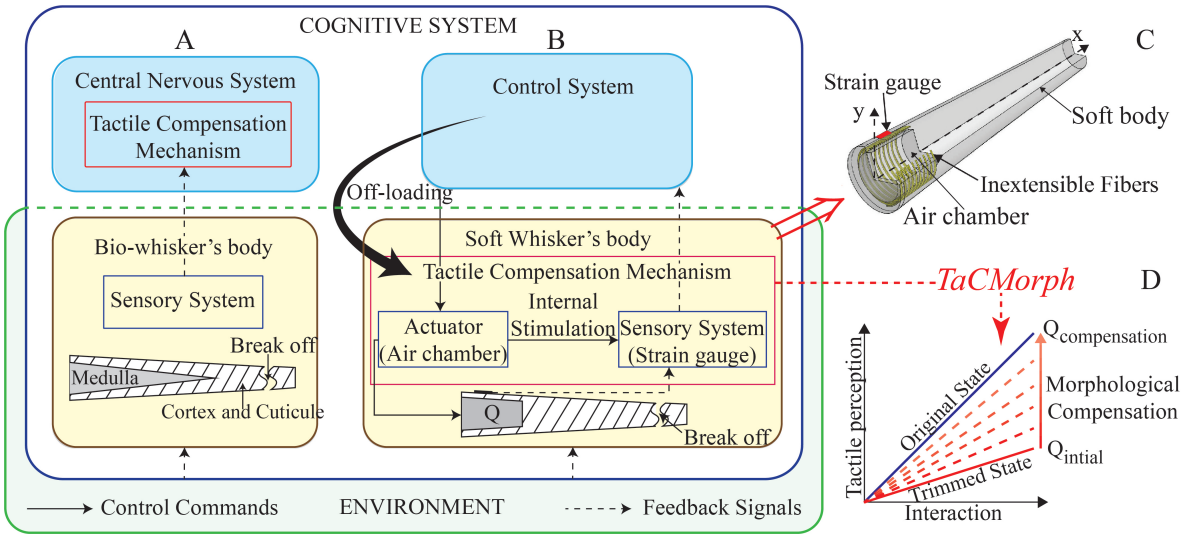

FIGURE 3.4: (A) An illustration diagram of how lost tactile information is compensated using a neuron compensation mechanism in rodent's brains [54] in comparison with (B) the information flows of our morphology-based compensation method which assigns the compensation tasks to the whisker's body. Whereas, (C) describes the bio-inspired design of the artificial whisker presented in this thesis; (D) illustrates how *TaCMorph* enable resilience by changing whisker's morphology alone (Morphological Compensation)

Assuming that such mechanism introduced from section 3.2 was implemented in a robotic system, the control system integrated with data-based learning techniques should be exploited to address the scenario of losing tactile information due to broken structure. However, this implementation generally requests the controller to share its limited resources for computation tasks when the whisker was broken. To reduce such computation burden in biomimetic systems, in this study, we approached differently by assigning the adaption process from the central system to the whisker's body itself as inspired by the proposal of morphological computation (see Fig. 3.4). It poses a challenge to integrate an actuator component within the whisker body in order to achieve a hybrid design. To satisfy this requirement, a

pneumatic actuator (*i.e.,* the chamber) was created inside the whisker body as can be seen in Fig. 3.4(B).

The main inspiration for this design came from the bio-structure of the actual rat whisker. In the whisker system, since mechanotransductive cells embedded within the whisker follicle will perceive all mechanical signals generated from whisker's physical interaction with the environment [99]. Hence, each whisker's geometry will have a critical contribution on its mechanics and thus on the tactile perception. According to Lucianna *et al.* [100], bio-structure of a real whisker consists of three separate layers: cortex, cuticle, and medulla as shown in Fig. 3.4(A), in which the medulla layer, which tapers from the base toward the tip, is the softest layer of the whisker and its geometrical characteristic such as length or diameter varies dependently with the whisker body [101]. This suggests that different whisker would produce different levels of *elasticity* as reflected in Young's modulus E (explained in the next chapter) because of non-identical the medulla layer [102]. Unlike insects antennae which contains sensing element within the antennae's body, the rodent whisker is simply non-sensorized hair. However, in this study, my whisker sensor will directly measure the mechanical properties through a sensing element (strain gauge) bonded onto the body (Fig. 3.5).

To achieve the soft changeable morphology in our device, we replicated the shape of a linearly-tapered natural whisker using silicon rubber and introduced a unique presence of the medulla chamber inside the whisker as introduced in my article [5]. The proposed whisker was divided into three separate regions to facilitate construction of the analytical model: cap (region 1), chamber (region 2), and whisker body (region 3) (see Fig. 3.5). Firstly, the chamber (region 2) is tapered at an equivalent degree of taper as the outer layer, that means the thickness t remains constant. Second, a thin cap (region 1) covers the chamber to prevent air leakage and to house a cylindrical hose that feeds pressurized air in or out. Third, a strain gauge is fixed to the top (outside wall) of the chamber with the sensitive direction toward x-axis. To prevent all unwanted influences of chamber expansion in other directions but x-direction to the strain gauge, two inextensible fibers (Nylon nano-filament of

TABLE 3.1: Artificial whisker parameters (see Fig. 3.4)

Parameter	Value (mm)	Parameter	Value (mm)
D_1	18	L_2	178
$D_2 = d_1$	17.8	L_3	165
$D_3 = d_2$	16.5	$\overline{L_2}$	148
$\overline{D_2}$	14.8	L_m	120
D_m	12	x_{ss}	6
$\overline{d_2}$	13.5	c	2
d_3	11	t	3
d_m	10.5	l	15
L_1	180	e	2

diameter $\phi = 0.38\,\text{mm}$) are wrapped helically with angles α and β around the chamber as illustrated in Fig 3.4. Bishop-Moser *et al.* [103] suggested that α and β should be larger than 54.7° and 234.7° respectively, in order to constrain mobility in all directions but the axial translation in x-direction. Thus, to meet this requirement, we designed the helical path to have the pitch $r = 3\,\text{mm}$. All essential parameters for the analytical model and visualization are presented in Table 3.1 and Fig. 3.5, respectively. Therefore, if we change the inner pressure of the chamber, it is theoretically expected to not only vary the geometry of the whisker but also material stiffness in a well-anticipating and directly measurable manner. In the next chapter, a detailed dynamical characterization of the sensor's output corresponding to the variation of the whisker's morphology during the air pressurization inside the chamber as well as in-contact states with the object as a morphological computation procedure will be presented.

3.4.2 Fabrication Process

The fabrication procedure is summarized in Fig 3.6(A). We used silicone-rubber Dragon Skin 00-30 (Smooth-on Inc., PA, USA) to make the soft whisker body. Molds were designed using 3D-CAD software (Solidworks) and fabricated in a 3D printer (Zortrax M200, Zortrax, Olsztyn, Poland). Two different sets of core molds were used in sequence due to the complicated design. First, core molds of *set I* were used to form the double-helical trench to make ease for wrapping the inextensible fibers in the next step. Then, *set II* was used to obtain all the dimensions of the outer

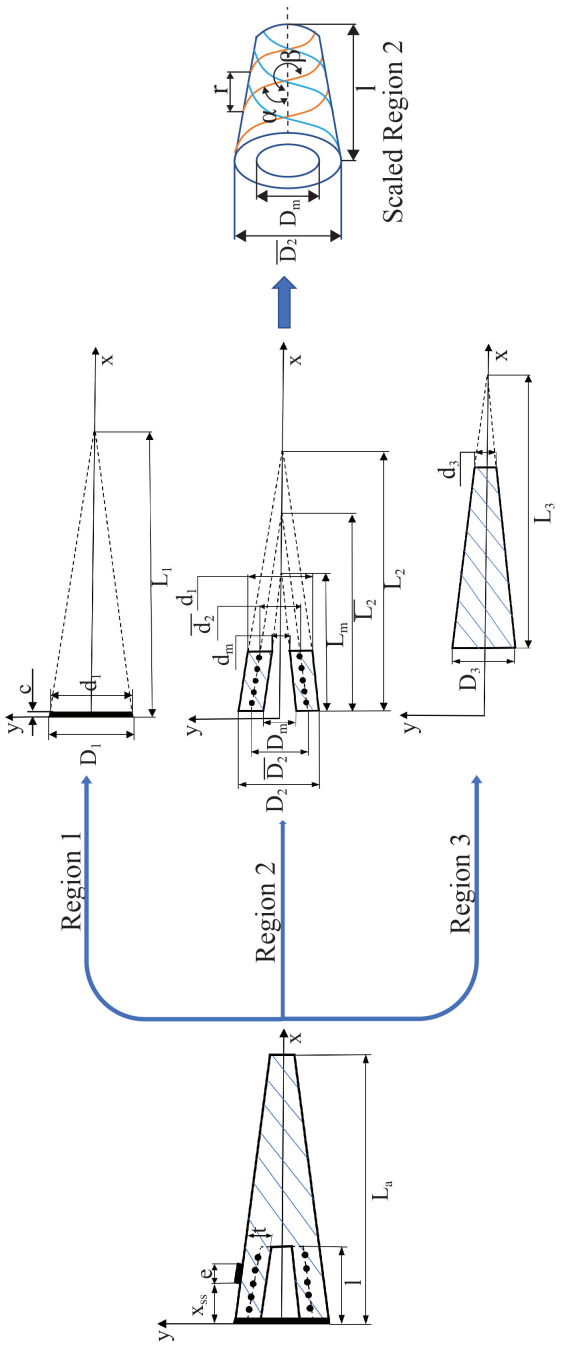

FIGURE 3.5: Geometrical design and parameters of the proposed whisker are represented into three regions: Region 1 - the cap, Region 2 - the chamber region and Region 3 - the body

layer as designed in Table 3.1. Both sets shared the same medulla mold which was not removed until finishing step 3. The model was then set on a cap mold with a cylindrical air hose (outer diameter 2 mm) and a thin layer of Dragon skin 30 was used to create the cap. Finally, a strain gauge was bonded by glue at the designate site x_{ss} and covered by a thin layer of silicone glue to enhance its robustness against external loads. The strain gauge used in this paper is KFGS-2-120-C1-11 L1M2R with gauge factor $GF = 2.21 \pm 1\%$, grid length $e = 2$ mm and was bonded with adhesive glue CC-3A, both from Kyowa Electronic Instrument Co. (Japan). The fabrication procedure was completed by fitting the model to the base and the curing process was implemented at a warm temperature with help from the vacuum dryer AVO-200NB-CR to avoid pockets of air bubbles.

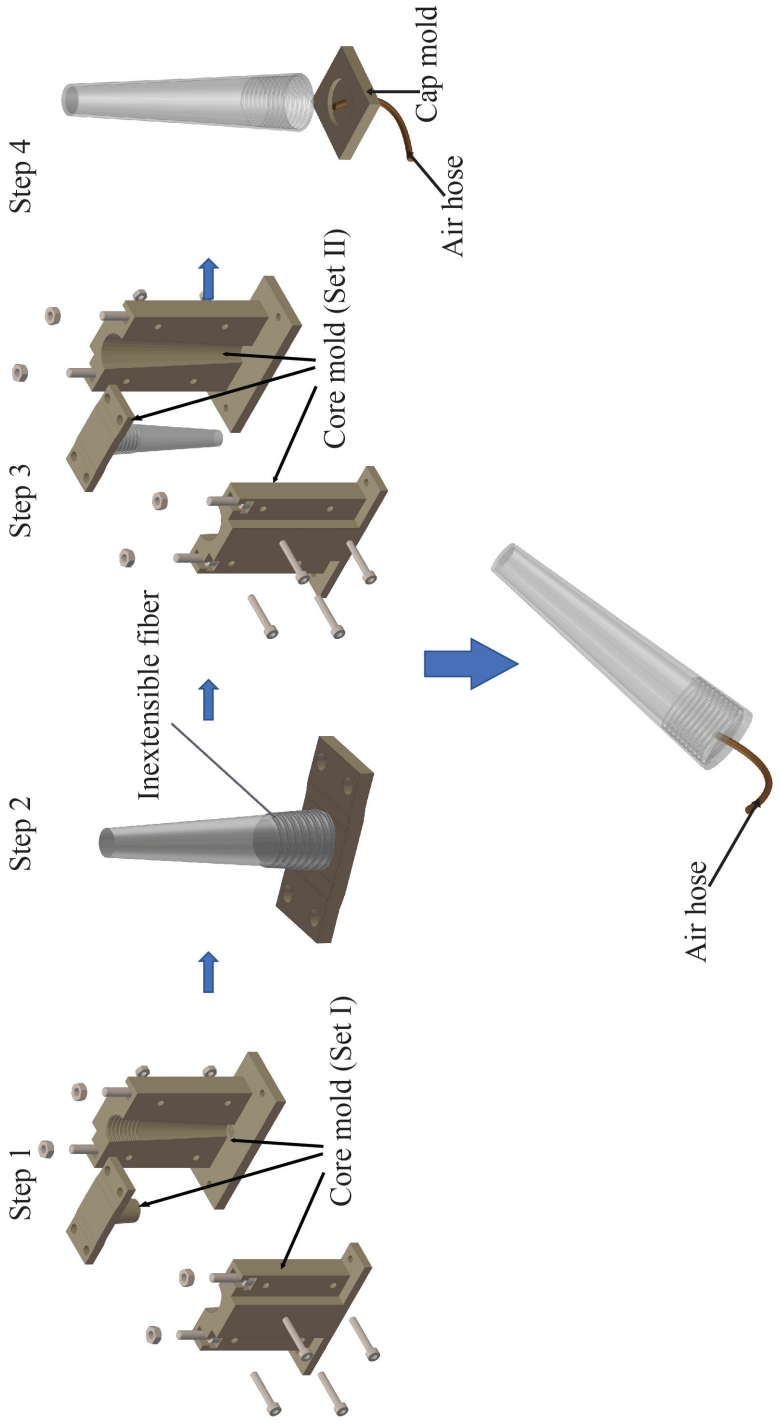

FIGURE 3.6: Fabrication procedure consisting of 4 consecutive steps: Step 1: Mold the inner layer of the whisker body using the core molds *set I*. Step 2: remove the body's mold but leave the medulla mold to hold the shape of the chamber, then wrap slightly with the nylon fiber. Step 3: Coat an outer skin to keep the reinforced fiber in place with the core mold *set II*. Step 4: remove the body and the head mold then dip the big end into a thin layer of Dragon Skin 30 inside the combination of cap mold and an air hose.

4 On the Variation of Tactile Perception upon Morphological Change: An Analytical Approach

As aforementioned, a typical whisker-like sensing system accomplished various tactile exploration tasks that happened on the whisker length. However, within this thesis, I particularly focused on radial distance discrimination ability to verify the feasibility and applicability of the Morphological Compensation concept. This sensing modality is used to specify where contact occurs along the body of the whisker. In fact, it is still vague about how the change of whisker's morphology will affect the tactile sensing performance of intact and broken whiskers. To acquire the best understanding of this regard, the following sections will propose an analytical approach to investigate the relationship between whisker's morphology (geometrical and material properties) and tactile feedback (*i.e.*, strain gauge output) used for detecting contact location. This relationship will help us to numerically estimate how much tactile perception has lost when a certain level of damage occur (*e.g* the body is trimmed in a length of Δ mm). Based on the difference in terms of tactile perception of the broken whisker with its previous state, we can identify a proper modulation of the whisker morphology in order to minimize this gap, *i.e.*, perform resilience. Finally, experimental results will be compared with numerical results (calculated from the model) to evaluate the success of the recovery process based on the suggested strategy for morphological change and offer some improvements. Note that the resilient ability is executed with a trivial intervention from the controller to compute parameters for morphological control. It means control tasks, now, are performed

in a more efficient manner in terms of time, memory, power and so on, than would be possible with conventional solution. For the sake of simplicity, the following assumptions were made:

- All possible interactions will be assumed to exert only in region 3 of the whisker body to minimize estimation error due to high rotational stiffness. In practice, this hypothesis is biologically relevant to the fact that rats tend to make whisker-environment collisions near the tip to avoid the increasing spike rate of some cells in follicle when contact is close to the snout [104].
- Lateral slip at the contact location is neglected.
- Deformation of the whisker is within the measurable range and principle measuring plane of the strain gauge. Furthermore, the whisker curvature during the contact phase, which is equivalent to the deflection is assumed to be relatively small, so that the soft whisker body can be linearly analyzed.
- A single-point contact is solely considered.

4.1 Analytical Modelling

The analytical model was constructed to describe the correlation between tactile sensory feedback (*i.e.,* mechanical strain ε) in response to a specific contact condition (*i.e.,* contact force P and contact location) and geometrical features as well as material stiffness (as reflected by Young's modulus E). As suggested by Solomon *et al.* [105], the contact distance is generalized for any whisker by following equation: $Contact\ distance = a \times L_a$, where a is the contact ratio. I modeled rodent whiskers as truncated cones with a tapered angle α, base diameter D_2, tip diameter d_3 and the body length L_a. The rest of geometrical parameters, their amplitudes and notations required for analytical model are shown in Table 3.1. A great deals of evidence shows necessity of linearly-tapered structure for active tactile sensation of the rodent's whiskers compared to cylindrical whisker [106]: 1) Behavioral observations

show that conical whiskers can sweep across objects or texture with relative ease for a larger range of informative data, whereas cylindrical whiskers normally encounter with a globally high curvature of the body in such cases. It can be explained with help of classical beam theories which implies that, as a given force is applied at increasing location from the whisker base, the conical whisker will experience a larger bending angle than the cylindrical one thanks to the decrease of bending stiffness with a fourth order of the contact distance as described in my work [4]; 2) Secondly, since the rats use distance-dependent mechanics as a ruler to localize the contact location [107], thus, tapered structure will most likely have a higher measurement resolution than its opponent due to larger deviation in bending stiffness among cross-sections of the body.

In this section, the most important challenge is to figure out the correlation between the morphology of the whisker model and the medulla chamber is of particular interest with an intrinsic effect on the response of the sensor system. To achieve such goal, my model will be divided into two types: normal model and compensation model. While the former model is particularly for the whisker as its original geometry (*i.e.*, no air pressure initialization inside the chamber), the latter one investigate the transition of whisker morphology within a wide range of inner pressure Q and corresponding tactile feedback.

4.1.1 Normal model

When the whisker encounters an obstacle, the contact force exerted at a location along the body generates a bending moment as illustrated in Fig. 4.1(A). To my best knowledge, there are two fundamental approaches to build up the closely related mechanical model of the whisker in analytic forms. One is based on natural frequencies experienced by a whisker in the contact phase and the non-contact phase afterward, and the other relies on mechanical consequences (*e.g* torque, strain) generated from the bending moments across the whisker body. In this research, I particularly exploit the second approach. My preliminary analysis of the whisker as a homogeneous cantilever beam which performed active sensing strategy, especially

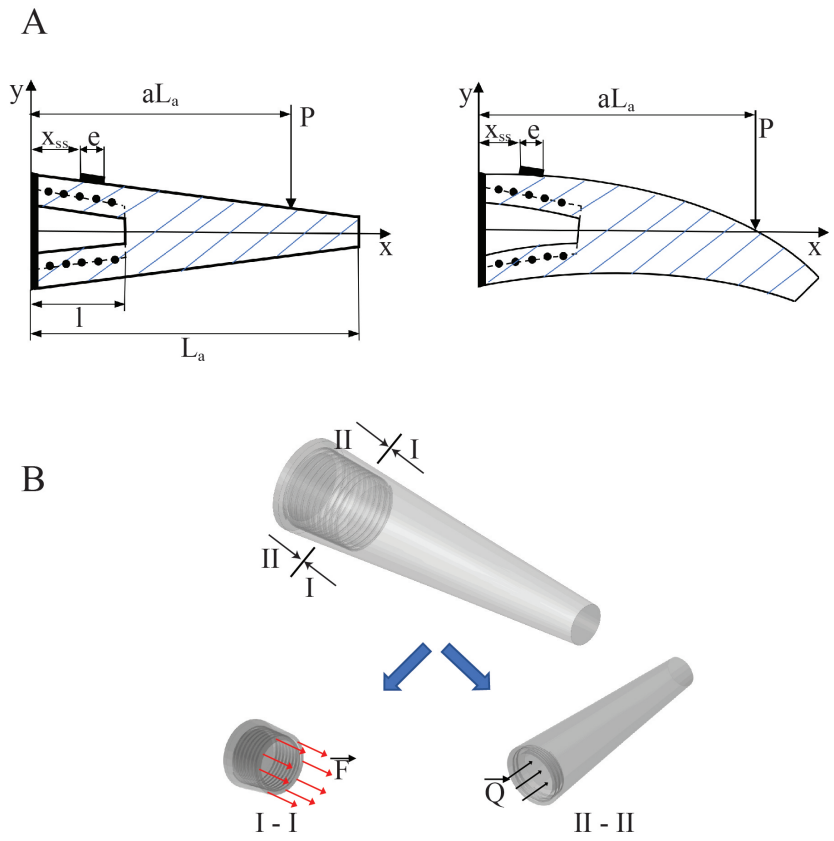

FIGURE 4.1: (A) When the whisker encounters the contact force P, then the change in form of the whisker and the mechanical signal generated in the strain gauge will be analyzed. (B) Schematic analyzing the internal force exerted in each cross-section along the length of region 2

equation (8) in [4], demonstrated that: the contact location a is linearly proportional to the ratio of strain signal ε and angular displacement θ. Hence, it is assumed that, instead of perceiving the absolute value of contact location a, the whisker sensor (whether both bio- and artificial whiskers) would rather sense the change rate in moment reflected by sensor feedback (here is mechanical strain) throughout the impact duration. See [4] for further analysis and validation for such concept.

For the construction of the normal mode, a similar procedure to find out the expression of $\frac{\varepsilon_n}{\delta_n}$, where ε_n is measured strain, δ_n is vertical body's deflection (in y-direction) measured at contact point δ_n (equivalent to angular displacement θ) and subscript n represents for normal mode, was executed. However, it should be noted that the proposed whisker shown in Fig. 4.1(A) has *inhomogeneous* structure because of the region 2 and the material stiffness of this region is expected to be variable upon morphological change. Therefore, classical beam theories such as

Euler-Bernoulli is not applicable for such whisker design. To tackle this problem, I made use of Castigliano's theorem [108] that relates to strain energy generated at each section of the whisker body. The main aim of this theorem is utilized for finding deflection δ_n of the whisker body based on strain energy stored in a soft structure during its deformation. Consider a small segment of the whisker length ds subjected to the bending moment M. The work done by the bending moment M to rotate a single cross section about another one with a small angle $d\phi$ will be stored in respective segment as strain energy dU:

$$dU = \frac{1}{2} M d\phi \tag{4.1}$$

$d\phi$ is calculated from:

$$d\phi = \frac{M}{EI} ds, \tag{4.2}$$

where EI is the flexural rigidity of the beam since it is a measure of bending resistance. Substituting $d\phi$ into equation 4.1, we get:

$$dU = \frac{1}{2} \frac{M^2}{EI} ds \tag{4.3}$$

Integration of equation 4.3 over the length L_a is taken to acquire full strain energy stored within each single region of the whisker body. Thus,

$$U = \sum W_i = \int_0^{aL_a} \frac{M(x)^2}{2E_i I_i(x)} dx, \tag{4.4}$$

where U denotes the strain energy, W_i is total work done by internal forces, $M(x)$ is bending moment internally generated in the whisker body, $I_i(x)$ and E_i $(i = 1, 2, 3)$ represent the second moment of cross-section area and Young's modulus for each region, respectively. $I_1(x)$, $I_3(x)$ and $M(x)$ are calculated as following equations:

$$I_1(x) = \frac{\pi {d_1}^4(x)}{64} = \frac{\pi {D_1}^4 (L_1 - x)^4}{64 {L_1}^4}, \tag{4.5}$$

$$I_3(x) = \frac{\pi {d_3}^4(x)}{64} = \frac{\pi}{64}\frac{{D_3}^4}{{L_3}^4}(L_1 - x + l)^4, \tag{4.6}$$

$$M(x) = P(aL_a - x), \tag{4.7}$$

where $d_i(x)$ is the diameter of the cross-sectional area at position x from the base. In regards to the term $I_2(x)$, the expression for second moment of section area for region 2 is supposed to be: $I_2(x) = \frac{\pi({d_2}^4(x) - {d_m}^4(x))}{64}$. Nevertheless, we realized that it is a challenge to solve Equation 4.4 with explicit output. To deal with this issue, an approximation approach by considering region 2 as a thin tube was applied. Specifically, let us consider the big end of region 2, we assumed that $D_2 \approx \overline{D_2} \approx D_m$, and $t = D_2 - D_m$. As a result, the formulation of second moment of area for this cross-section $I_2(x)$ is derived as follows:

$$I_2(x) = \frac{\pi}{64}\left(D_2^4 - D_m^4\right) = \frac{\pi}{64}\left(D_2^2 + D_m^2\right)(D_2 + D_m)(D_2 - D_m) \approx \frac{\pi}{8}\overline{D_2}^3 t \tag{4.8}$$

Then, the generalized formulation of $I_2(x)$ can be re-written as:

$$I_2(x) = \pi\frac{\overline{d_2}^3(x)}{8}t = \frac{\pi}{8}\frac{\overline{D_2}^3}{\overline{L_2}^3}\left(\overline{L_2} - x + c\right)^3 t. \tag{4.9}$$

According to Castigliano's second theorem [108], displacement $\delta_n(x)$ at the contact spot aL_a is equal to the partial derivative of the total strain energy with respect to contact force P:

$$\delta_n(aL_a) = \frac{\partial U}{\partial P} = \int_0^{aL_a} \frac{M(x)^2}{2E_i I_i(x)}dx \tag{4.10}$$

Expanding Eq. 4.10 yeilds:

$$\delta_n(aL_a) = \int_0^c \frac{M(x)}{E_1 I_1(x)}\frac{M(x)}{\partial P}dx + \int_c^l \frac{M(x)}{E_2 I_2(x)}\frac{M(x)}{\partial P}dx + \int_l^{aL_a} \frac{M(x)}{E_3 I_3(x)}\frac{M(x)}{\partial P}dx \tag{4.11}$$

While Young's modulus (E) for bio-whisker is an approximation at best, because this materials are typically anisotropic, heterogeneous, and nonuniform, in this research, the material used for my whisker sensor is isotropic throughout the body. Hence,

in regards to normal model (*i.e,* original shape), Young's modulus E_i for each region $i = 1 - 3$ of the whisker body is assumed to be constant and equal to each other $E_1 = E_2 = E_3 = E$. Then, substitute equations 4.5, 4.6, 4.7 and 4.9 into 4.11 we get:

$$\begin{aligned}\delta_n(aL_a) = \frac{64PL_1{}^4}{E\pi D_1{}^4}\int_0^c \frac{(aL_a-x)^2}{(L_1-x)^4}dx + \frac{8P\overline{L_2}^3}{E\pi t\overline{D_2}^3}\int_c^l \frac{(aL_a-x)^2}{\left(\overline{L_2}-x+c\right)^3}dx \\ + \frac{64PL_3{}^4}{E\pi D_3{}^4}\int_l^{aL_a} \frac{(aL_a-x)^2}{(L_3-x+l)^4}dx\end{aligned} \tag{4.12}$$

This equation can be shortened as:

$$\delta_n(aL_a) = \frac{P}{E\pi}\left(\delta_1 + \delta_2 + \delta_3\right), \tag{4.13}$$

where:

$$\begin{aligned}\delta_1 = \frac{64L_1{}^4}{D_1{}^4}\left[\frac{L_1{}^2+L_1aL_a-3L_1c+(aL_a)^2-3aL_ac+3c^2}{3(L_1-c)^3}\right. \\ \left. - \frac{L_1{}^2+L_1aL_a+(aL_a)^2}{3L_1{}^3}\right]\end{aligned} \tag{4.14}$$

$$\begin{aligned}\delta_2 = \frac{8\overline{L_2}^3}{t\overline{D_2}^3}\left[\ln\left(\frac{\overline{L_2}}{\overline{L_2}+c-l}\right) + \frac{\left(\overline{L_2}-aL_a+c\right)\left(3\overline{L_2}+aL_a-c\right)}{2\overline{L_2}^2}\right. \\ \left. - \frac{\left(\overline{L_2}-aL_a+c\right)\left(3\overline{L_2}+aL_a+3c-4l\right)}{2\left(\overline{L_2}+c-l\right)^2}\right]\end{aligned} \tag{4.15}$$

$$\delta_3 = \frac{64L_3{}^4}{D_3{}^4}\frac{(aL_a-l)^3}{3L_3{}^3(L_3-aL_a+l)} \tag{4.16}$$

Consequently, equation 4.16 denotes the dependence of contact deflection $\delta_n(aL_a)$ on the contact location aL_a, contact force P, geometrical parameters of the whisker's body and material characteristic E. In which, the determination of Young's modulus E for soft material is a difficult task due to highly nonlinear behaviors. In this circumstance, we attempted to describe the ratio of the strain generated in the outer layer, which is linearly proportional to contact force and material stiffness, to the curvature of the whisker.

In order to achieve that, Hooke's law is applied to construct the relationship between bending stress σ and the mechanical strain ε_n of region 2 measured by the sensing element. Even though Hooke's law is the law of elasticity indicating that the strain ε (deformation) of an elastic object or material is proportional to the stress σ

applied to it, however, in this case, if the curvature of the whisker body (equivalent to whisker's deflection $\delta(x)$ is relatively small, it can be assumed that the linearity of the soft body will be held. Evidence for such assumption is presented in section 5.2.4.

$$\varepsilon_n = \frac{\sigma}{E} = \frac{yM(x)}{EI_2(x)}, \tag{4.17}$$

where y is radius of the outermost layer of the chamber's wall where the strain is measured:

$$y = \frac{1}{2}\left[\frac{\overline{D_2}}{\overline{L_2}}\left(\overline{L_2} - x + c\right) + t\right]. \tag{4.18}$$

Let us substitute y, $M(x)$ and $I_2(x)$ into Eq. 4.17 to get the final form:

$$\varepsilon_n = \frac{4P\overline{L_2}^3}{E\pi t\overline{D_2}^3} \int_{x_{ss}}^{x_{ss}+e} \frac{\left[\frac{\overline{D_2}}{\overline{L_2}}\left(\overline{L_2} - x + c\right) + t\right](aL_a - x)}{\left(\overline{L_2} - x + c\right)^3} dx = \frac{4P\overline{L_2}^3}{E\pi t\overline{D_2}^3}\kappa, \tag{4.19}$$

where, x_{ss} and e are location and measuring grid length of the strain gauge as shown in Fig. 4.1(A), and:

$$\kappa = \int_{x_{ss}}^{x_{ss}+e} \frac{\left[\frac{\overline{D_2}}{\overline{L_2}}\left(\overline{L_2} - x + c\right) + t\right](aL_a - x)}{\left(\overline{L_2} - x + c\right)^3} dx \tag{4.20}$$

Combining equation 4.13 and 4.19 yields:

$$\frac{\varepsilon_n}{\delta_n(aL_a)} = \frac{4{L_2}^3}{t{D_2}^3}\frac{\kappa}{\delta_1 + \delta_2 + \delta_3} = f_n(aL_a) \tag{4.21}$$

Then, the mechanical strain measured by strain gauge can be estimated as:

$$\Leftrightarrow \varepsilon_n = f_n(aL_a) \times \delta_n(aL_a) \tag{4.22}$$

Equations 4.21 and 4.22 imply that the tactile signal in the form of mechanical strain relies on the geometry, the location of the stimuli source and the deformation of the whisker (candidates for contact force P and Young's modulus E). Validation results

of the above model will be discussed later. The analytical model offered in this section is served as an efficient method to not only characterize the inhomogeneous geometry of my whisker sensor but also a typical morphological computation process to incorporate the strain gauge's output ε_n with the change of whisker curvature (reflected by whisker deflection $\delta_n(aL_a)$ for tactile information (contact location aL_a) acquisition. To enable resilience, variation of sensor's feedback corresponding to the change of chamber's inner pressure Q (*i.e.*, whisker's morphology) will be studied.

4.1.2 Compensation model

The proposed whisker is able to employ the compensation mode when it was trimmed or broken along its body. In this mode, the air pressure inside the medulla chamber is varied, bringing change in chamber morphology, which results in an adjustable output of the strain gauge (attached to the chamber outside wall). For the accomplishment of this purpose, the analytical model must predict outputs of the sensing element (strain gauge) for different dimensions of chamber morphology (see Fig. 4.2). At first, it is necessary to picture how the whisker body looks like when the inner pressure Q of the chamber is varied. It is obvious when all the change of the morphology will occur on the region 2 (the chamber region). In more detail, thanks to two reinforcement fibers wrapped around, when the value of Q goes upward the chamber region is supposed to not be expanded in x- and y-axis but in axial z-direction where has no blocker. Moreover, the thickness t of the chamber wall is expected to be reduced as a consequence from the extension of the length L_a. Since it is difficult to precisely measure the variation of the thickness t within air pressurization process, in this work, I tackle this challenge with an approximation approach relying on classical theory for material mechanics. The detail will be explained in the rest of this section.

Let us introduce variable $\Delta l(x)$ representing the axial deformation at any cross-sectional area of the chamber when the inner pressure changes. With this notation, $\Delta l(l)$ is the total axial deformation of the chamber, which is directly measured by a laser sensor (discussed in the experiment section). The ultimate aim is to obtain the

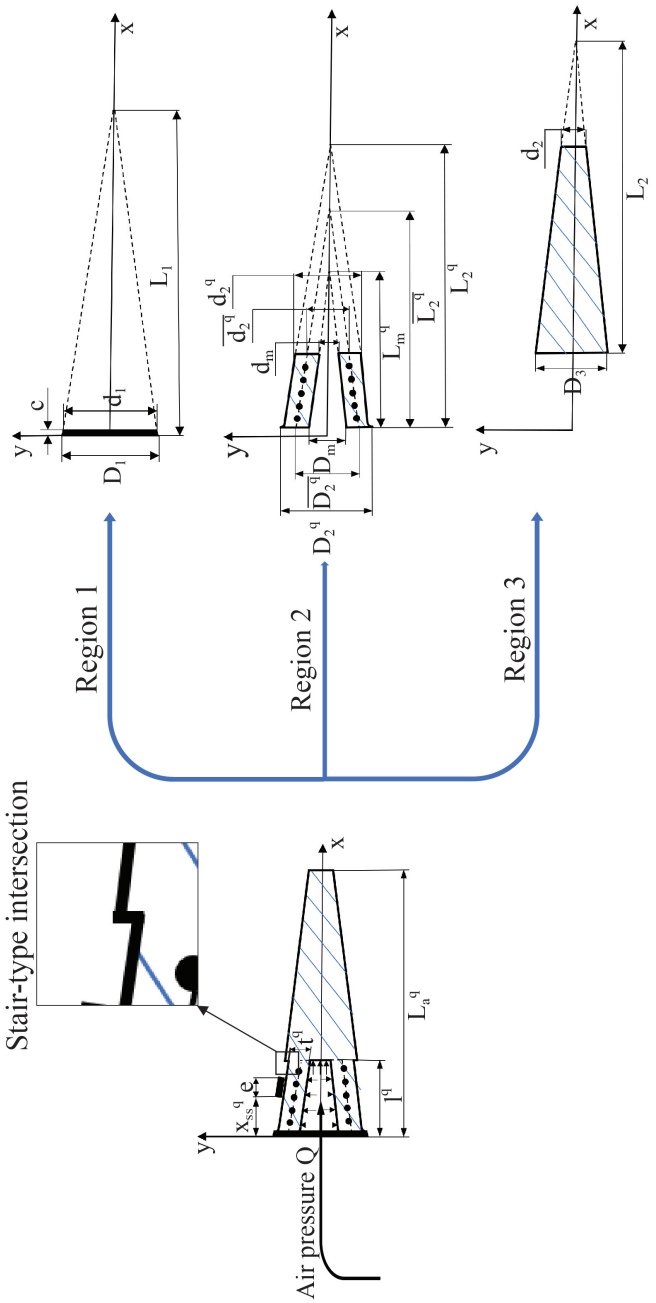

FIGURE 4.2: Transformation of the whisker body after air compression inside the chamber. Note that, the structure of the whisker after air pressurization process and most of the changed variables belong to the region 2. See Table. 4.1 for details.

new configuration of the whisker model after pressurization with respect to $\Delta l(l)$ by updating the expression of equations 4.14 - 4.16. In which, the extension length $\Delta l(x)$ and the variation of the chamber wall's thickness $t^q(x)$ of each cross-section area of region 2 are the most of interest. For ease of modeling, several assumptions were made as follows:

- The whisker remains straight throughout the air pressurization of the chamber.
- Possible deformation upon pressurization of the chamber was assumed to be in region 2. As a result, the morphology region 1 and region 3 remains unchanged under any pressure value. Extension in the length of region 2 may only be caused by pressure force Q (represented by black arrows in Fig. 4.1(B)) in the x-direction because of reinforced fibers.
- The diameter at each end of the chamber does not change during air pressurization. Region 2, in general, and the chamber, in particular, remain linear-tapered upon pressurization.
- The intersection of region 2 and region 3 was stair-like type as illustrated in Fig. 4.2(B), instead of a fillet shoulder.
- Thickness t^q, corresponding to the pressure Q in the chamber, was considered to remain a linear distribution across region 2. Thus, t^q is calculated as the average value of thickness at two arbitrary cross-sectional areas near two ends of region 2 (we chose $t^q(2.5)$ and $t^q(l)$). We estimated the approximation error rate was about 7.3% according to the highest examined pressure (discussed further in the experiment section).

The estimation equation for $t^q(x)$ is derived by using the ratio of transverse strain ε_t (change in radius of the chamber wall) to longitudinal strain ε_l (change in whisker length) which is simply represented by the Poisson's ratio coefficient v, and calculated as follows:

$$v = \frac{\varepsilon_t}{\varepsilon_l} \tag{4.23}$$

where ε_t and ε_l can be calculated as follow:

$$\varepsilon_t = \frac{\Delta R_2(x)}{R_2(x)} \tag{4.24}$$

$$\varepsilon_l = \frac{\Delta l(l)}{l - c} \tag{4.25}$$

Then, the equation 4.23 becomes:

$$v = \frac{\frac{\Delta R_2(x)}{R_2(x)}}{\frac{\Delta l(l)}{l-c}} \tag{4.26}$$

From this equation, the change in radius $\Delta R_2(x)$ or thickness $\Delta t(x)$ of the region 2 and the resulting thickness $t^q(x)$ are as:

$$\Delta R_2(x) = \Delta t(x) = \frac{v \Delta l(l) R_2(x)}{l - c} \tag{4.27}$$

$$t^q(x) = t - \Delta t(x) \tag{4.28}$$

According the fifth assumption listed above, the equation for calculating the finally estimated value for thickness t^q in response to inner pressure Q is as:

$$t^q = \frac{t^q(2.5) + t^q(l)}{2}, \tag{4.29}$$

where, $t^q(2.5)$ and $t^q(l)$ are thickness of the cross-section at $x = 2.5$ mm and $x = l$, respectively. These equations 4.27 - 4.29 indicate that as long as the change in chamber length is known, we can directly estimate the variation of the chamber in terms of the outer surface's radius to fully emulate the geometry of the whisker with different stages of pressure modulation. Note that Poisson's ratio of a typical silicone-rubber material was estimated in a tension experiment as approximately equal to 0.5 [109], in this study, we chose the value of 0.49. The next challenge is to measure the change in length for each cross sectional area of the chamber region with respect to the inner pressure Q. Elastic mechanic theory was applied to derive

TABLE 4.1: Re-identification of whisker's structure

Original Param.	Param. after pressurization
$\overline{D_2}$	$\overline{{D_2}^q} = D_m + t^q$
$\overline{d_2}$	$\overline{{d_2}^q} = d_m + t^q$
$\overline{L_2}$	$\overline{{L_2}^q} = \frac{\overline{{D_2}^q}(l^q - c)}{\overline{{D_2}^q} - \overline{{d_2}^q}}$
l	$l^q = l + \Delta l(l)$
L_a	${L_a}^q = L_a + \Delta l(l)$
x_{ss}	${x_{ss}}^q = x_{ss} + \Delta l(x_{ss})$

the axial deformation $\Delta l(x)$ by the expression below:

$$\Delta l(x) = \frac{F}{E_2} \int_c^x \frac{1}{A(x)} dx, \tag{4.30}$$

in which, F is an internal force generated on the cross-section area at x (indicated by red arrows in Fig. 4.1(B)) with area $A(x)$. It is clearly that the internal force F is equal to the total pressure exerted on the chamber's small end:

$$F = Q\frac{\pi {d_m}^2}{4}, \tag{4.31}$$

and the area $A(x)$ is computed by:

$$A(x) = \frac{\pi {d_2}^2(x)}{4} - \frac{\pi {d_m}^2(x)}{4} = \frac{\pi {D_2}^2}{4{L_2}^2}(L_2 - x + c)^2 - \frac{\pi {D_m}^2}{4{L_m}^2}(L_m - x + c)^2 \tag{4.32}$$

Re-writing Equation 4.30, we obtain followed relation:

$$\Delta l(x) = \frac{Q{d_m}^2{L_2}^2{L_m}^2}{E_2} \int_c^x \frac{1}{{D_2}^2{L_m}^2(L_2 - x + c)^2 - {D_m}^2{L_2}^2(L_m - x + c)^2}. \tag{4.33}$$

From equation 4.33, the relation between the extension length of each cross-section $\Delta l(x)$ and the total change in length $\Delta l(l)$ can be derived as follow:

$$\Delta l(x) = \frac{\int_c^x \frac{1}{{D_2}^2{L_m}^2(L_2 - x + c)^2 - {D_m}^2{L_2}^2(L_m - x + c)^2}}{\int_c^l \frac{1}{{D_2}^2{L_m}^2(L_2 - x + c)^2 - {D_m}^2{L_2}^2(L_m - x + c)^2}} \Delta l(l). \tag{4.34}$$

Consequently, Table 4.1 shows all changed parameters for re-constructing the original analytical model introduced in the previous section, and their new approximation equations. In short, if the extension length $\Delta l(x)$ corresponding to a specific value of inner pressure Q (which can be easily measured by laser sensor) can be detected, the whole new configuration of the whisker is directly re-constructed through equations 4.27 - 4.29, 4.33, 4.34 and those in table 4.1. With new configuration as specified above, we need to come up with the new equation for whisker deflection $\delta_c(aL_a)$ by updating equations 4.14-4.16 as follow:

$$\delta_1^q = \frac{64{L_1}^4}{{D_1}^4}\left[\frac{{L_1}^2+L_1aL_a^q-3L_1c+(aL_a^q)^2-3aL_a^qc+3c^2}{3(L_1-c)^3} - \frac{{L_1}^2+L_1aL_a^q+(aL_a^q)^2}{3{L_1}^3}\right] \tag{4.35}$$

$$\delta_2^q = \frac{8\overline{L_2^q}^3}{k_2t^qD_2^{q3}}\left[\ln\left(\frac{\overline{L_2^q}}{\overline{L_2^q}+c-l^q}\right) + \frac{\left(\overline{L_2^q}-aL_a^q+c\right)\left(3\overline{L_2^q}+aL_a^q-c\right)}{2\overline{L_2^q}^2} - \frac{\left(\overline{L_2^q}-aL_a^q+c\right)\left(3\overline{L_2^q}+aL_a^q+3c-4l^q\right)}{2\left(\overline{L_2^q}+c-l^q\right)^2}\right] \tag{4.36}$$

$$\delta_3^q = \frac{64{L_3}^4}{{D_3}^4}\frac{\left(aL_a^q-l^q\right)^3}{3{L_3}^3\left(L_3-aL_a^q+l^q\right)} \tag{4.37}$$

Equation 4.20 also need to be remade. However, as discussed in *section* 3.4.1, Young's modulus of region 2 (E_2) is expected to vary corresponding to the change in chamber morphology with pressurization. Hence, there should be a proper way to express the changeability of E_2 in Eq. 4.20. Hereafter, this variation is described by variable k_2 with the following relation: $E_2^q = k_2E_2 = k_2E$. Then, equation 4.20 becomes:

$$\varepsilon_c = \frac{4P\overline{L_2^q}^3}{k_2E\pi t^qD_2^{q3}}\int_{x_{ss}^q}^{x_{ss}^q+e}\frac{\left[\frac{D_2^q}{\overline{L_2^q}}\left(\overline{L_2^q}-x+c\right)+t^q\right]\left(aL_a^q-x\right)}{\left(\overline{L_2^q}-x+c\right)^3}dx = \frac{4P\overline{L_2^q}^3}{k_2E\pi t^qD_2^{q3}}\kappa^q, \tag{4.38}$$

where:

$$\kappa^q = \int_{x_{ss}^q}^{x_{ss}^q+e}\frac{\left[\frac{D_2^q}{\overline{L_2^q}}\left(\overline{L_2^q}-x+c\right)+t^q\right]\left(aL_a^q-x\right)}{\left(\overline{L_2^q}-x+c\right)^3}dx \tag{4.39}$$

Finally, the final equation to compute the numerical strain in the compensation mode is:

$$\frac{\varepsilon_c}{\delta(aL_a^q)} = \frac{4\overline{L_2^q}^3}{kt^q\overline{D_2^q}^3}\frac{\kappa^q}{\delta_1^q+\delta_2^q+\delta_3^q} = f_c(aL_a^q) \Leftrightarrow \varepsilon_c = f_c(aL_a^q)\times\delta(aL_a^q). \tag{4.40}$$

In summary, equation 4.40 takes into account the variation of both material stiffness E and geometrical parameters (as listed in table 4.1) in response to the change of inner pressure Q to approximately estimate the sensor feedback with the same stimuli condition (*i.e.,* same contact ratio a). In addition to equation 4.22, it gives a hint to come up with an compensation strategy and an efficient tool to predict the desired morphology state that satisfies such strategy. The experimental procedure to comprehensively evaluate feasibility and reliability of the predicted compensatory actions based on above analytical models will be presented in the next chapter.

5 Verification on Tactile Resilience based on Variable Morphology

5.1 Compensation strategy

Although the concept of "*compensation*" in nature varies among species, it is worthwhile investigating this function in a robotic device. The compensation strategy for my whisker sensor is particularly applicable for the contact localization ability in which the ratio of the absolute value of radial contact distance and the body length as presented by the parameter a is desired tactile information. Based on this assumption, we propose a compensation concept: with the same contact ratio a, the tactile information perceived by intact whiskers in an array (either longer or shorter) is supposed to be as close to the broken one as possible. At the same time, for a sole whisker that requires a self-calibration procedure, compensation will be activated to obtain updated sensitivity (in the broken case) that is close to the original one. These cases will be discussed and experimentally validated in the next section. Let me mathematically explore the above strategy by assigning the whisker before and after cut off as the *origin* and *compensator*, resspectively. Then, according to the compensation concept, the tactile perception of the *compensator* is expected to be regained as close as that of the *origin* (*i.e.*, ε_{c1} and ε_{c2}, respectively), thus:

$$\varepsilon_{c1} = \varepsilon_{c2} \tag{5.1}$$

Hence, from analytical model for the compensation mode in section 4.1.2, in order to obtain at the similar response of the strain gauge for the *compensator* and *target*, a suitable configuration of the whisker that satisfied the concept of compensation was

estimated by the following equation:

$$f_c(aL_{a1}^q) \times \delta_c(aL_{a1}^q) = f_c(aL_{a2}^q) \times \delta_c(aL_{a2}^q) \tag{5.2}$$

By solving this equation, we can identify the proper morphology (or inner pressure Q) to recover the loss sensitivity due to damaged structure. Note that this compensation strategy would not always be applicable for other tactile sensibilities such as texture discrimination or contour extraction. Depend on the requirements and contribution of the whisker body on a specific task, suitable compensatory behaviors can be established. In future works, I plan to explore how MorphCom is beneficial to other whisker's sensing abilities and develop a comprehensive contingency plan for self-recovery against different types and levels of damages.

5.2 Experiment and Validation Results

5.2.1 Experiment setup

To evaluate the reliability of the analytical model and compensation strategy in the self-maintenance for the proposed whisker's sensibility against a range of damages, an experimental setup was design as illustrated in Fig. 5.1. It comprised an artificial whisker and an obstacle (with a rigid, sharp edge), fixed onto two linear motorized stages (PG750-L05AG-UA, Suruga Seiki, Japan) perpendicular to each other as shown in Fig. 5.1(B). They were driven precisely at a resolution of $2\,\mu m$ by a stepping motor controller (DS102, Suruga Seiki, Japan). The strain output was measured by an instrument EDX-15A connected with a bridge box UI-54A-120 and sent to the computer for post-processing by data acquisition program DCS-100A (these devices are from Kyowa, Electronic Instrument Co., Japan). The sampling rate for the data recording system was set at 100 Hz. To acquire information on pressure value and axial deformation of the chamber in the compensation mode, a digital pressure sensor ISE20A-R-M (SMC Co., Japan) and an analog laser sensor IL-030

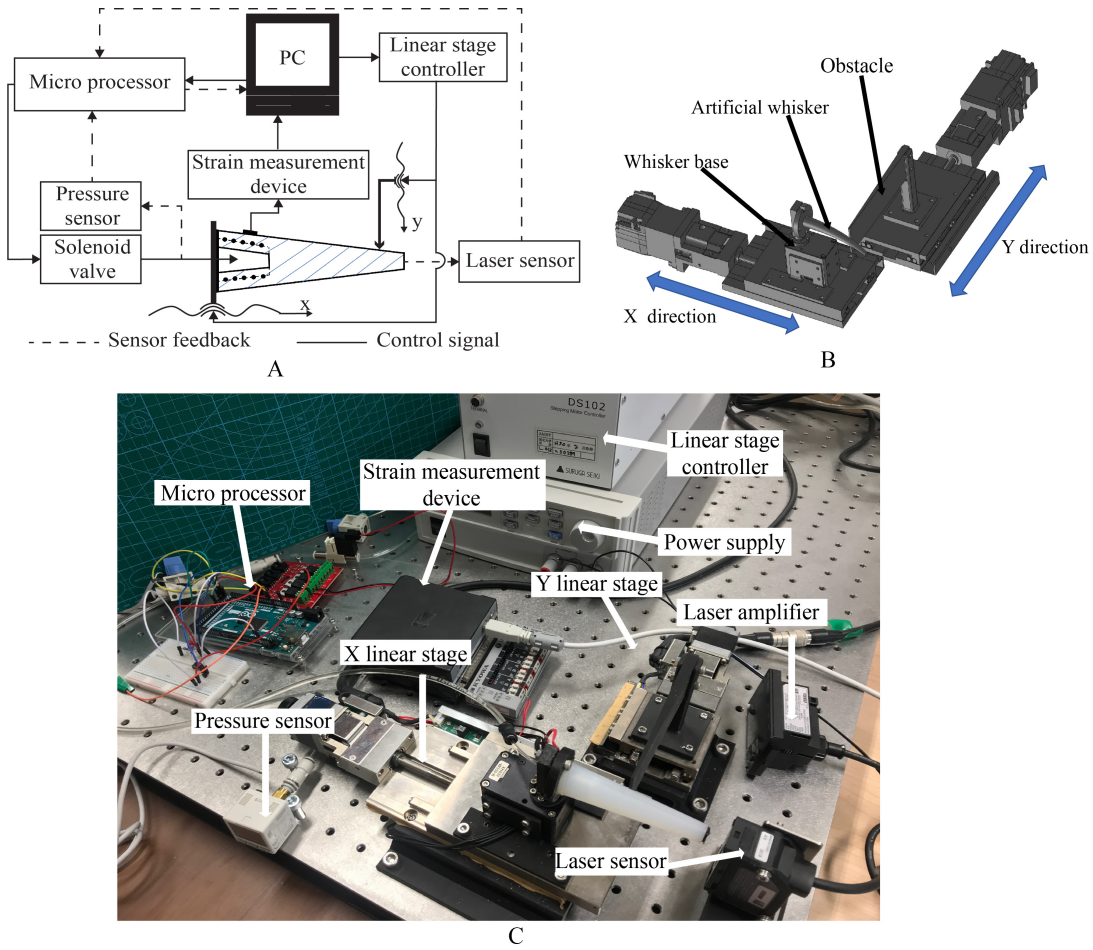

FIGURE 5.1: Experimental setup: (A) Block diagram of the experimental setup, in which, (B) a linear stage, in x-direction, controls the contact distance, whereas, the one in y-direction produces the contact deflection as desired. (C) Experimental setup includes the data acquisition system, sensors (pressure sensor and distance sensor) and power supply.

integrated with amplifier IL-1050 (KEYENCE Co., Japan) were employed. A microprocessor (Arduino MEGA 2560) is responsible for controlling a solenoid valve to ensure a stable amount of air inside the chamber during testing. The sensor head of the laser was fixed in a mounting bracket so that the laser light from the transmitter was coincident to the centerline of the whisker. Moreover, to ensure the laser light absorption or excessive reflection did not affect the measurement, a black layer of silicone covered the free end of the whisker. All analog signals from these devices were recorded by a microprocessor and transmitted to the computer. Finally, Matlab R2019a was used for data analysis. In this research, we examined two prototypes of artificial whisker with equivalent structure parameters as listed in Table 3.1 but different length: $L_{a1} = 70\,\text{mm}$ and $L_{a2} = 65\,\text{mm}$, to represent an intact and

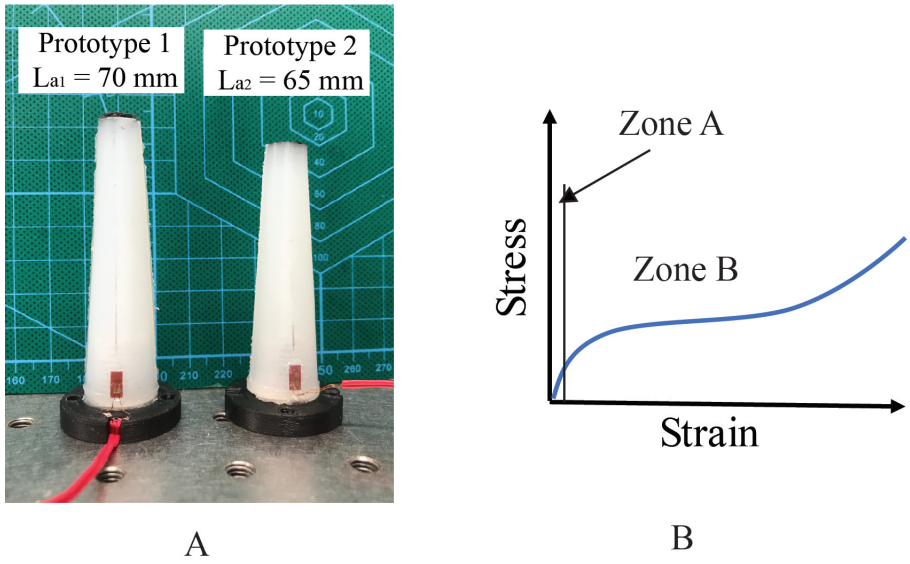

FIGURE 5.2: (A)Tested prototypes 1 and 2 have the identical dimensions as listed in Table 3.1 except the actual length $L_{a1} = 70\,\text{mm}$ and $L_{a2} = 65\,\text{mm}$, respectively. (B) The typical stress-strain curve for silicon-rubber material

trimmed whisker (see Fig. 5.2(A)). The X linear stage was used to ensure the contact was exerted at the desired distance from the base, whereas the Y linear stage drove the obstacle back and forth for expected deflection with velocity $v = 0.5\,\text{mm/s}$. By moving stimuli source toward the whisker, it means that the passive sensing strategy has been applied since I wanted to simultaneously measure the transition in body length by using laser sensor, so that the whole experiment can be operated in a complete automatic fashion. It should be noticed that the proposed method for recovery function also works for whiskers those exploit active sensation.

5.2.2 Procedure for Young's modulus estimation

Thanks to the softness of silicon-rubber, the morphology of a soft structure is actively changed by the integration of a simple pneumatic actuator. It is worth noting that the response of a soft material to stress highly depends on the applied strain, and the stress-strain relationship may vary significantly as illustrated in Fig. 5.2(B). More importantly, the linear theory of elasticity is only valid for a very small deformation that corresponds to zone A of the stress-strain curve, which obeys Hooke's law, and is characterized by a constant Young's modulus. As stress increases slowly with high deformation in zone B, it is expected that the applied Young's modulus in

this region reduces, which may result in a change of the soft body morphology. This characteristic is applied in our method to achieve the changeable morphology of an artificial whisker.

Generally, the measurement methods for Young's modulus E can be done by constructing a strain-stress curve through a standardized tensile test or three-point bending test. However, these methods are valid for any homogeneous, isotropic materials like metals, while methods for nonlinear elastic material are not well established. Moreover, a number of specialized test procedures, instruments are required making it difficult to carry them out in a cost-effective way. To tackle this bottleneck, I proposed a measurement method to approximately estimate the trend of Young's modulus E that is reflected by strain gauge output upon the variation of the whisker body. More specifically, in this section, a static test to observe the variation of the material property of region 2 (E_2) under increased air pressure in the chamber was conducted. We evaluated the response of the strain gauge generated by expansion in the x-direction of the chamber to compute the value of k ($E_2^q = kE_2 = kE$) in equation 4.40. Note that sensitivity adjustment only relied on the change in morphology of the chamber, while a typical response of an individual sensing element did not remarkably change. At first, the signal of strain gauge ε_a generated by axial stress during air pressurization can be derived as follows:

$$\varepsilon_a = \frac{\Delta l_{ss}}{e}, \tag{5.3}$$

where ε_a is the measured strain and Δl_{ss} is the total change in length observed in the section area that the gauge length e cover up and can be calculated by using Eq. 4.33. Consequently, the equation 5.3 becomes:

$$\frac{Q{d_m}^2{L_2}^2{L_m}^2}{eE_2^q} \int_{x_{ss}}^{x_{ss}+e} \frac{1}{{D_{2o}}^2{L_m}^2(L_{2o}-x+c)^2 - {D_m}^2{L_2}^2(L_m-x+c)^2} \tag{5.4}$$

Then, Young's modulus of region 2 is computed by regressing strain output ε_a and pressure Q:

$$E_2^q = \frac{Q{d_m}^2{L_2}^2{L_m}^2}{e\varepsilon_a} \int_{x_{ss}}^{x_{ss}+e} \frac{1}{{D_{2o}}^2{L_m}^2(L_{2o}-x+c)^2 - {D_m}^2{L_2}^2(L_m-x+c)^2}. \tag{5.5}$$

Then, a series of experiments with the setup in Fig. 5.1 in order to pre-calculate E using Eq. 5.6 corresponding to a wide range of inner pressure Q were conducted. We regulated pressure Q within the range $0.002 \div 0.2\,\text{MPa}$ and repeatedly recorded the response of the strain gauge five times. The examined range of Q is decided to minimize the error of the estimation method for Young's modulus (see section 5.3.3 for detailed explanation), or permanently ruin the original structure. The recorded strain signal are plotted in Fig. 5.3(A). Output in $\mu m/m$ from the measuring device is converted by the equation:

$$\varepsilon_a = \frac{\varepsilon_{read}}{GF} \times 10^{-3} \tag{5.6}$$

where ε_{read} is read from the software and GF stands for the gauge factor provided by the vendor ($GF = 2.21 \pm 1\%$). Then, by substituting the mean values of recorded strain for each trial into Equation 5.6, we can derive the variation of E_2^q in Fig. 5.3(B). Fig. 5.3(B) witnesses a significant decreasing trend of Young's modulus corresponding to the increase of pressure inside the chamber as expected. Note that at very low chamber pressures of the chamber ($Q_1 = 0.002\,\text{MPa}$ and $Q_2 = 0.005\,\text{MPa}$), *i.e.*, with small deformations of the chamber, the value of E_2^q slightly falls which reminds us about the early stage of the strain-stress curve (zone A in Fig. 5.2(B)). Thus, hereafter, the value of Young's modulus corresponding to pressure value $Q_1 = 0.002\,\text{MPa}$ is set as the primitive value for the whole whisker at its original state. As a result, the value of k_2, then, can be directly calculated and plotted in Fig. 5.3(C) (note that $E_2^q = kE_2$). Finally, for application to the entire examined range of pressure, we used

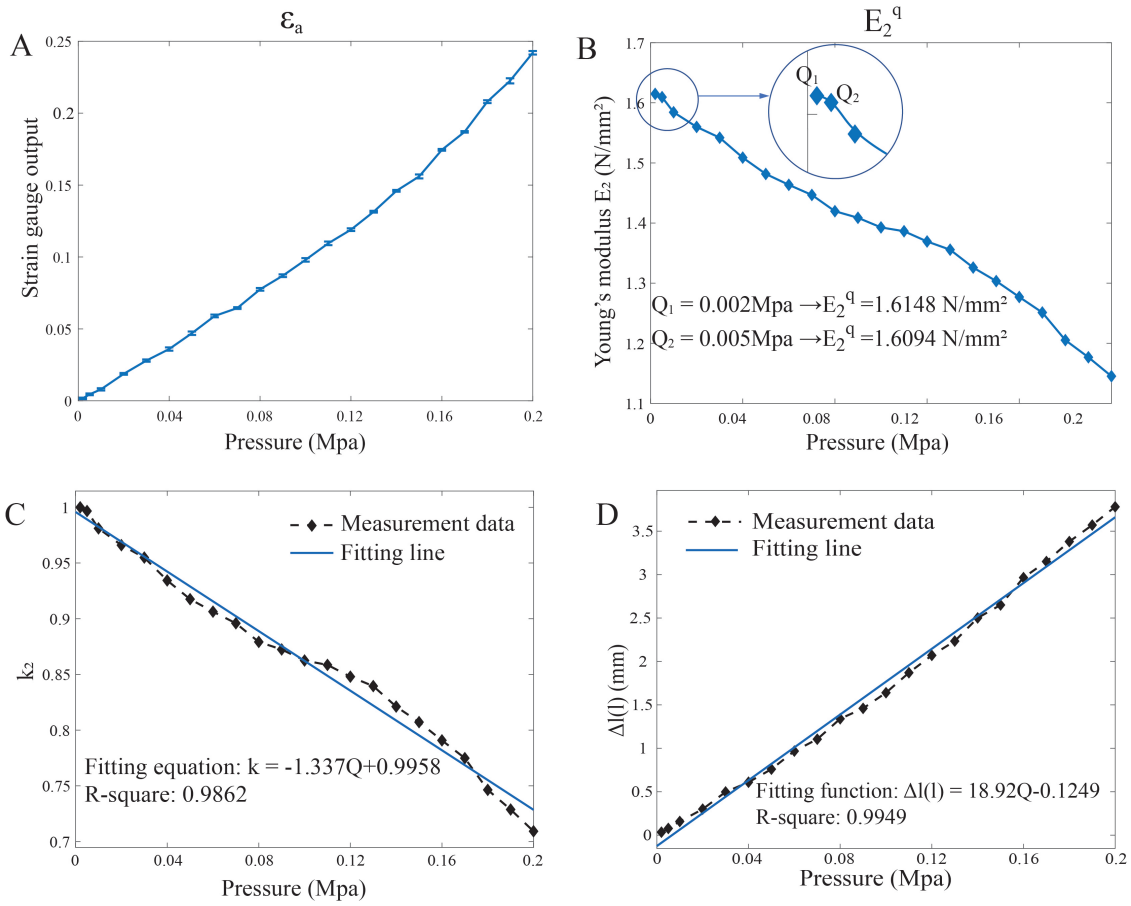

FIGURE 5.3: Variation of material characteristics with respect to a range of pressure Q: (A) Sensor signals with standard deviation due to the axial elongation of the chamber were recorded in five times. (B) Young's modulus E_2^q estimation result in which, at low pressures, E_2^q shows insignificant variability. (C) The corresponding value of k_2 and the approximate function depends on the pressure Q. (D) Deformation of the whisker model in x-direction measured by the distance sensor

Matlab's curve fitting tool to find out the best-fit equation as follow:

$$k = -1.337 \times Q + 0.9958 \tag{5.7}$$

In conclusion, the results prove our concept that variation of the inner pressure would lead to morphological change (including softness and shape) of the whisker, as well as the response of the strain gauge. This was exploited to implement the broken whisker compensation strategy presented in section 5.1.

5.2.3 Validation of the analytical model

In this section, we report an experimental method for validation of the proposed analytical model for two modes (normal and compensation) and demonstration of the feasibility of using the model to predict an appropriate chamber morphology for the compensation process (of a broken whisker). Measurement of the strain gauge response with different value of pressure in the chamber ($Q = 0$ MPa for normal mode and $Q = [0,\ 0.002,\ 0.05,\ 0.1,\ 0.15,\ 0.2]$ MPa for compensation mode) were recorded, then compared to the numerical ones derived from the analytical model. All experiments were conducted within the strain gauge's sensing range. Before each trial, change in length $\Delta l(l)$ corresponding to an input air pressure of the chamber was measured by a laser sensor. Figure 5.3(D) shows the obtained result and the fitting function of $\Delta l(l)$ w.r.t Q.

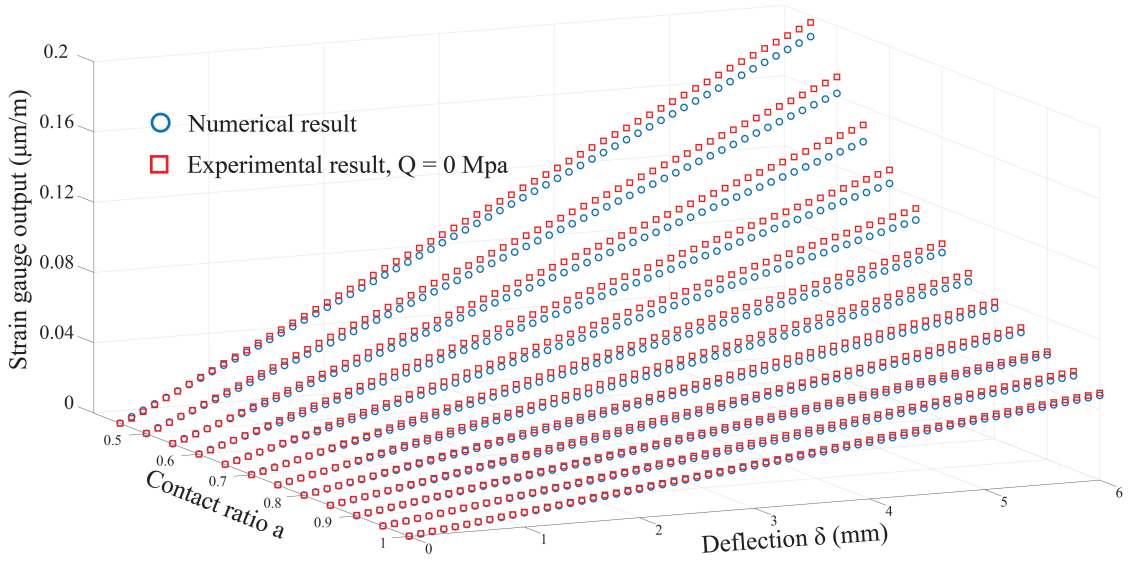

FIGURE 5.4: Numerical solution versus experimental result in normal mode ($Q = 0$ MPa)

First, we validated the proposed model for the normal mode ($Q = 0$) using prototype 1 (original whisker length $L_{a1} = 70$ mm as illustrated in Fig. 5.2(A)). In this experiment, X and Y linear stages drove the whisker and the obstacle, respectively, to make contact at different contact rates ranging from $a = 0.45 \div 1$ in steps of 0.05 along the body of the whisker, and in a range of deflection $\delta(aL_a) = 0 \div 6$ mm.

Measurement of strain gauge output was synchronized with contact onset. The investigated ranges of contact location and deflection were chosen based on the observation that rodents tend to make subsequent touches (after an unexpected collision) in locations far from the base (along the whisker), as the whisker sweeps over an obstacle without requiring large deflection [110]. Furthermore, any measuring inaccuracy due to exceeding the sensor threshold could be prevented. The results are analyzed and plotted in Fig .5.4. The output of the strain gauge, shown in Fig. 5.4, has a quite small variance in amplitude in comparison with the numerical results. Figure 5.5 shows average differences (in magnitude and rate) between numerical and experimental results with respect to each deflection δ (Fig. 5.5A, B) and contact ratio a (Fig. 5.5C, D) calculated using equation 5.10. At the first glance, we can see the increase of deviation magnitude as the increase of deflection δ and the decrease of contact ratio a. These trends are equivalent to higher internal bending stress which will cease the linearity of silicon rubber (zone B in Fig. **??**). However, let review these gaps as mean ratios (in percent) with respect to measured strain signal ϵ_{exp} that only fluctuate around the range of 4 - 7 % (for all cases) even at critical values (high deflection δ or small contact ratio a). These findings demonstrate the feasibility of the normal model.

$$\text{Deviation magnitude} = \sum_{i}^{61} \left| \varepsilon_n^j - \varepsilon_{\text{exp}}^j \right| \text{ and } \sum_{j}^{12} \left| \varepsilon_n^i - \varepsilon_{\text{exp}}^i \right| \tag{5.8}$$

$$\text{Deviation rate} = \sum_{i}^{61} \left| \frac{\varepsilon_n^j - \varepsilon_{\text{exp}}^j}{\varepsilon_{\text{exp}}^j} \right| \times 100 \text{and} \sum_{j}^{12} \left| \frac{\varepsilon_n^i - \varepsilon_{\text{exp}}^i}{\varepsilon_{\text{exp}}^i} \right| \times 100 \tag{5.9}$$

where: i and j are measuring steps of deflection δ and contact ratio a, respectively.

Regarding the model in the compensation mode, a similar procedure was applied with different values of compressed air Q in the chamber, and the results are presented for the entire range of examined contact location and deflection (see Fig. 5.6). At first glance, both graphs share a similar trend compared to the normal mode results in Fig. 5.4, which highlights an increase in strain amplitude with pressure Q increase under the same interaction conditions (location and deflection). It can

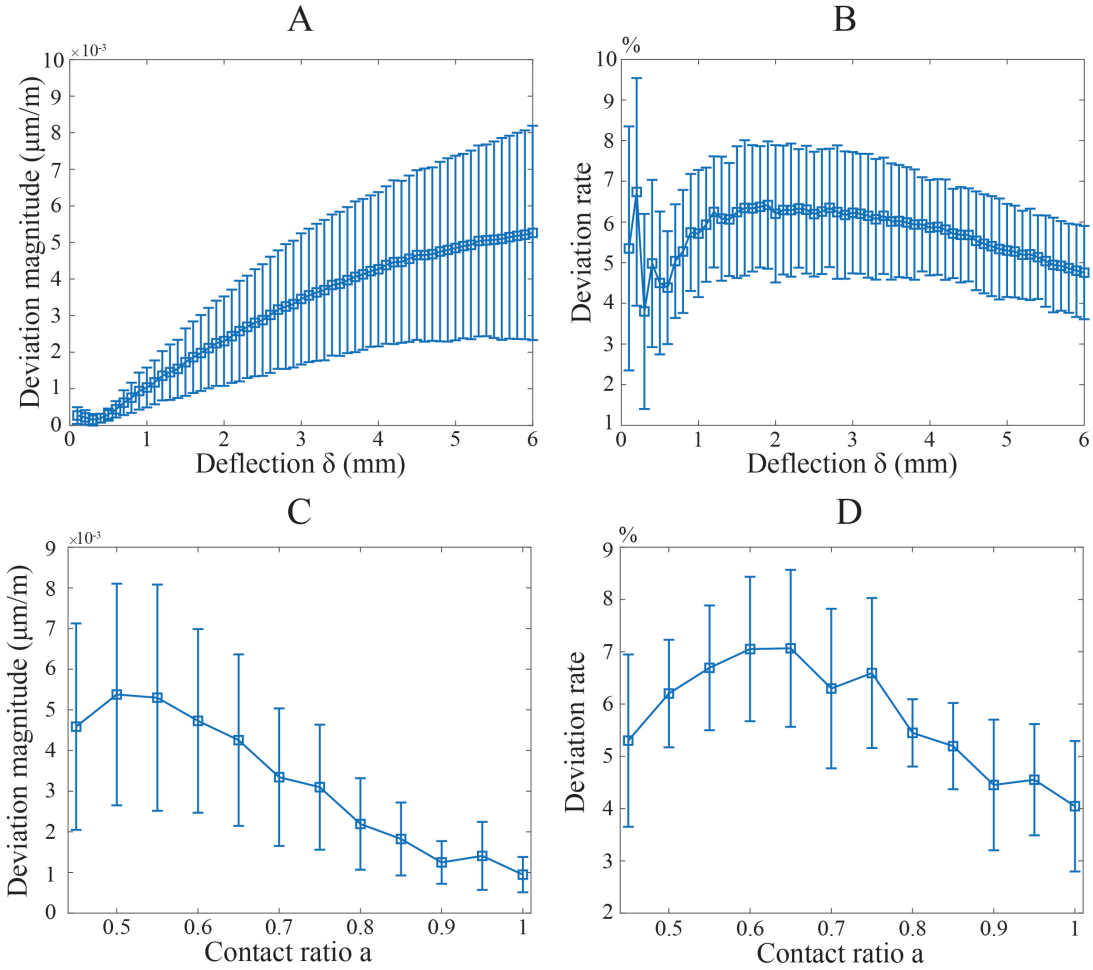

FIGURE 5.5: Average differences (in (A)(C) magnitude and (B)(D) rate) between experimental and numerical results estimated by normal model (Eq. 4.22) with respect to each deflection δ (A)(B) and contact ratio a (C)(D) calculated using equation 5.10

be explained by Fig. 5.3(B) where the value of E_2^q reveals a rapid decrease at high value of compressed air in the chamber, resulting in larger mechanical strain on the chamber's wall. Results in Fig. 5.6 also implies that, by variation of inner pressure, the sensitivity of the strain gauge could be actively adjusted, which supports our original idea on the morphological change that leads to a change of sensor output and sensitivity. Figure 5.7 shows the differences in rate (calculated by using Eq. 5.9) between experimental results and ones predict by compensation model when $Q = [0.05,\ 0.1,\ 0.2]$ MPa . Generally speaking, the deviation rates in all cases are a bit larger than those in the normal model (see Fig. 5.5 for comparison), but not significantly. In more detail, we can clearly observe the rise up of error rates as the inner pressure Q goes higher. The most straightforward explanation lies in the fact that

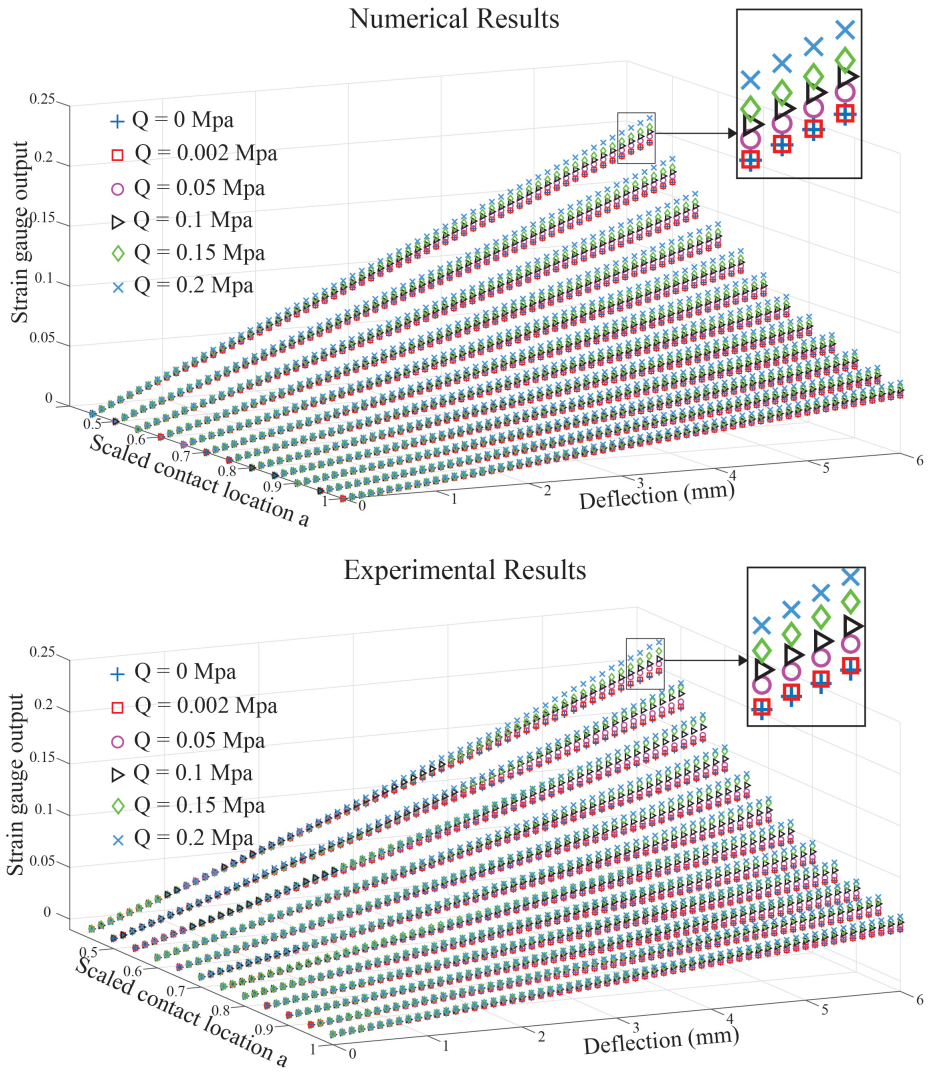

FIGURE 5.6: Numerical solution versus experimental result in the compensation mode: The gradient of the strain output gets higher as the input of air pressure increases.

the non-linearity in the variation of geometrical factors (table 4.1) and material stiffness E (Eq. 5.6) are achieved in an approximation manner with various assumptions and. But after all, within the examined pressure range, the maximum error that can be observed (at the highest pressure 0.2 MPa) in Fig. 5.7 is only around 13%. Interestingly, although the contributions of the geometrical change of each parameter in table 4.1 are still unclear and possibly overlapped by others, but we might confirm that the change in material stiffness, in this research, outperform the change in shape in terms of increasing the sensitivity of the strain gauge. The blow-ups reveal that the strain output at $Q = 0.002$ MPa is nearly coincident to that of $Q = 0$ MPa. Hence, it is acceptable to take the value of E_2^q corresponding to the pressure $Q = 0.002$ as the

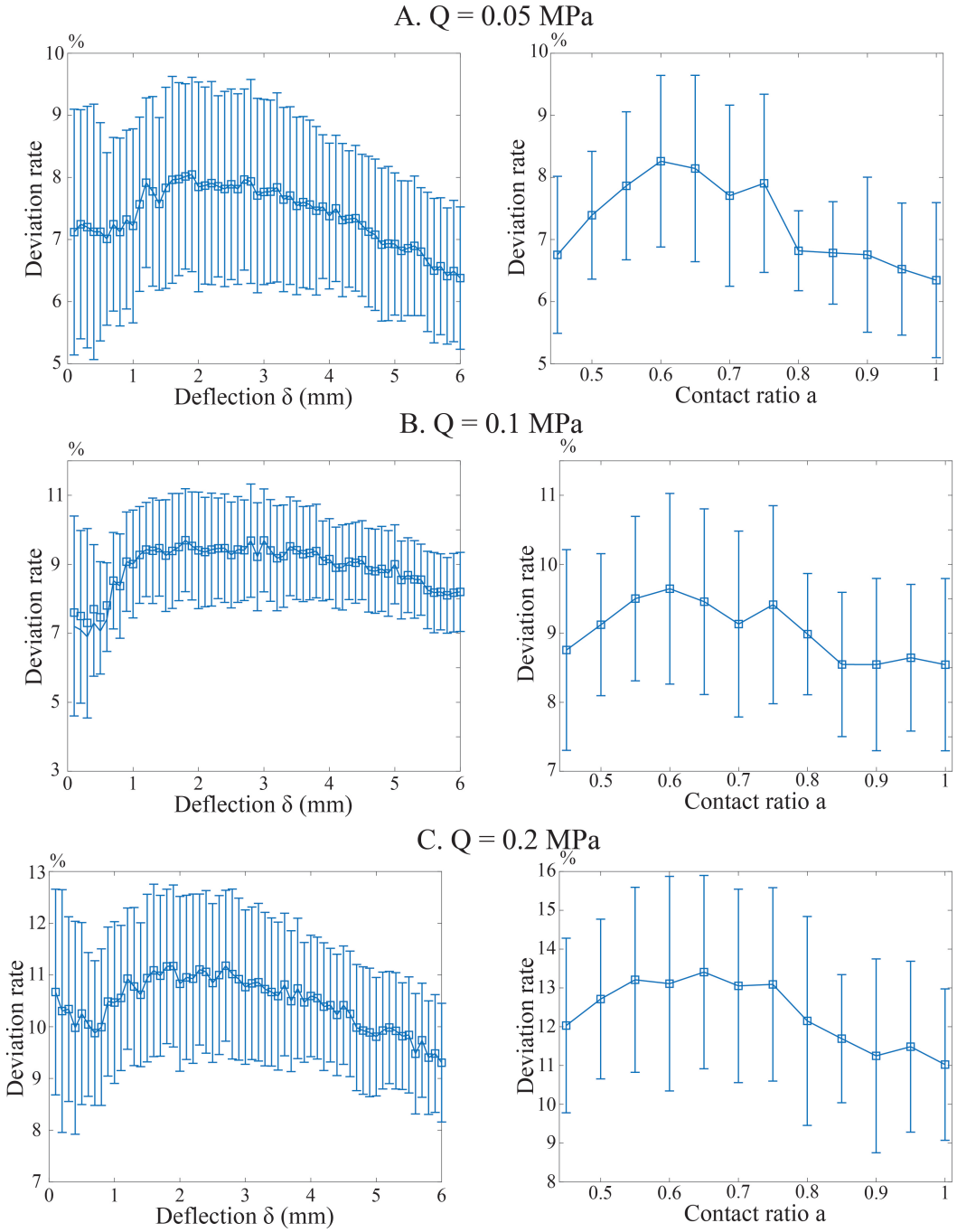

FIGURE 5.7: Average differences in rate (calculated by Eq. 5.9) between experimental results and numerical results estimated by compensation model (Eq. 4.40) when inner pressure $Q = [0.05,\ 0.1,\ 0.2]$ MPa

initial value of the chamber's inner pressure as we claimed in previous section. Accordingly, it is sufficient to keep the whisker's medulla chamber with a small value of pressure, to be more resilient to change from normal to compensation mode upon being trimmed. Based on this evaluation, the proposed whisker and the analytical model can be used as a *body* and *brain* for selection of suitable morphology to the response of different sensing tasks, especially for recovering a broken whisker.

5.2.4 Tactile compensation experiments

In this section, two study cases regarding a broken whisker compensated by its neighboring shorter whisker *(Case 1)* as well as longer whisker *(Case 2)*, are introduced in evaluation of the suggested compensation strategy for broken whiskers. While these cases are inspired by the natural behaviors of rodents, another *sub-case* of *Case 1*, which is more appropriate for a robotic system, is also investigated:

- *Case 1*: A short whisker compensates for a neighboring long whisker. In this case, the experimental Prototype 2 (65 mm in length, see Fig. 5.2(A)) plays the role of *compensator*, and the Prototype 1 (70 mm in length) plays the role of *origin*. In fact, an artificial whisker system is not always constructed as an array of whiskers as natural ones, whilst a sole whisker system is also a good choice. To fulfill the requirement of a resilient capability for such system, I additionally investigate the self-recovery strategy, *i.e.,* a broken whisker (the short one) compensates for *itself* after being trimmed from its original (long) state.

- *Case 2*: A long whisker compensates for a neighboring broken (shorter) whisker. In this case, the experimental Prototype 1 (70 mm in length, see Fig. 5.2(A)) plays a role of *compensator*, and the Prototype 2 (65 mm in length) plays a role of *origin*.

The compensation technique is based on the proposed analytical model for calculation of an appropriate value of chamber pressure Q so that the updated sensitivity

of the *compensator* is close to that of the *origin* one. The experiment procedure can be summarized in the following steps:

- First, we selected the initial air pressure $Q_1 = Q_2 = 0.1\,\text{MPa}$ for prototypes 1 and 2. These choices are based on the tested scenarios which require the *compensator* to become more (Case 2) as well as less (Case 1) sensitive to the stimuli Then, we estimated the geometrical structure and the material characteristics caused by morphology change by using equations mentioned in *section* 4.1.2 and parameters listed in Table 4.1.

- Second, from the analytical model for the compensation mode in section 4.1.2, in order to obtain at the similar response of the strain gauge for the *compensator* and *origin* (*i.e.*, ε_{c1} and ε_{c2}, respectively), a suitable value k for the *compensator* that satisfied the concept of compensation presented in section 5.1 was estimated by the equation 5.2. In this evaluation, we chose the input of contact location $a = 1$ (at the tip of the whiskers) and deflection $\delta(aL_{ai}^{q}) = 1\,\text{mm}$ for simplification purpose.

- Third, we substituted the value of k from the previous step to the relation equation 5.7 to determine the necessary amount of air to be compressed into the chamber.

- Finally, the strain gauge output was recorded under different interaction conditions ($a = 0.45 \div 1$ and $\delta(aL_{ai}^{q}) = 0 \div 6$ mm ($i = 1, 2$) in steps of 0.05 and 0.1 mm, respectively) for each whisker model. Recorded signals are presented by blue circle markers (the original *compensator*), red square markers (the *origin*) and black plus markers (the tuned *compensator*) for comparison as illustrated in Fig. 5.8 and 5.9.

Case 1:

In this scenario, the *compensator* (prototype 2) attempted to adjust its sensitivity (*i.e.*, change pressure value Q) to match that of the *origin* whisker (prototype 1). Since

the *compensator* (short whisker prototype) is more sensitive than its target, hence, to accomplish resilience task, the *compensator*'s sensitivity equivalent to the pressure Q is expected to be reduced. Substituting the required variables to solve Eq. 5.2, reveals the desired value of air pressure is $Q_2^q = 0.048\,\text{MPa}$ (as expected) resulting with $k = 1.5033$. Simultaneously, experimental outputs of the strain gauge were recorded as shown in Fig. 5.8(A). One can observe that by decreasing the pressure from the initial value to $Q_2^q = 0.048\,\text{MPa}$, the response of the *compensator* decreases significantly (from blue circle markers to black cross markers) towards the *target* (red square markers) over the entire range of contact distance and deflection, regardless a small deviation. This result guarantees the *compensator* is able to perform similar responses in comparison with those of the *origin* whisker, by solely changing pressure Q.

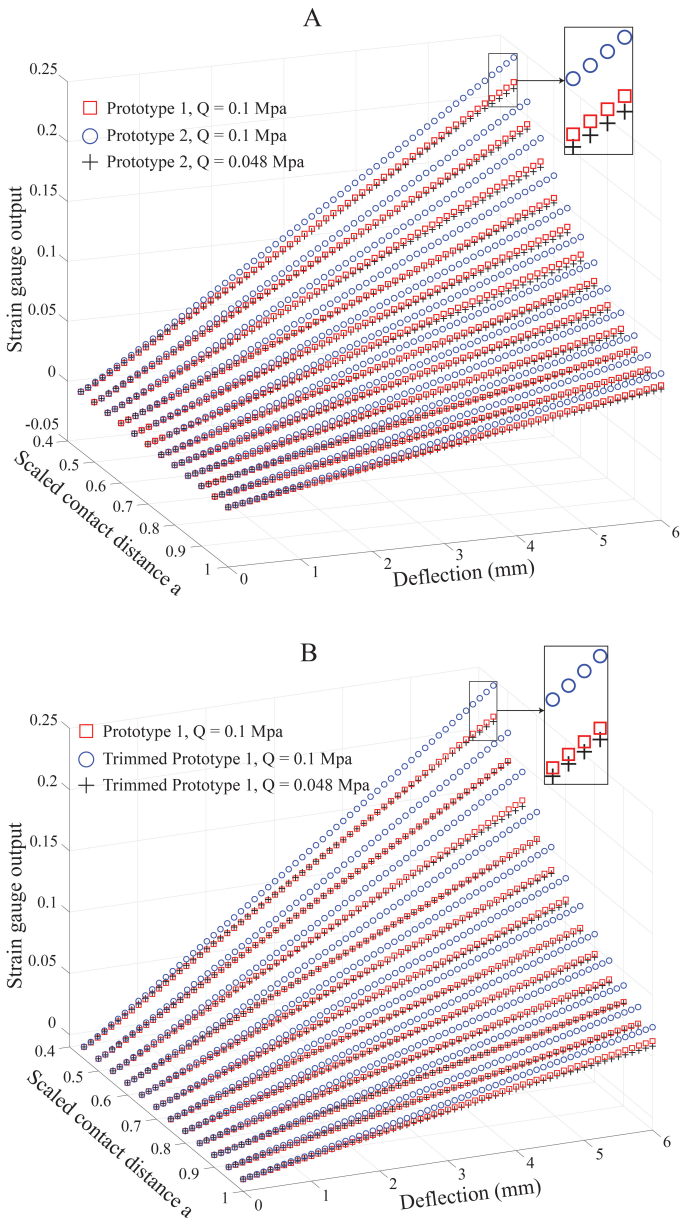

FIGURE 5.8: Compensation test results. Graphs in (A) and (B) are obtained strain signal at various condition of contact location ratio and deflection of Case 1 (short whisker compensates for the neighboring long whisker) and its sub-case (Shelf-compensation: a trimmed whisker compensates to itself), respectively

We also conducted a special case for this scenario to whether a single whisker system would enable resilient capability by using this strategy, called *self-compensation*. Specifically, prototype 1 was trimmed by 5 mm (*i.e.*, length change from 70 mm to a value $L_{a1} = 65$ mm), then compressed air was discharged at the calculated value of 0.048 MPa. The tactile perception of prototype 1 was re-measured and compared to its own performance before being trimmed. The compensation result, as shown in Fig. 5.8(B), reveals that it is possible to adjust the sensitivity of the whisker so that it

performs similarly to its own previous state (before being trimmed).

Case 2:

In this case, the *compensator* (length $L_{a1} = 70\,\text{mm}$) was set to adjust its sensitivity to match the sensing performance of the neighboring *target* whisker (being trimmed with length $L_{a2} = 65\,\text{mm}$). In constrast to Case 1, the sensitivity of the *compensator* should be increased by compressing more air inside the chamber. In order to accomplish this situation, the estimated value of k and air pressure Q_1^q were approximately 0.7365 and 0.192 MPa (as expected), respectively. Then, the response of the *compensator* whisker under various contact locations and deflections was recorded and illustrated in Fig. 5.9. One can see that by increasing chamber pressure from its initial value to the estimated one (0.192 MPa), the compensated response of the *compensator* (black plus markers) set to leave its original response (blue circle markers) toward and match the response of the *target* whisker (red square markers). Again, by a change in chamber morphology (by internal pressure), whisker sensing performance can be actively adjusted, demonstrating morphological compensation in tactile sensing. In conclusion, from comparison results, it is clearly seen

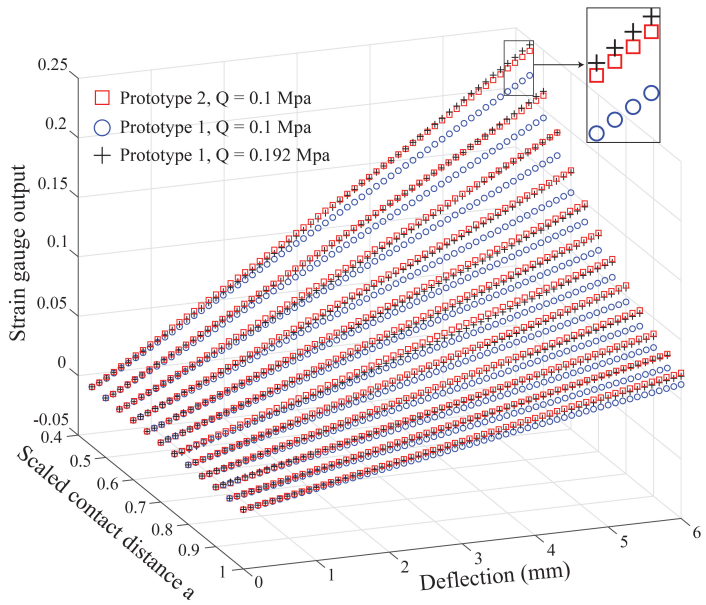

FIGURE 5.9: Compensation test results for Case 2 (long whisker compensates for a neighboring broken (shorter) whisker)

the performance of the broken whisker is exact as our expectation in both cases. By evaluation of two showcases on morphological compensation, despite a small difference among calculated and experimental values, the proposed whisker could actively adjust its sensitivity to match sensing performance of itself (or a neighboring whisker) when the body length shortened (trimmed or broken). At the same time, the proposed whisker design and compensation strategy can be exploited to develop an *active* robotic whiskers that can actively change their sensitivity to match various sensing tasks, or even to compensate itself when it is accidentally broken.

5.3 Discussion

5.3.1 Artificial whisker design with changeable morphology

The design of our artificial whisker was inspired by the structure of a rodent whisker but still remain some differences. First, the scale of each constitutive components do not obey that of actual whiskers. For example, the real whiskers are approximately tapered across the body from base to tip with a ratio of 10 and those who have this value below 10 can be assumed that their tips have been torn [110]. The performance of the sensing element (strain gauge) is highly dependent on the morphology of the chamber layer, which differs from a natural whisker in proportion (as illustrated in Fig. 3.3(A) and (B)). In detail, the conical-shaped medulla of a natural whisker extends further towards the tip than the chamber in our artificial whisker, which provides different levels of elasticity. Furthermore, the radius of cross-section area of the medulla layer, in fact, is linearly reduced from the base and nearly equal to zero at its tip. Generally, we kept the chamber's length at around $15 \div 25\%$ of the overall length for two main reasons. First, the area of the small end of the chamber was kept as large as possible to produce more internal force F with a little compressed air Q (see Fig. 4.1(B)). Second, we tried to avoid physical interaction between the chamber body (region 2) and the surrounding environment, which might result in complications in deriving the numerical solutions. Also, the damaged zone (broken,

trimmed) must not be *within* the length of the region 2, otherwise, the calculations for the artificial whisker become invalid. Additionally, the design of my whisker sensor is actually more practical for a robotic device in many aspects such as easy to fabricate, avoid "$slightflicking$" circumstances of the tip, magnify the sensor feedback when contacts occur near the tip.

On the other hand, the precision of the morphology analysis relies on the stable expansion of the chamber in the direction of measurement by the strain gauge, thanks to the reinforcement fiber. However, in experimental trials, a slight bend of the chamber was observed at high inner pressure. Due to this observation, the resulting strain output shown in Fig. 5.3(A) may include not only pure axial translation. However, this may little affect whisker performance as long as the screw pitch r (see Fig. 3.4) of the helical path is sufficiently small. Also, we ignored any possible impact of the nylon fiber in the analytical model and evaluation test of the material characteristics, even though they were assembled without twisting or tightening.

5.3.2 Applicability: Haptic sensing system for autonomous robots

A changeable morphology whisker is considered appropriate for embodied intelligence [111] and behavior adaptation. Our aim was to provide an efficient solution to active sensing which allows us to actively re-configure the sensing components to fulfill specific purposes or adapt to critical uncertainty (*e.g.* partly-broken state). In this section, I will introduce two potential configurations (see Fig. 5.10 of our whisker sensory system that could be integrated into actual robotic applications:

Type 1: An array of whiskers

An array of whiskers is capable of tactile exploration since all whisker tips lie in a plane, such that, an obstacle will be swept over by multiple whiskers to obtain rich information [112]. This case deploys the biological compensation procedure discussed in section 5.2.4 which is summarized as follows: the broken whisker will be completely and functionally replaced by its neighboring whiskers in an array of

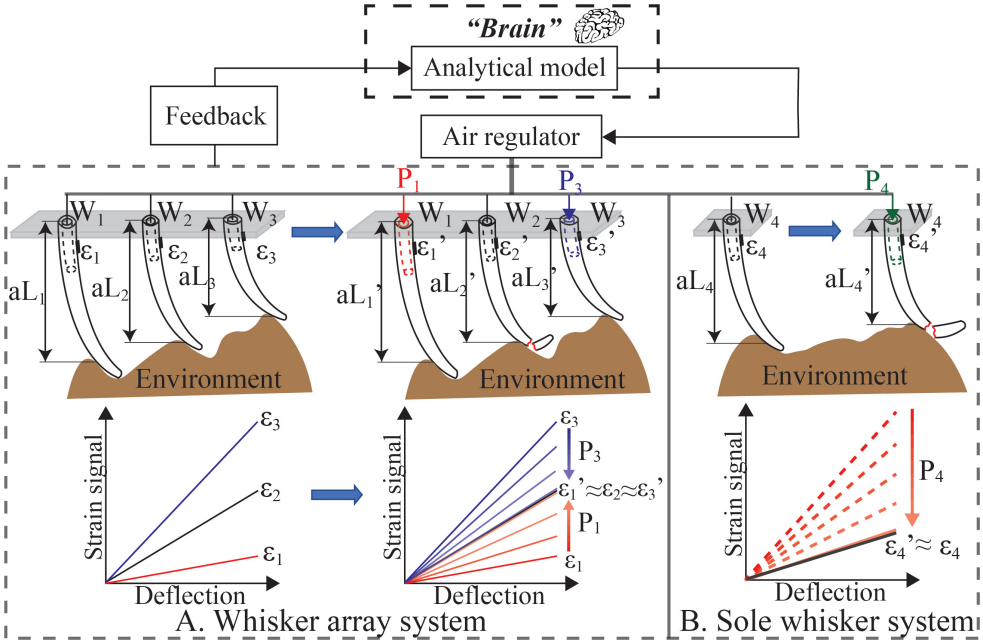

FIGURE 5.10: Compensation test results for Case 2 (long whisker compensates for a neighboring broken (shorter) whisker)

whiskers. Furthermore, whiskers in this system would require the ability to compensate for either longer (Case 1) or shorter (Case 2) which were validated by two experiment cases in section 5.2.4. Hence, stability is highly required for both working states. We will demonstrate how this configuration hardly meets such criteria in the next section. On the other hand, the potential combination between the arrangement of the whisker array and the morphology of each member would enable some intriguing properties facilitating texture discriminability. Since this direction is out of the scope of this study, hence, future works will tackle this challenge.

Type 2: A single whisker

For a sole whisker system (or more than one located independently), in order to deal with unexpected situations (*e.g.* broken or trimmed whisker), it needs to be able to self-calibrate its performance. The experimental results, discussed in the previous section (Fig. 5.8(B)), demonstrate the potential of our whisker system for such application. Obviously, only air decompression is sufficient in this case. Nevertheless, the robot must be able to acquire feedback about the new configuration of the whisker

after trimming to select an appropriate chamber morphology for exact compensation. This feature will be further examined in the next study. Furthermore, along with the investigation of sensing ability, we target this sensing device as a new communication protocol that a mobile robot can use to send a *message* to their allies in a swarm through *touching*, whereas the content of the message depends on the morphology of the chamber.

5.3.3 Reliability of the analysis model

As mentioned before, since construction of the analytical model shown in this chapter has done under the spirit of *morphological computation* concept. The main idea is to express mathematically the dependence of strain gauge's output on mechanical properties (Young's modulus E) and geometrical parameters of the whisker body when the chamber is under actuation. The convenience of this approach lies in the independent expression of the material characteristic for each region which is significantly important for the non-uniform structure proposed in this study. Nevertheless, the inherent relationship between the air modulation inside the chamber and the morphological (including geometrical and material) properties were only approximated (by equations as introduced in section 4.1.1 and 4.1.2). Among those equations, the expression of the second moment of cross-section area for region 2, which is approximated by Equation 4.8, is considered to be a major factor affecting the accuracy of the model. Because of that, there is still a gap between the numerical results calculated from the analytical model and experimental results as clearly seen in Fig. 5.4 and 5.6. We compared the approximated expression $I_2(x)$ with an exact one, then calculated the maximum approximation error which ranged from 4.7% to 11.51% with chamber width (Fig. 3.4) from 33% to 50% of the outer radius of the large end. Thus, to enhance the accuracy of the analytical model, the value of t should be set as small as possible while ensure the possibility of the fabrication process.

On the other side, the feasibility of this model depends on whether the linearity of material is held. Hence, it is essential to understand the mechanical responses

of silicon rubber through the typical strain-stress curve for such kind of material. Like elastomers, silicon rubbers are isotropic nonlinear elastic incompressible or nearly incompressible materials that can be deflects by changing its shape rather than changing volume. The typical stress-strain curve for such kinds of material can be seen in Fig. 5.2(B). Generally, the stress-strain curve of silicon rubber has an unusual shape. The curve may comprise two regions I and II. When the whisker starts making contact with the object, the ratio of stress from the strain measured by strain gauge is a constant corresponding to region I. This feature is true whether the strain is applied in tension or compression (*i.e.*, no dependent on the direction of bending moment). Thus, Hooke's law is valid within this proportionally limit, in the other words, the . In contrast, linearity ceases as the strain increase, a large strain is observed for small increases in stress and the gradient of the graph decreases as evident in region II.

As presented in section 5.2.4, quasi-static tests to observe responses of the embedded sensing element under different contact conditions were conducted with a wide range of chamber morphology. Comparison results in section 5.2.2 and 5.2.2 show consistency with the hypothesis we made at the beginning of this chapter. The first agreement is related to the decreasing trend of Young's modulus E_2 when the air pressure in the chamber increases (as illustrated in Fig. 5.3(B)) which conforms to the stress-strain curve. The second agreement is that the experimental results of the analytical model could predict the overall performance of the system. Thus, the model could be utilized to serve as a *brain* to actively control the whisker *body* depending on various tasks such as adaptive functions.

Although the performance of the whisker prototypes in compensation mode (see Fig.5.9) seems to agree with the hypothesis, some challenges still remain. Some errors in the measurement data may have arisen during analog-to-digital conversion by the microprocessor system, or the proposed analytical model itself does not fully consider all potential factors affecting system performance. For overall evaluation, we examined how the parameters of actual length L_a and air pressure Q influenced the *compensator* performance in the compensation mode. Moreover, we evaluated

how accuracy of the proposed model changed in compensation mode, when the whisker was trimmed at different locations. An experimental procedure similar to that introduced in section 5.2.4 was conducted on the *compensator* whisker with the length varied from 65 mm to 69 mm in Case 1, and 66 mm to 70 mm in Case 2. Under each condition of trimmed whisker, the desired inner pressure Q was estimated from the model and applied to the chamber. Then, the difference between the strain signal of *compensator* whisker and its *origin* one after implementing the compensation was computed through Equation 5.10.

$$\text{Compensation error}(\%) = \left| \frac{\varepsilon_{ac} - \varepsilon_t}{\varepsilon_{bc} - \varepsilon_t} \right| \times 100, \tag{5.10}$$

where ε_{ac}, ε_{bc} and ε_t are tactile responses of *compensators* after and before compensation process and its target, respectively. In short, the smaller the compensation error is, the more accurate the compensation process is. Figure 5.11 compares the average compensation error with respect to a specific range of deflection at three different contact locations, *i.e.*, the contact location ratio a was varied from 0.45 (contact location is near the tip of the chamber), 0.7 (contact location is near the center of the trimmed whisker), and 1 (contact location is at the tip of the trimmed whisker). Generally, the error of Case 1 (Fig. 5.11A-C) was rather consistent in most conditions of length and pressure; and smaller than those of Case 2 (Fig. 5.11D-F), especially when contact occurred near the tip of the chamber (*i.e.*, $a = 0.45$). The main factors affecting the overall accuracy of Case 2 can be characterized as below:

- Figure 5.11(D) illustrates that, at the early stage of whisker bending (very small deflection), the larger the value of the chamber inner pressure, the larger the compensation error. This can be explained by the fact that at high pressure, the chamber is stretched resulting in a significant increase of tension of the chamber wall which requires greater contact force even with small deflection. As a result, the outer surface of region 3 experienced a *local deformation* at the interacted region, leading to an amount of strain output absorbed.

- Whereas, at higher deflection ranges, the bending stress increases enormously

producing larger mechanical strain output complying with the stress-strain curve in Fig. 5.2(B). Thus, the compensation error decreases dramatically which can be observed more clearly for the high-pressure cases (*e.g.* blue and orange columns). As can be seen from Fig. 5.11(E)-(F), the influence of such factors was no longer significant due to the inversely proportional relation between contact location and contact force.

For other cases (Fig. 5.11(A)-(C)), the results were consistent with the above arguments. Generally, the greatest error occurred with contact close to the base ($a = 0.45$). However, there was no remarkable difference compared with the other contact location since the air compressed in the chamber was relatively small for all testers.

According to above investigation, we conclude that, with the morphology of the artificial whisker suggested by the analytical model, the *compensator* in *Case* 1 accomplished the compensation task with more stability and lower overall average error (20.385%) for the whole range of contact locations and deflections, compared to *Case* 2 (36.1837%). This suggests it is better to configure the proposed device according to *type* 2, whose chamber pressure is always lower than the initial value in compensation mode, rather than *type* 1. More precisely, a broken whisker in either sole whisker or a system of whiskers should itself accomplish recovery process rather than assigning this task to neighboring whiskers. This strategy is more practical for robotic devices since it does not constraint the arrangement for a system of whiskers on a simple array configuration as similar as that of rodents.

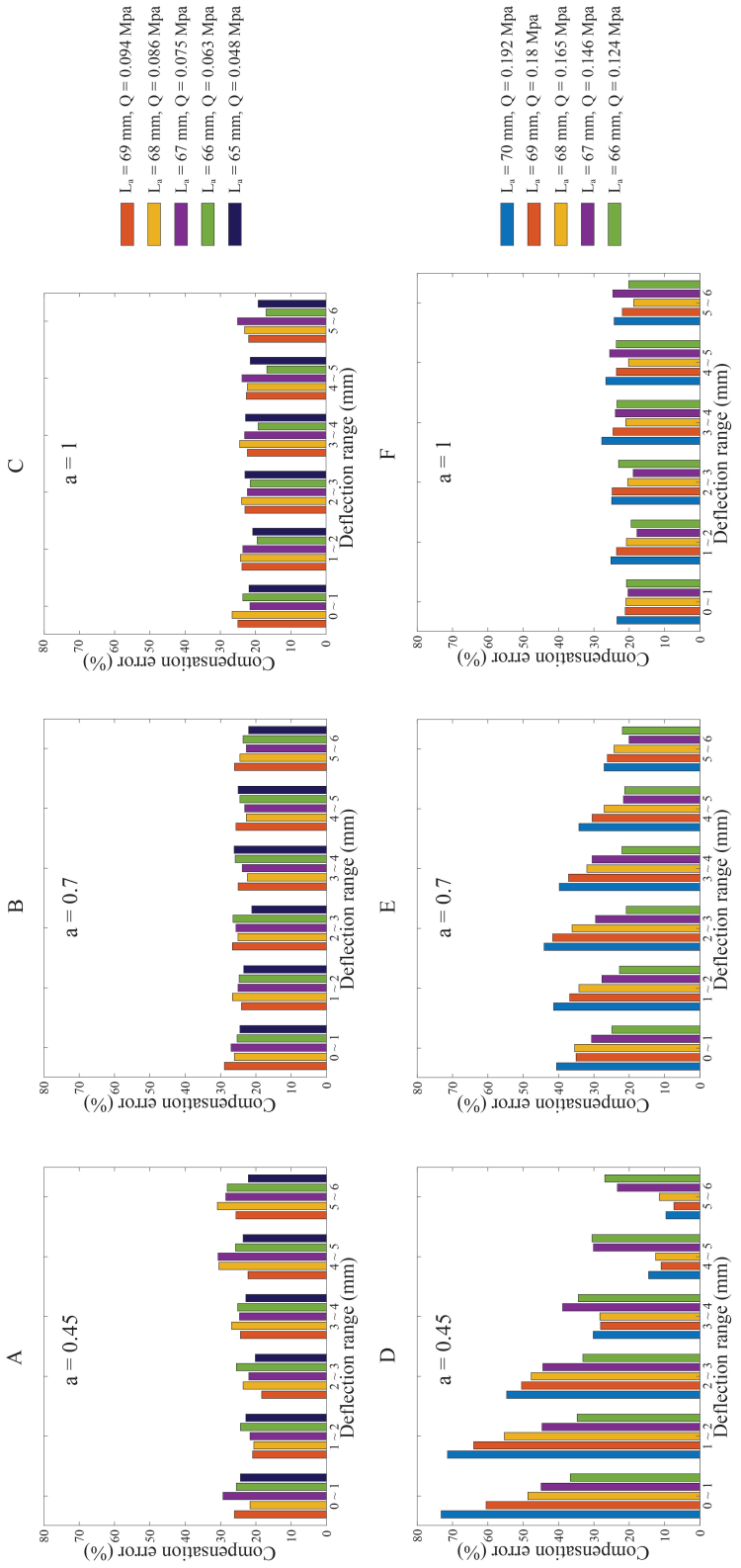

FIGURE 5.11: Compensation error analysis for Case 1 (A)-(C) and Case 2 (D)-(F) with different actual length (L_a) and chamber pressure (Q^q) of *compensator*. The contact location ratio a was varied from 0.45 (contact location is near the tip of the chamber), 0.7 (contact location is near the center of the trimmed whisker), and 1 (contact location is at the tip of the trimmed whisker); while the pressure Q^q was estimated from the analytical model. Error was calculated based on experimental results as shown in Eq. 5.10.

6 On the influence of whisker geometry for self-recovery function

Previous chapter demonstrates that stiffening the chamber region (equivalent to decreasing Young's modulus E) comparably contribute to resilience based on morphological change. Meanwhile, although deformable geometrical parameters listed in table 4.1 can be measured or analytically estimated, however, their explicit roles on recovery performance still remain unclear. This chapter focus on how to maximize the contribution of geometrical factors on the tactile compensation process. Most of content in this Chapter are reported in [6].

6.1 Analysis of Compensation Range

In the proposed whisker sensory system, the largest compensable range of a shortened whisker is considered as a fundamental feature of the compensation ability. This feature is also understood as the maximum and minimum level of tactile perception that a whisker can actively adjust to accomplish compensation tasks with an acceptable accuracy rate. According to the compensation principle clarified in section 3.4.1 and 5.1, this range is strongly dependent on the morphological transformation of the chamber. As introduced in previous chapter, we tested two scenarios with trimmed length up to 5 mm. However, worthy questions arise: Is it possible to improve the compensable range? and to what level?. To tackle these concerns, the value of the initial air pressure Q_i (i = 1; 2) assigned in the experiment section 5.2.4 need to be altered to 0.2 MPa for Case 1 and 0 MPa for Case 2, respectively. As a result, the changeable range of air pressure inside the chamber, which is proportional

to the morphological transformation level, will be increased accordingly.

Nevertheless, increasing the adjustable range of the compressed air inside the chamber to claim a better compensation range is not always advantageous due to a higher resulted compensation error (as pointed out in section 5.3.3). Furthermore, in such attempt, the air regulating system needs a more power-consuming and bulkier compressor which is not suitable especially for a small-scale robotic system. An alternative approach is to optimize the geometrical variables of the whisker body especially the chamber such as the chamber length l, the thickness t and outer diameters of each region (see Fig. 3.4) to achieve the maximum compensable range (upon application's demand) with a small value of compressed air Q. That poses a demand for an efficient investigation framework for studying the dynamics of the soft whisker body with different geometrical inputs. This allows us to seek the optimized body structure for the whisker sensor that outperforms others in terms of recovery tasks as well as evaluate the contribution of geometrical changes in resilient ability compared to that of material properties. The main achievements of this step are summarized as follows:

1) Investigation of critical geometric factors that affect the compensation ability of the proposed whisker sensor system and consideration of its integration in an actual robotic system.

2) Construction of a simulation model based on Finite Element Analysis (FEA) to precisely analyze both sensing and compensation functions.

3) Introduction of an optimization framework based on a combination of the above FE model and Genetic Algorithm (GA) method to suggest an optimal set of decision variables for satisfying various performance objectives.

6.2 Optimization framework for geometrical design

In this section, we introduce an optimization framework to determine optimum geometrical parameters for the whisker sensor to improve its resilient functionality,

TABLE 6.1: Artificial whisker's parameters

Pre-defined variables	parameterized variables
Base diameter $D = 18\,\text{mm}$	Cone angle α
Whisker length $L = 70\,\text{mm}$	Chamber length l
Strain gauge's location $x_{ss} = 6\,\text{mm}$	Chamber wall thickness t

while the material is the same as that used in chapter 4. To serve this aim, I parameterized the design of the whisker sensor chamber with the chamber length, l, cone angle, α, and chamber wall thickness, t, meanwhile, the rest are defined as shown in Table 6.1. First, we listed the performance requirements in descending order of importance as shown below:

- *Objective 1*: The adaptive range describes the extent to which the adaptive mechanism can accomplish a compensation task. For instance, the adaptive range of an artificial whisker is the longest trimmed length, Δ_{max}, that can be compensated with an acceptable error rate. As stated in previous section, this feature strongly depends on the capacity of the whisker morphology to change (the chamber region in particular) within the working range of inner pressure. Hence, in order to adjust this feature, there are two solutions as detailed below:

  - One way is to tune the transmission capacity of the actuating system (pneumatic actuation). This is done by increasing (*i.e.*, larger adaptive range) or decreasing (*i.e.* smaller adaptive range) initial pressure, Q_i, while compensation pressure, Q_c, is reduced to zero.
  - The other way is to change geometric variables l, α, and t, which directly correspond to strain gauge sensitivity.

  Technically, the adaptive range is desired to be as large as possible. Nonetheless, it is worth noticing the responsive range of the embedded strain gauge.

- *Objective 2*: The adaptive range depends on the chamber air pressure, however, the wider the working range of air pressure the more power the compressor requires, which is inefficient for small-scale robotic systems. For this reason,

the value of Q_i should be as small as possible, which may conflict with the first objective.

Based on the above discussion, the main objective of the proposed optimization framework is to produce a set of decision variables including l, α, t, and Q_i for an artificial whisker with maximum adaptive range, Δ_{max}, as requested while keeping Q_i as small as possible. The details are presented in the next sub-section.

6.2.1 Dynamic investigation using Finite Element Method (FEM)

FE model construction

The most challenging mission is to accurately replicate dynamics changes of a soft body under either internal or external actuation due to its complex and highly non-linear mechanical behaviors of hyper-elastic materials. In this matter, there are several approaches to tackle this problem, in which, two most widely used method are:

- The soft body is modeled as a set of nodes (points masses) connected by elastic spring (thus, Hooke's law is available) which takes inspiration from muscle-skeleton systems of biological systems [113]. Then the behaviors of the soft body discretized by a mass-spring system is observed as interactions between the particles driven by the springs as well as external impacts. Then the local deformation of springs will be used to form the global deformation of the object. This is widely used in many applications, for example, medical simulation of soft tissues [114] thanks to its ease to implement, simple calculations and applicable with any topological modifications.

- The second method also the most popular choice for studying non-linear dynamic is Finite Element Method (FEM) [115]. In more details, the soft body as a continuous volume will be discretized into a number of topological element whose partial differential equations (PDE), or normally called basis functions, are solved using the principle of minimization of the energy to obtain a

static solution in an equilibrium state. This method gives outstanding precision in the results, therefore, FEM is not only used for simulation of deformable bodies [116], but also airflow [117], heat transfer [118], fluids [119] and many others. Thanks to its wide application, there are many commercial products in the market offering off-the-shelf FE solvers. In this section, we describe the construction of an FE model for dynamic investigation of the proposed whisker sensor under highly deformed states during interaction with obstacles by utilizing the commercial FE solver Abaqus/Standard (Simulia, Dassault Systemes)

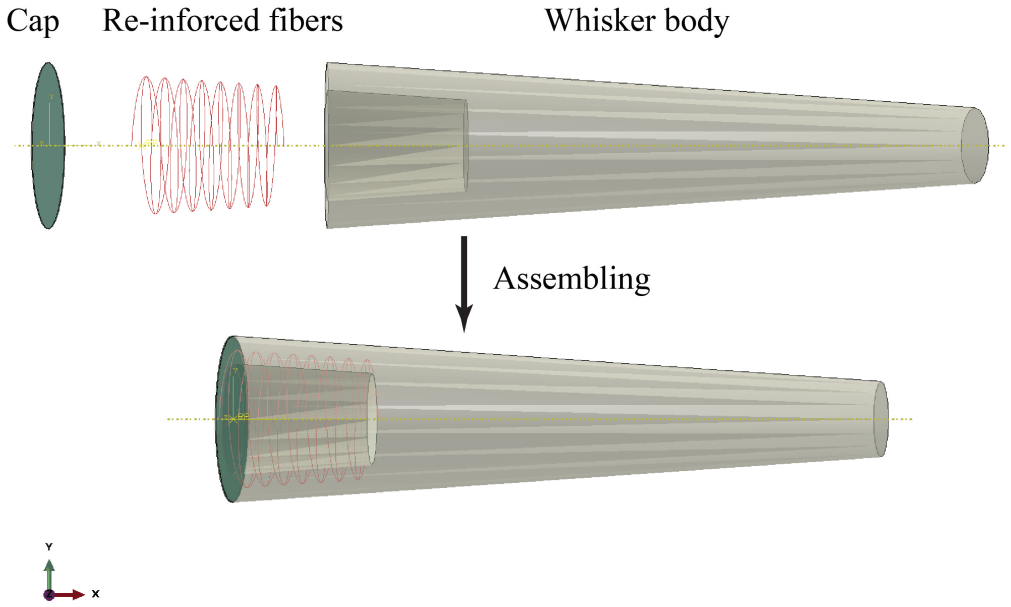

FIGURE 6.1: Construction of the FE model (in Abaqus) for the proposed whisker sensor which consists of three separated parts (similar to analytical model shown in Fig. 3.4): The cap, reinforced fibers and the whisker body.

First of all, let me clarify how to build a FE model for my whisker sensor. The whisker sensor comprises three main parts: body, reinforced-fibers, and cap as shown in Fig. 6.1. The cap was fused into the body end wall to prevent relative motion between them by using *Tie* constraint. Whereas, the reinforced-fibers were embedded within the chamber wall with help of *Embedded region* constraint to complete the CAD whisker model. Then, a symmetrical boundary condition (BC) at the base end of the whisker model was applied. Another critical point is to define the

material characteristic for each component to precisely describe the nonlinear mechanical behaviors of the whisker body. For simplification, the reinforced-fiber was treated as an elastic material with Young's modulus $E = 31,067\,\text{MPa}$ and Poisson's ratio of $\nu = 0.36$. Meanwhile, the body and the cap are classified as hyperelastic materials. As a matter of fact, there exists many approximately mechanical models to describe such kind of material. In this study, in order to precisely describe the nonlinear behavior of silicon rubber (Dragon skin 30, Smooth-on Inc., PA, USA), a hyperelastic Neo-Hookean model was utilized. The Neo-Hookean model is the simplest form of all commonly used hyperelastic models. The elastic strain energy potential energy is shown as:

$$W = C_{10}\left(\overline{I_1} - 3\right) + \frac{1}{D_1}(J-1)^2 \tag{6.1}$$

where W is the strain energy per unit of volume, C_{10} and D_1 are temperature-dependent material parameters, $\overline{I_1}$ is the first deviatoric strain invariant and J is the elastic volume ratio. Since the silicon-rubber material is incompressible, the second term in Eq. 6.1 is equal to zero. In our model, D_1 is set to be zero whereas $C_{10} = 0.14$. These value were taken from the set of material coefficients in [120]. Finally, the model was meshed with hybrid 20-node quadratic elements (C3D20RH) whose edge size was set equal to the grid length of the strain gauge (KFGS-2-120-C1-11 L1M2R from Kyowa Electronic Instrument Co., 2 mm grid length was used in this paper). The final mesh model for the whisker is shown in Fig. 6.2. The simulation process included two steps, as indicated in Fig. 6.3: Pressurization of the air chamber to a pre-set value (see Fig. 6.3(A)), followed by deflection of the whisker in the negative y-direction at a certain point along its length (aL_Q), with translation distance, δ, set at 5 mm in all simulation trials (see Fig. 6.3(B)). Logarithmic strain data generated at the centroid of the element where the strain gauge is bonded was extracted for further data processing.

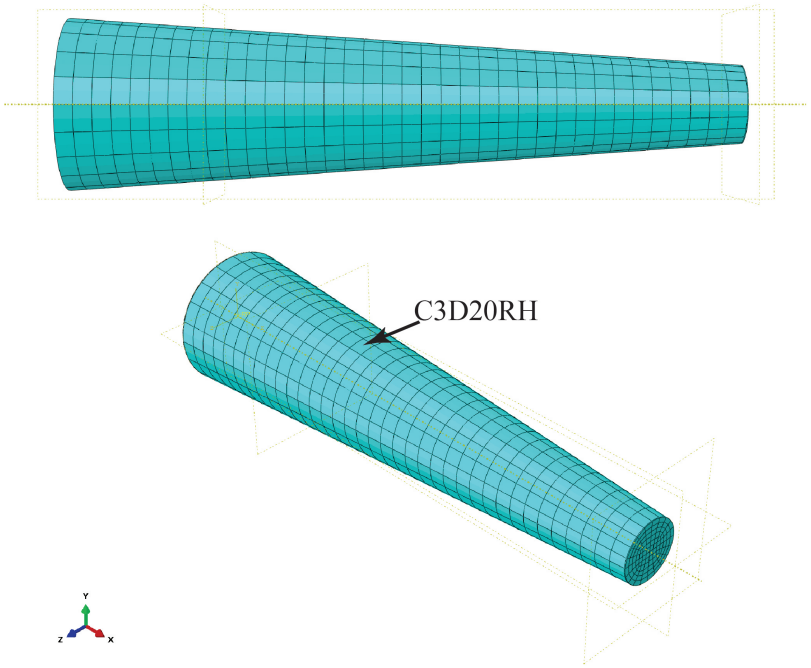

FIGURE 6.2: Meshed whisker body

Validation

To validate the FE model, simulation trials were conducted in a prototype whisker with the following parameters: $[\alpha \ \ l \ \ t] = [2.862 \ \ 15 \ \ 3]$ and the results of axial translation of the whisker tip in the x-direction during air pressurization were compared to practical data measured by a laser sensor (the experimental setup is the same as shown in Fig. 5.1). Figure 6.4(A) shows the comparison results where the estimated extension of chamber length under a wide range of compressed air ($0 - 0.2$ MPa) was nearly coincident to the actual data. Moreover, since there is a deviation between actual strain gauge responses (electrical signals) and simulated mechanical strain produced by Abaqus, a calibration procedure (similar to method described in [4]) is necessary. More specifically, I conducted a practical test to observe the tactile signal of the strain gauge ε under different measuring conditions (*i.e.*, varied contact ratio a along the whisker length) to compare with numerical results obtained from Abaqus. It was found that to eliminate the difference the simulated values should be multiplied by coefficient, ξ, ranging from $3.8 - 4$ corresponding to the contact ratio from $1 - 0.5$ (examined range), respectively. In this study, we chose $K = 3.9$ for data post-processing, and a series of simulations was performed with different

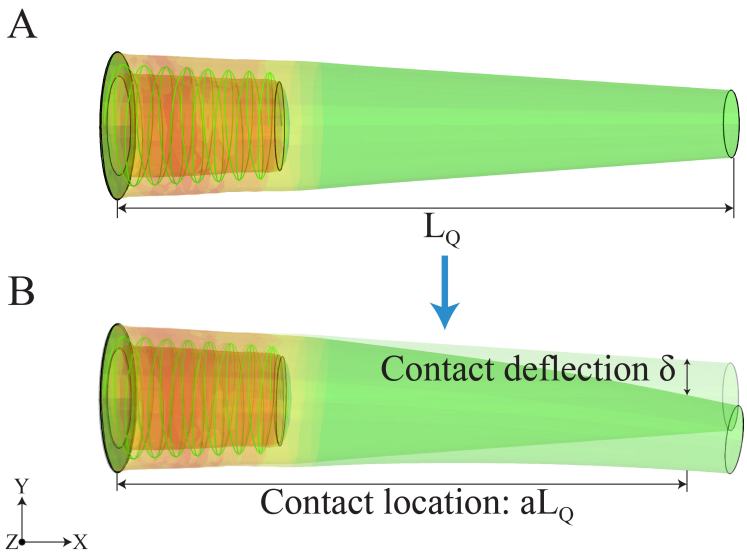

FIGURE 6.3: The FE simulation process consists of two stages: (A) Pressurizing the air chamber at a specific pressure Q MPa; (B) then, deforming the whisker body with contact deflection δ mm at location aL_Q where "a" and "L_Q" are contact ratio and current whisker length, respectively.

values of inner pressure, contact ratio and body deflection. Figure 6.4(B) illustrates the strain gradients generated by the strain gauge. These simulated results demonstrated that the sensitivity of the strain gauge was proportional to Q regardless of contact location, similar to experimental results in section 5.2.3.

6.2.2 Genetic algorithm-based optimization method

Searching the optimal solution for the design of the whisker sensor was done by using a combination of FE simulation model and a metaheuristic optimization algorithm called Genetic Algorithm (GA) based on Darwin's theory of evolution and Mendel's genetics [121] (see Fig. 6.5. GA stochastically searches the solution space for an optimal individual containing the value of design variables as "*chromosomes*" which best fits with the pre-defined *survival* conditions (*i.e.*, fitness function). Such progress is done in the fashion that mimics the operation of evolution - a number of best individuals from an initial *population* is chosen upon the rule that the fitter the individual, the more likely that individual will be able to save their genes to the next generation, thus improving successive generations; then each of them will go through an evolving procedure with two genetic operators: *Cross-over* and *Mutation*

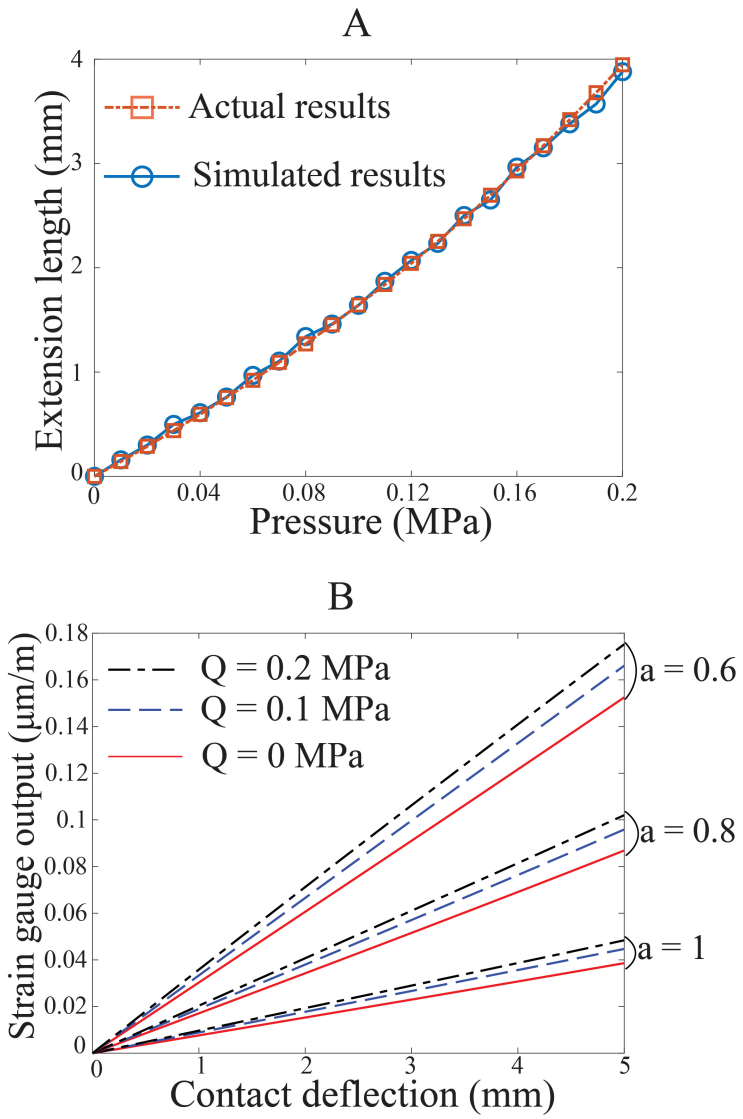

FIGURE 6.4: Performance evaluation of the FE model is validated by (A) a comparison of results among simulated and actual extension lengths as well as (B) perceived tactile responses of the strain gauge under a wide range of chamber pressures and contact ratio a.

to produce the new $offsprings$ for the next generation. The Tournament selection method [122] was chosen as selection strategy because of its easiness of adjusting the selection pressure by changing the tournament size s ($s = 2$ in this work). The whole process is repeated until the termination conditions are satisfied such as the max generation is reached or the fitness value of the best individual is sufficiently low. The fitness function of a specific design of the artificial whisker is determined based on performance and functional requirements declared in the previous section. Since there are two major objectives conflicting to each other (Objective 1 and 2), thus, a multi-objective problem, where the optimized individual need to be taken in

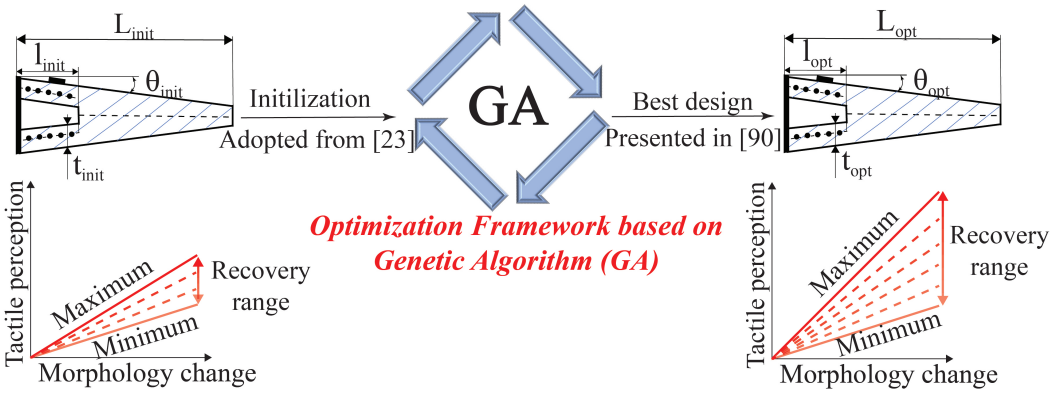

FIGURE 6.5: Evaluation framework for compensation performance

a trade-off between them, is commonly used. However, the evolution in fitness score of each individual is expected to compromise all Objectives. Hence, after a number of generation, all individuals have stuck at local optimal with respect to either Objective 1 or 2. It is crucial to aware that the adaptive range, or in other words, the compensation capability must be paid more priority than others. Within this study, we tackled this issue differently by considering compensable range as the main target in a constrained single-objective optimization problem. Constrained optimization problems are common in engineering, science and operation researches which define a feasible region so that, if a vector $\overrightarrow{x}$ satisfy with all constraints (defined by main objective and sub-objectives) then it is within the feasible region. There are many traditional approach to constrained optimization, in which penalty functions is the most popular. Theoretically, this method turn a constrained problem into a "non-constrained" ones by following expression:

$$F(\overrightarrow{x}) = \begin{cases} f(\overrightarrow{x}) & \overrightarrow{x} \in feasible\ region \\ f(\overrightarrow{x}) + penalty(\overrightarrow{x}) & \overrightarrow{x} \notin feasible\ region \end{cases} \tag{6.2}$$

Selections for penalty function are reviewed in [123]. Among them, I choose dynamic penalty function to address the problem presented in this chapter, where its own fitness function $f(\overrightarrow{x})$ is combined with a summation of penalty functions respective to each remaining objective to form the final penalized fitness function $F_p(\overrightarrow{x})$. By doing so, GA algorithm is forced towards the Objective 1 in the direction governed by other minor objectives whose distributions are determined based on

their weight of influence. According to the concept expressed in Eq. 6.2, equation 6.3 introduces the formulation of $F_p(\overrightarrow{x})$ as formulation to calculate the fitness score included with penalty function:

$$F_p(\overrightarrow{x}) = f_1(\overrightarrow{x}) + \sum_{j=2}^{4} \rho_j(\overrightarrow{x}) \tag{6.3}$$

where $\overrightarrow{x}$ is the vector containing four decision variables (*i.e.*, chromosomes) $\overrightarrow{x} = [\ \alpha \quad l \quad t \quad Q_i\ ]$, $f_1(\overrightarrow{x})$ and $\rho_j(\overrightarrow{x})$ are fitness function regarding compensable range (*i.e.*, Objective 1) and penalty functions for other objectives, respectively. In term of penalty function, we utilized the dynamic type for this case where the general formulation can be seen below:

$$\rho_j(\overrightarrow{x}) = C_j \times \kappa_j, \tag{6.4}$$

where C_j are user-defined coefficients which put a control on the distribution of each objective in the design space. On the other hand, κ_j is a dynamic measure changing over the time of the GA progress. Specifically, κ_j is equal to the product of fitness value $f_1(\overrightarrow{x})$ of solution $\overrightarrow{x}$ and the distance metric measured from solution $\overrightarrow{x}$ to the best one. For instance, the dynamic term for the Objective 2 κ_2 where the decision variable Q_i is preferred to be close to the minimum bound value Q_{imin}, is illustrated as follows:

$$\kappa_2 = f_1(\overrightarrow{x}) \times \frac{Q_i - Q_{i\,\min}}{Q_{i\,\max} - Q_{i\,\min}}. \tag{6.5}$$

Similar formulations can also be withdrawn for the other two objectives. Equation 6.5 has the property of eliminating every low-preference individuals when the $f_1(\overrightarrow{x})$ is still relatively large (resulting a big penalty cost), while gradually decreasing the penalty value to accept those individuals if the fitness improvement of $f_1(\overrightarrow{x})$ is significant. Additionally, our GA-based optimization framework applied this type of fitness function was witnessed to converge to the feasible region more quickly and not being trapped at a non-optimal solution or area in the searching space. As regards the coefficient C_j, a trial and error procedure was made to determine the value

of $C_{2\div4}$ to ensure that they are not too lenient leading the final outcome is not even near the optimal solution or too intense resulting in an increase in the cost time. We realized that $[C_1;C_2;C_3] = [0.5; 0.2; 0.2]$ works perfectly for our case.

In the next section, several simulation trials and a thorough experimental validation upon the suggested design by GA will be conducted for practical scenarios to strengthen the novelty of the TaCMorph platform as well as the proposed optimization tool.

6.3 Optimization Results and Validation

6.3.1 Optimization procedure

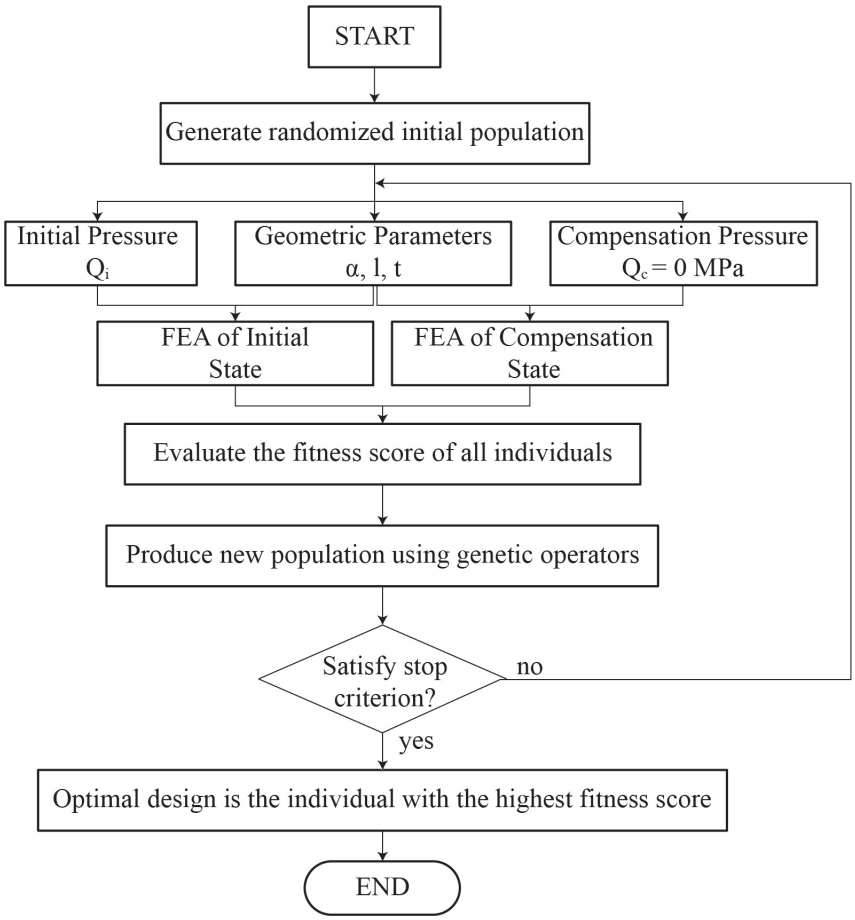

FIGURE 6.6: Flowchart of the proposed optimization framework

In order to demonstrate the effectiveness of this optimization framework, in this section, two optimization problems with respect to two adaptive ranges *Case*

1: $\Delta_{max1} = 5\,\text{mm}$ and *Case 2*: $\Delta_{max2} = 10$, were solved. The boundaries for each design variable were chosen as $\alpha \in [2.5; 6]^{\circ}$, $l \in [10; 15]\,\text{mm}$, $t \in [2; 6]\,\text{mm}$ and $Q_i \in [0.01; 0.2]\,\text{MPa}$ to span feasible values. The remaining geometric variables for the whisker design are given in Table 3.1. The function *ga* from Matlab Global Optimization toolbox was implemented to run GA algorithm with population size n and tolerance set to 50 and 10^{-9}, respectively. To determine the fitness score regarding Objective 1, two FE simulations corresponding to the initial state of the whisker (inner pressure $Q = Q_i$ and trimmed length $\Delta = 0$) and the compensation state ($Q = Q_c = 0$ and $\Delta = \Delta_{max}$) were conducted in sequence. The fitness score $f_1(x)$ was calculated as an absolute average of the difference of strain signals (*i.e.*, $f_1(x) = \frac{\sum_n |(\varepsilon_i(x) - \varepsilon_c(x))|}{n}$ where n is the number of measuring steps) extracted from the simulation results for each step of the whisker's deflection (step size of 0.01 mm) exerted at the same contact ratio of $a = 1$. A protocol for evolution termination is essential to ensure the best candidate is achieved within a reasonable time. Thereon, the termination protocol will be activated when either: 1) The number of iterations performed by GA is equal to 50; 2) The best fitness value, $F_p(x)$, is lower/equal to 10^{-3}; 3) The average relative improvement in the best fitness value over 20 consecutive generations is less than or equal to the tolerance. These stopping criteria are chosen based on the following reasons:

- In general, Abaqus took approximately 8 minutes to run an evaluation test for an individual. Thus I chose the maximum number of generations to be 50 to make sure we will get the final results within two weeks.

- The second condition is based on the fact that the contributions of sub-objectives to the final fitness score $F_p(x)$ will be gradually reduced with the improvement of the score for the main objective (*i.e.*, $f_1(x)$ is nearly equal to zero) as can be reviewed in equations 6.3 - 6.5. With this concept, The desired value of $F_p(x)$ is supposed to be sufficiently small so that $F_p(x) \approx f_1(x)$ which directly indicates the gap between sensory feedback before (initial state) and after (broken state) compensation. After several trials, I decided to choose the stopping

value for $F_p(x) = 10^{-3}$, because at the end of the evolutionary process (*i.e.*, generation 50), the final score of the best individual usually converge around this value and did not significantly improve the final score afterward. From the engineering point of view, this value is considered a negligible tolerance in practical robotic sensory systems and also denotes the success of the tactile compensation process.

- The final condition was used to check the feasibility of the optimization framework.

Figure 6.6 outlines the optimization procedure exploited for the whisker sensing system in this chapter. In short, our single-objective optimization problem can be generalized as shown in the expression below:

$$\begin{aligned} \textbf{minimise}: & \frac{\sum_n |(\varepsilon_i(x) - \varepsilon_c(x))|}{n} \\ \textbf{subject to}: & 3 \leq \alpha \leq 6[^\circ], 10 \leq l \leq 15[\text{mm}], \\ & 3 \leq t \leq 6[\text{mm}], 0.01 \leq Q_i \leq 0.2[\text{MPa}] \\ \textbf{to yield}: & \varepsilon_i = \varepsilon(Q_i, \Delta = 0), \\ & \varepsilon_c = \varepsilon(Q_c = 0, \Delta_{\max} = [5; 10]) \end{aligned} \tag{6.6}$$

6.3.2 Optimization results

Figure 6.7 illustrates the performances of the GA algorithm (including the best fitness score and average score over the evolving duration) for Case 1 (see Fig. 6.7(A)) and Case 2 (see Fig 6.7(B)). In more detail, the optimization process of the former case was terminated at generation 29 since the best fitness (0.0009986 as shown in Fig. 6.7(A)) was lower than the threshold value, meanwhile, the progress of the latter problem was ended after 41 generations due to the third stopping criteria. Table 6.2 presents whisker designs with different sets of examined parameters, in which, the first two sets are the optimized designs qualifying two objectives Δ_{max1} and Δ_{max2}, respectively. The third set belongs to a random individual in the final generation of the first case. The calculated fitness score for each design is also given.

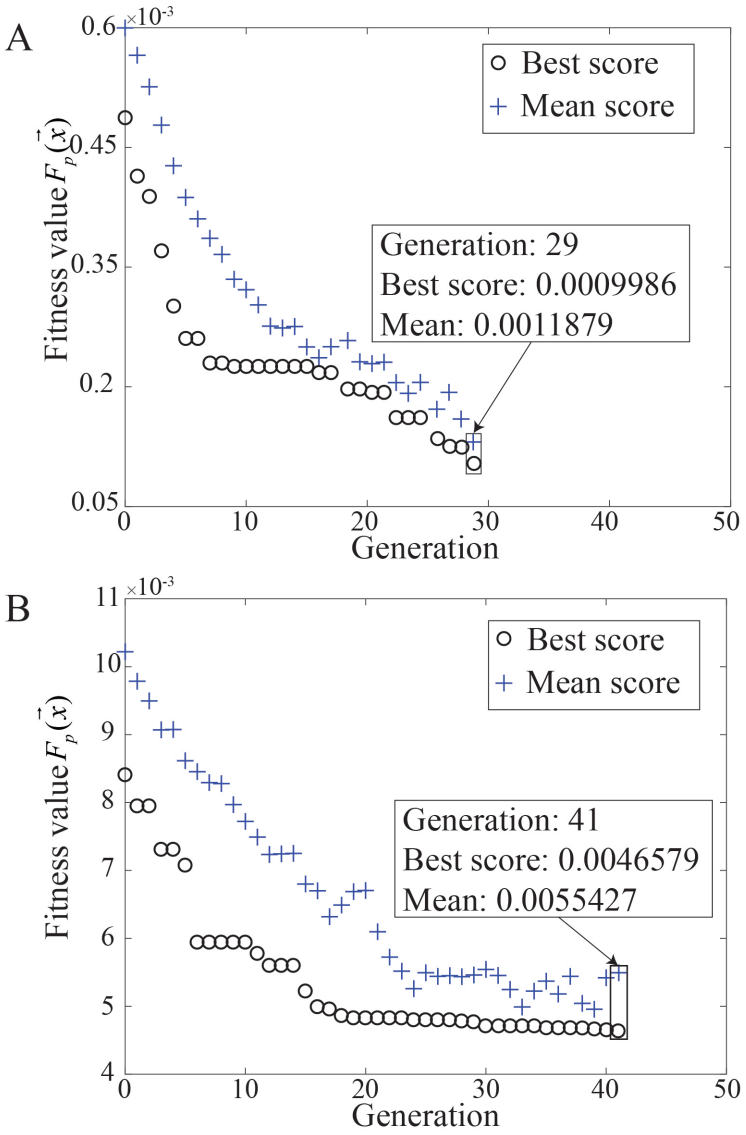

FIGURE 6.7: Convergence results of GA runs in cases (A) 5 mm and (B) 10 mm maximum broken length, respectively.

In comparison with design No.3 (in Table 6.2), optimized design No.1 could accomplish the compensation task for 5 mm trimmed length more precisely but at lower initial pressure ($Q_i = 0.087$ MPa for No.1 compared to $Q_i = 0.106$ MPa for No.3) together with the value of t and α are more reasonable according to Objectives 3 and 4. The fitness score calculated for Objective 1 $f_1(x)$ of design No.1 (7.85×10^{-4}) is even higher than that of No.3 (7.702×10^{-4}), which proves the efficiency of additional penalty functions in guiding the GA to the more feasible region. Additionally, we found that the pressure variable, Q_i, of design No.2 was stuck at its up-boundary (around 0.199 MPa) over generations (starting from generation 18). As a result, the

TABLE 6.2: Compensation performance corresponding to different sets of decision variables

No.	α (°)	l (mm)	t (mm)	Q_i (MPa)	$F_p(x)$
1	3.744	12.04	3.715	0.087	0.0009986
2	3.465	13.54	4.06	0.199	0.0046579
3	4.58	14.27	3.078	0.106	0.0011519

improvement of its fitness score was far below the expected milestone. This suggests that to improve this result, all investigated decision variables, especially the initial pressure, should be searched within a wider domain. However, it also violates Objective 2. Alternatively, another solution without increasing the input pressure may take into account parameters such as whisker length (*i.e.*, L), base diameter (*i.e.*, D), or material property as decision variables for the optimization problem.

6.3.3 Experimental validation

Tactile compensation performance of the fabricated prototypes was practically evaluated by using the same testbed and experiment procedure as described in Fig 5.1 and section 5.2.1, respectively, to assess the reliability of the GA-based optimization framework. Two tests were conducted under the conditions of intact whisker and broken whisker. At first, the sensing performance of the intact whisker was evaluated. After compressing air into the chamber with the pressure, Q_i, as listed in Table 6.2 and measuring the body length, L_Q, the obstacle sequentially made contact with the whisker at different locations $a = [0.55 \;\; 0.7 \;\; 0.85 \;\; 1]$ for 5 mm in deflection at a speed of 1 mm/s. The synchronized strain signal was recorded and saved for further analysis. In the second test, the whisker was trimmed by $\Delta_{max1} = 5$ mm for design No.1 and $\Delta_{max2} = 10$ mm for design No.2, respectively. Chamber's inner pressure was set to zero. A similar procedure was repeated and the results were compared with those of intact whiskers. The results of the validation tests are presented in Fig. 6.8. The response of the strain gauge to the contact deflection changed significantly after being trimmed/broken (green lines) compared to the original one (red lines).

Interestingly, from computational and experimental data, it can be observed that by activating the compensation mode (*i.e.*, $Q_c = 0$ MPa), the response of the

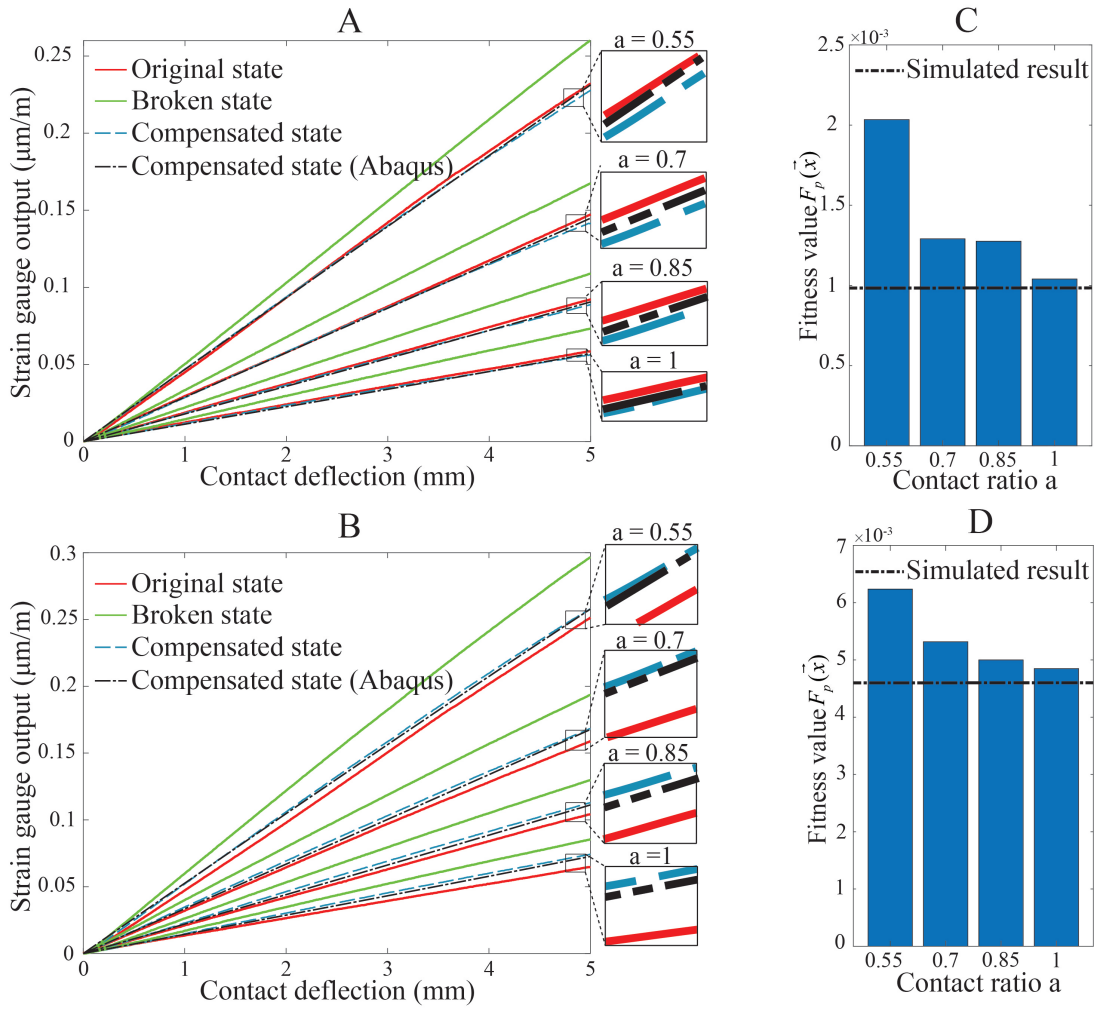

FIGURE 6.8: Compensation results of the trimmed whisker based on optimal design No.1 (trimmed length $\Delta_{max1} = 5\,\text{mm}$) and No.2 (trimmed length $\Delta_{max1} = 10\,\text{mm}$) in both experiment and simulation scenarios. (A) Compensation results when $\Delta_{max1} = 5\,\text{mm}$. (B) Compensation results when $\Delta_{max2} = 10\,\text{mm}$. (C) Actual value of $F_p(x)$, *i.e.* compensation error, when $\Delta_{max1} = 5\,\text{mm}$. (D) Actual value of $F_p(x)$, *i.e.* compensation error, when $\Delta_{max2} = 10\,\text{mm}$.

trimmed whiskers after compensation (blue dashed lines) approximated its original state (red solid lines) with at least 87% and 72% improvement (calculated by equation 6.7) for Case 1 and Case 2, respectively, regardless of contact location ($a = 0.55 - 1$).

$$\text{Recovery rate}(\%) = \left(1 - \left|\frac{\varepsilon_c - \varepsilon_o}{\varepsilon_b - \varepsilon_o}\right|\right) \times 100, \tag{6.7}$$

where ε_c, ε_b and ε_o are the response of strain gauge (reported in Fig. 6.8) in compensation, broken and original states, respectively.

As a result, after compensation, the relative sensitivity of the whisker was unchanged. In addition, the compensation results showed good agreement with the

optimization framework outcomes (see Fig. 6.8(A)(B)). Design No.1 outperformed design No.2 regarding compensation accuracy. A similar conclusion can be obtained from Fig. 6.8(C)(D). From the presented results, the experimental outputs were approximately close to the simulated value, implying the proposed combination of FE model and GA algorithm is feasible. As can be seen in Fig. 6.8(C)(D), compensation error $F_p(x)$ slightly increases with decrease in contact ratio due to higher non-linearity when contact occurs near the base. This was deemed acceptable since the magnitude and difference between the max and min value of $F_p(x)$ for both cases (around 1×10^{-3}) are insignificant. Note that, to compensate for other sizes of trimmed length, we only need to set Q to a specific value within the range of $[0; Q_i]$, which is predicted by the FE model.

6.4 Discussion

In this phase, we aimed to enhance the feasibility of a sensory compensation mechanism in a soft whisker sensor system in response to the whisker being broken, trimmed, or suffering critical change in morphology. The underlying idea relies on controlling the morphology of the soft body to change its geometric and material properties in order to re-calibrate the sensing element to its original state. A design optimization framework, comprising an FE model and Genetic Algorithm that improved the compensation functionality in various perspectives, especially adaptive range, was investigated. Experimental results of tested whisker prototypes suggested by our GA-based optimization method were confirmed to successfully accomplish compensation tasks under stringent quantitative as well as qualitative conditions. On the other hand, two critical challenges remain for this idea to be applied in an actual robotic system. First, in order to appropriately adjust the whisker body morphology for compensation task, the size of the broken length must be determined beforehand. Hence, an algorithm to detect and evaluate the breakage condition is needed. Second, robust evidence is required to prove that allocating the tactile compensation task to a robot body is more practical in terms of costs and

resources than allocating it to a central processing system. Therefore, further investigation is necessary to address thoroughly the aforementioned issues.

Furthermore, as mentioned in the beginning of this chapter, the contribution of each geometrical parameter on the the tactile compensation performance based on morphological change has so far not been explicitly clarified. In comparison with the first whisker version as parameterized in table 3.1, the optimal design in table 6.2 and all best individuals of each generation reveal the varying trends of examined parameters toward higher performance of resilience. Taking design No.1 as an example shows that, while cone angle α and thickness t witnessed a slight increase, the chamber length l seems to decrease in order to improve the outcome of recovery process. These transitions can be seen in Fig. 6.9. In summary, through Chapter 4, 5 and 6, we have obtained a relatively comprehensive knowledge about how MorphCom can enable resilience with trivial supervision from the controller. In the future, the proposed method is expected to become an underpinning strategy to exploit the idea of morphological control in development of tactile sensing systems. Moreover, the present design and idea of controlling tactile perception may be tailored to potentially suit various applications that require enduring frequent external interaction with changeable sensitivity. Some promising scenarios include rescue robots such as legged-robots, surgical devices, or rehabilitation robots.

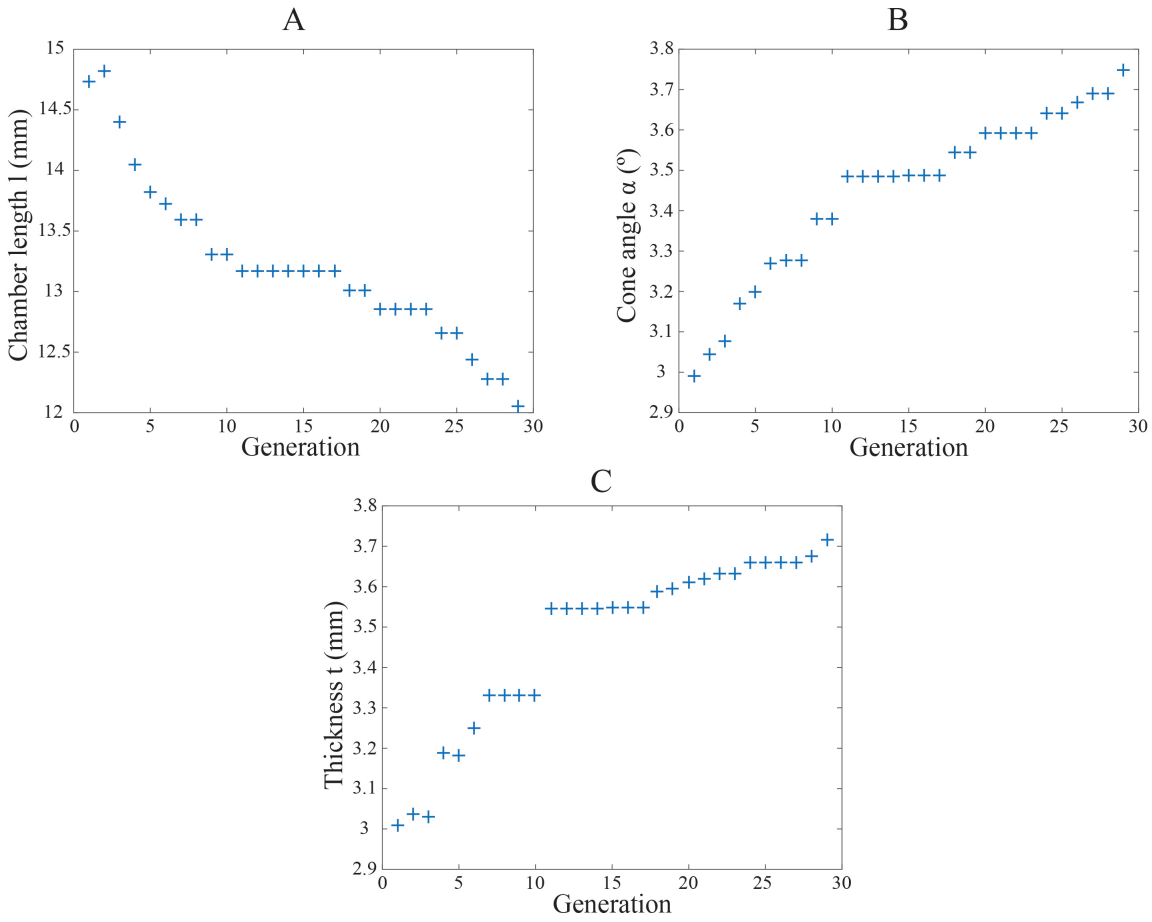

FIGURE 6.9: Performance evaluation of the FE model is validated by (A) a comparison of results among simulated and actual extension lengths as well as (B) perceived tactile responses of the strain gauge under a wide range of chamber pressures and contact ratio *a*.

7 Conclusion and Future Works

7.1 General Summary

This thesis embarks on the field of resilient robots aiming to provide capability to self-recover from malfunctions (here is tactile sensing function) caused by broken body parts. The idea is inspired by a vast of biological systems which use morphological features to enable remarkable resilience, whilst existing robotic systems would simply cease their operation until getting intervention from humans. This prevents the engagement of autonomous robots in more challenging missions in hazardous environments. Thus, much approaches have been proposed, every single one of them focus on either updating the control policy or re-configure the mechanical structure. Unfortunately, this process is often quite complex and sometimes not even able to counteract the damage at all. Taking inspiration from biological systems, I introduced a novel paradigm to design soft tactile sensory systems called *TacMorph* (presented in Chapter 3) that can actively enable resilient ability, *i.e.*, regain sensitivity as close to original state as possible, by allowing their morphology to adapt. I named this strategy as *MorphCom*. Chapter 4, 5 and 6 threw a light on it by studying a showcase on bio-inspired whisker sensory system. To demonstrate the feasibility of this paradigm, this device exhibited resilience against physical damages by changing its resting morphology through selective compression and decompression of the air chamber implanted inside the whisker body. To my best knowledge on every similar efforts reported in the literature to date, my whisker sensor is the first actual robotic device exploiting its own body morphology to enable self-recovery ability.

These findings are given in Chapter 5, 4 and 6 prove that adaptive morphology is not only beneficial to sensing and perception, but also to robot's adaptability. Although the underlying mechanics for morphological change have not been fully clarified before, I suspected the key roles could be geometrical as well as material attributes. And the experimental results are shown in Chapter 5 and 6 certify my prediction by clearly pointing out the explicit contribution of material stiffness (Young's modulus E) and geometrical parameters on the variation of tactile perception. Hence, to perform tactile compensation, the morphology of a whisker (after being trimmed) will be driven to a specific state that generate similar mechanical feedback from the embedded sensing element to that of intact whisker. To provide the best understanding of the underlying mechanics related to this idea, two specific concerns have been studied:

1. The correlation between the change of the morphology reflected by the variation of geometrical parameters (listed in table 4.1) and material stiffness (Young modulus E) with perceived sensor feedback (discussed in Chapter 4 and Chapter 5).

2. The role of each factor on the overall recovery performance (discussed in Chapter 5, section 5.2.3 and Chapter 6).

Clarifying the first concern would help us to establish a proper transformation strategy for whisker's morphology in order to compensate for a certain loss of tactile perception. Such strategies can be reviewed in section 5.1. The general idea is to tune the amplitude of the factor of interest due to impaired conditions as close to the desired state (which normally is initial state) as possible. Note that the concept of resilient ability presented in this thesis can also be tasked for other applications. For example, resilient strategy in legged-robot with an amputated leg would be to maximize the locomotion distance to be achieved within a given time while controller features are unchanged (similar to [61]). On the other hand, although the analytical method shown in this thesis unfolds the mechanical insights of resilient function based on the morphological change, nevertheless, this approach exposes

considerable limitations as discussed in section 5.3.3. Potential solution for these defects will be discussed in the section of future works.

For the second issue, I established a framework to evaluate compensation rate for a set of different initialization of the whisker geometry (see Fig. 6.8), which are suggested by the evolutionary algorithm. Interested geometrical parameters will go through a similar process as ontogenetic development to enhance the efficiency of the recovery functionality. At the end of the evolution, the optimal whisker design with the best resilience will be given. The simulation results are in the same agreement with experiment results in that a wrong choice of initialized body morphology would result in a low performance even with an optimal compensatory action. Therefore, it gives a hint that considering the morphology as a part of the design process for low-cost but strong resilient robots is necessary.

Overall, the exploration of tactile compensation ability provides the fundamental insight on great potential of embodied intelligence via adaptive morphology to enable desirable functions that have been untouched by conventional robots. Yet, while most of the existing rigid and soft robots have been designed with limited tasks, it has shown that each state of body morphology could be respective to specific functionality or a certain level of system performance. Such argument might refresh our philosophy for designing intelligent machines that have no longer been limited to repetitive tasks in a pre-defined environment but are aggressively involved in uncertain workplaces where robustness and adaptability are achieved by activating different forms of morphology. More interestingly, there is a fact that biological systems are not just born with a set of pre-programmed intelligent actions, but they acquire such abilities from an interactive and continuously exploratory process throughout their lifetime and generations. This observation shakes a hint for classical machine learning methods applied to modern robots to constantly optimize the controller and body's morphology simultaneously (even from scratch) to incrementally adapt to more challenging tasks. More investigations associated with this idea should be done in the future.

7.2 Future Research Directions

The first avenue for my future works is based on remaining limitations mentioned in section 5.3.3 and 6.4. With respect to searching for suitable compensatory actions. The method used in Chapter 4 is to solve the equality equation (*i.e.,* Eq. 5.2) between estimated sensor magnitude perceived by intact whiskers and broken whiskers for finding the proper value of inner pressure Q (equivalent to searching new morphology). The accuracy of the outcome totally relies on the reliability of the analytical model. Aforementioned, To build up a sufficiently precise analytical model, it is essential to estimate all changeable geometrical parameters via the body transformation and variation of material properties which are sometimes impossible. Not to mention the fact that the dynamic of whisker body during physical interaction has not been fully identified throughout this model. In this scenario, FE-based simulation tools (*e.g,* Abaqus) was used to clarify the dynamic aspects of a soft body stimulated by internal as well as external stimulation. Nonetheless, commercial FE solvers such as Abaqus will take a significant amount of time to finish a single evaluation session for a sample of compensatory behaviour, thus, it is definitely inappropriate especially if searching space is high-dimensional. Currently, there have been an increasing trend of open-sources engines that offer advanced physics simulation in real-time, in which, SOFA (Simulation Open Framework Architecture) developed by INRIA, France catches the most attention of mine. Taking advantage of simulation-based dynamical investigation and powerful data-driven techniques would be a promising solution to facilitate design procedure as well as the construction of a table of compensatory behaviors for other high-skilled tactile sensibilities, especially those acquire dynamical feedback from the complex environment such as texture discrimination or contour recognition, in response to different types of uncertainty. Further implementations on different parts of robotic systems with intricate sensory-actuator networks will provide additional evidences for the idea of morphology-based resilience.

Secondly, it is worth mentioning that, the resilient performance by changing

morphology is eventually prescribed by the limits of its transformation capacity through the number of locally controllable degree of freedom (LC-Dof) within the body. Since the number of actuators and their operation ranges are normally limited resulting in a deficiency of available compensatory actions (*e.g* in my works, there are only two compensatory actions: compressing and decompressing the chamber corresponding to 1 LC-DoF). On the other side, the damage conditions for tested showcases in this thesis are already known in advance. This is obviously not true for real robotic systems. Therefore, identifying the classification of robot failures and developing methods to discover when, where damages occur, and to what level, should be paid more attention as resilient capabilities. Yet, such self-diagnosis robots are expensive since they require embedding more sensors within the body and a program to self-monitor all sensors, but the success is not guaranteed. To efficiently address these challenges, instead of solely assigning the duty of adaptation to the body morphology, both characteristics of the controller and the robot's body should be adapted in parallel to maximize resilience performance. Morphology and controller co-evolution could highlight the fundamental aspects of motor-sensory coordination as a key principle of embodied intelligence.

Genetic algorithm and Reinforcement Learning (RL) method [124] could be tailored to seek an optimal geometry w among a design distribution $p(w)$ (*i.e.*, a set of possible designs which obey a certain number of LC-DoF and actuator arrangement rules) and control policy π_θ for LC-DoFs activation to achieve a specific compensation task. I already encountered several challenges of evolving the initial morphology to improve functional efficiency in Chapter 6. While this method works well in simulations, in practical implementations, it is not feasible in terms of computation cost. Thus, a fast and decentralized online searching algorithm is need. Whereas, RL acts a form of trial and error learning analogous to the method used by animals or even humans to continuously adapt throughout their lifetime [59]. Since the main aim of RL method is to maximize the reward gained from actual operation in fields for each single step with no interest in damage condition (*e.g* the gap between current (broken-state) and original sensitivity), therefore, fault diagnosis is

not necessary. Morever, RL is very highly individualistic, instead depending on a population of individuals.

According to above proposal, it is necessary to assess performances (or estimate the gained reward) of a morphology-changeable robots in varying conditions. It is a fact that manufacturing and testing multiple robots would require a massive amount of time and money. Therefore, SOFA simulation tools could be used as a testbed for either evaluation progress to eliminate undesirable robot design or learning process to come up with optimal morphology-control policies for resilience, sometimes both. Employing SOFA into RL model as described above would technically provide the answer for three critical issues for the emerging field of resilient robots:

- The learning process through co-evolution of morphology and controller parameters equip proprioception and intelligence to resilient robots to self-behave recovery process until the desired state is achieved without a monitoring system.
- The design process for novel resilient robotic devices can be optimized by using this framework.
- And finally, It paves a way to successfully transfer more highly functional designs for complex robotic systems (probably taking inspiration from *TacMorph*) to reality.

Bibliography

[1] J. Manyika, Susan Lund, Michael Chui, et al. “Jobs lost, jobs gained: What the future of work will mean for jobs, skills, and wages”. In: 2017.

[2] Anthony Holtmaat and Karel Svoboda. “Experience-dependent structural synaptic plasticity in the mammalian brain”. In: *Nature Reviews Neuroscience* 10.9 (2009), pp. 647–658. ISSN: 1471003X. DOI: https://doi.org/10.1038/nrn2699.

[3] Fritz Vollrath and Thiemo Krink. “Spider webs inspiring soft robotics”. In: *Journal of The Royal Society Interface* 17.172 (2020), p. 20200569. DOI: https://doi.org/10.1098/rsif.2020.0569.

[4] Nhan Huu Nguyen, Trung Dung Ngo, Dinh Quang Nguyen, et al. “Contact Distance Estimation by a Soft Active Whisker Sensor Based on Morphological Computation”. In: *2020 8th IEEE RAS/EMBS International Conference for Biomedical Robotics and Biomechatronics (BioRob)*. 2020, pp. 322–327. DOI: https://doi.org/10.1109/BioRob49111.2020.9224314.

[5] Nhan Huu Nguyen and Van Anh Ho. “Mechanics and Morphological Compensation Strategy for Trimmed Soft Whisker Sensor”. In: *Soft Robotics* 0.0 (0), null. DOI: 10.1089/soro.2020.0056.

[6] Nhan Huu Nguyen and Van Anh Ho. “Tactile Compensation for Artificial Whiskered Sensor System Under Critical Change in Morphology”. In: *IEEE Robotics and Automation Letters* 6.2 (2021), pp. 3381–3388. DOI: 10.1109/LRA.2021.3064460.

[7] Rolf Pfeifer and Josh C. Bongard. “How the body shapes the way we think - a new view on intelligence”. In: 2006.

[8] Rolf Pfeifer, Max Lungarella, and Fumiya Iida. "Self-Organization, Embodiment, and Biologically Inspired Robotics". In: *Science* 318.5853 (2007), pp. 1088–1093. DOI: 10.1126/science.1145803.

[9] René Descartes. *Discourse on Method*. Harmondsworth, Penguin, 1968.

[10] Herke van Hoof, Tucker Hermans, Gerhard Neumann, et al. "Learning robot in-hand manipulation with tactile features". In: *2015 IEEE-RAS 15th International Conference on Humanoid Robots (Humanoids)*. 2015, pp. 121–127. DOI: https://doi.org/10.1109/HUMANOIDS.2015.7363524.

[11] Visakha K. Nanayakkara, Giuseppe Cotugno, Nikolaos Vitzilaios, et al. "The Role of Morphology of the Thumb in Anthropomorphic Grasping: A Review". In: *Frontiers in Mechanical Engineering* 3 (2017), p. 5. ISSN: 2297-3079. DOI: https://doi.org/10.3389/fmech.2017.00005.

[12] "Are Wet-Induced Wrinkled Fingers Primate Rain Treads?" In: *Brain, Behavior and Evolution* 77.4 (2011), pp. 286–290. ISSN: 0006-8977. DOI: 10.1159/000328223.

[13] Julia Haseleu, Damir Omerbašić, Henning Frenzel, et al. "Water-Induced Finger Wrinkles Do Not Affect Touch Acuity or Dexterity in Handling Wet Objects". In: *PLOS ONE* 9.1 (Jan. 2014), pp. 1–6. DOI: 10.1371/journal.pone.0084949.

[14] Rolf Pfeifer, Fumiya Iida, and Gabriel Gomez. "Designing Intelligent Robots". In: 24.7 (2006), pp. 783–790. DOI: 10.7210/jrsj.24.783.

[15] Brian S. Peters, Priscila R. Armijo, and Dmitry Oleynikov. "Robotic Technologies (Past, Present and Future)". In: *Robotic Assisted Hernia Repair: Current Practice*. Ed. by Karl A. LeBlanc. Springer International Publishing, 2019, pp. 3–27. ISBN: 978-3-030-23025-8. DOI: 10.1007/978-3-030-23025-8_1.

[16] Kamran Shaukat Dar, Farhat Iqbal, Talha Mahboob Alam, et al. "The Impact of Artificial intelligence and Robotics on the Future Employment Opportunities". In: *Trends in Computer Science and Information Technology* (Sept. 2020). DOI: 10.17352/tcsit.000022.

[17] Keyan Ghazi-Zahedi, Carlotta Langer, and Nihat Ay. "Morphological Computation: Synergy of Body and Brain". In: *Entropy* 19.9 (2017). ISSN: 1099-4300. DOI: 10.3390/e19090456.

[18] Matteo Cianchetti, Maurizio Follador, Barbara Mazzolai, et al. "Design and development of a soft robotic octopus arm exploiting embodied intelligence". In: *Proceedings - IEEE International Conference on Robotics and Automation* (May 2012), pp. 5271–5276. DOI: 10.1109/ICRA.2012.6224696.

[19] Van Anh Ho, Hideyasu Yamashita, Zhongkui Wang, et al. "Wrin'Tac: Tactile Sensing System With Wrinkle's Morphological Change". In: *IEEE Transactions on Industrial Informatics* 13 (2017), pp. 2496–2506.

[20] ABK Grooming. *Dog anatomy*. 2017. URL: https://www.abkgrooming.com/blogs/news/anatomy-of-dog.

[21] Rolf Pfeifer, Fumiya Iida, and Josh Bongard. "New Robotics: Design Principles for Intelligent Systems". In: *Artif. Life* 11.1–2 (Jan. 2005), pp. 99–120. ISSN: 1064-5462. DOI: https://doi.org/10.1162/1064546053279017.

[22] Rolf Pfeifer, Fumiya Iida, and Gabriel Gomez. "Designing Intelligent Robots-On the Implications of Embodiment-". In: *Journal of the Robotics Society of Japan* 24 (Jan. 2006). DOI: 10.7210/jrsj.24.783.

[23] Noel E. Du Toit and Joel W. Burdick. "Robotic motion planning in dynamic, cluttered, uncertain environments". In: *2010 IEEE International Conference on Robotics and Automation*. 2010, pp. 966–973. DOI: 10.1109/ROBOT.2010.5509278.

[24] Helmut Hauser. "Resilient machines through adaptive morphology". In: *Nature Machine Intelligence* 1.8 (2019), pp. 338–339. ISSN: 2522-5839. DOI: 10.1038/s42256-019-0076-6.

[25] Josh Bongard, Victor Zykov, and Hod Lipson. "Resilient Machines Through Continuous Self-Modeling". In: *Science* 314.5802 (2006), pp. 1118–1121. DOI: 10.1126/science.1133687.

[26] "Long-range neural and gap junction protein-mediated cues control polarity during planarian regeneration". In: *Developmental Biology* 339.1 (2010), pp. 188–199. ISSN: 0012-1606. DOI: https://doi.org/10.1016/j.ydbio.2009.12.012.

[27] Peter Igelmund. "Morphology, sense organs, and regeneration of the forelegs (whips) of the whip spider Heterophrynus elaphus (Arachnida, Amblypygi)". In: *Journal of Morphology* 193.1 (1987), pp. 75–89. DOI: https://doi.org/10.1002/jmor.1051930108.

[28] Tønnes F Nygaard, Charles P Martin, Jim Torresen, et al. "Real-world embodied AI through a morphologically adaptive quadruped robot". In: *Nature Machine Intelligence* 3.5 (2021), pp. 410–419. ISSN: 2522-5839. DOI: 10.1038/s42256-021-00320-3.

[29] Josh Bongard. "Morphological change in machines accelerates the evolution of robust behavior". In: *Proceedings of the National Academy of Sciences* 108.4 (2011), pp. 1234–1239. ISSN: 0027-8424. DOI: 10.1073/pnas.1015390108.

[30] Yee Ling Yap, Swee Leong Sing, and Wai Yee Yeong. "A review of 3D printing processes and materials for soft robotics". In: *Rapid Prototyping Journal* ahead-of-print (June 2020). DOI: 10.1108/RPJ-11-2019-0302.

[31] Bruno Siciliano and Oussama Khatib. *Springer Handbook of Robotics*. Springer, Berlin, Heidelberg, 2008. ISBN: 978-3-540-30301-5. DOI: https://doi.org/10.1007/978-3-540-30301-5.

[32] Kostas Alexis. *Towards a Science of Resilient Robotic Autonomy*. 2020. arXiv: 2004.02403 [cs.RO].

[33] Dylan Shah, Bilige Yang, Sam Kriegman, et al. "Shape Changing Robots: Bioinspiration, Simulation, and Physical Realization". In: *Advanced Materials* 33.19 (2021), p. 2002882. DOI: https://doi.org/10.1002/adma.202002882.

[34] Alin Albu-Schaffer, Oliver Eiberger, Markus Grebenstein, et al. "Soft robotics". In: *IEEE Robotics Automation Magazine* 15.3 (2008), pp. 20–30. DOI: 10.1109/MRA.2008.927979.

[35] Vishesh Vikas, Paul Templeton, and Barry Trimmer. *Design and control of a soft, shape-changing, crawling robot*. 2015. arXiv: 1509.07569 [cs.RO].

[36] Vincent Wall, Gabriel Zöller, and Oliver Brock. "A method for sensorizing soft actuators and its application to the RBO hand 2". In: *2017 IEEE International Conference on Robotics and Automation (ICRA)*. 2017, pp. 4965–4970. DOI: 10.1109/ICRA.2017.7989577.

[37] Michael Wehner, Ryan L Truby, Daniel J Fitzgerald, et al. "An integrated design and fabrication strategy for entirely soft, autonomous robots". In: *Nature* 536.7617 (2016), pp. 451–455. ISSN: 1476-4687. DOI: 10.1038/nature19100.

[38] Andrew D. Marchese, Cagdas D. Onal, and Daniela Rus. "Autonomous Soft Robotic Fish Capable of Escape Maneuvers Using Fluidic Elastomer Actuators". In: *Soft Robotics* 1.1 (2014). PMID: 27625912, pp. 75–87. DOI: 10.1089/soro.2013.0009.

[39] Cecilia Laschi, Barbara Mazzolai, and Matteo Cianchetti. "Soft robotics: Technologies and systems pushing the boundaries of robot abilities". In: *Science Robotics* 1.1 (2016), eaah3690. DOI: 10.1126/scirobotics.aah3690.

[40] Julius E. Bernth, Van Anh Ho, and Hongbin Liu. "Morphological computation in haptic sensation and interaction: from nature to robotics". In: *Advanced Robotics* 32.7 (2018), pp. 340–362. DOI: https://doi.org/10.1080/01691864.2018.1447393.

[41] Marit Hagens and Serge Thill. "How Much Information Does a Robot Need? Exploring the Benefits of Increased Sensory Range in a Simulated Crowd Navigation Task". In: *Information* 11.2 (2020). ISSN: 2078-2489. DOI: 10.3390/info11020112.

[42] Daekyum Kim, Sang-Hun Kim, Taekyoung Kim, et al. "Review of machine learning methods in soft robotics". In: *PLOS ONE* 16.2 (Feb. 2021), pp. 1–24. DOI: 10.1371/journal.pone.0246102.

[43] Lucia Seminara, Paolo Gastaldo, Simon J. Watt, et al. "Active Haptic Perception in Robots: A Review". In: *Frontiers in Neurorobotics* 13 (2019), p. 53. ISSN: 1662-5218. DOI: 10.3389/fnbot.2019.00053.

[44] Chao Huang, Qizhuo Wang, Mingfu Zhao, et al. "Tactile Perception Technologies and Their Applications in Minimally Invasive Surgery: A Review". In: *Frontiers in Physiology* 11 (2020), p. 1601. ISSN: 1664-042X. DOI: 10.3389/fphys.2020.611596.

[45] Kazuhiro Shimonomura. "Tactile Image Sensors Employing Camera: A Review". eng. In: *Sensors (Basel, Switzerland)* 19.18 (Sept. 2019), p. 3933. ISSN: 1424-8220. DOI: 10.3390/s19183933.

[46] Perla Maiolino, Marco Maggiali, Giorgio Cannata, et al. "A Flexible and Robust Large Scale Capacitive Tactile System for Robots". In: *IEEE Sensors Journal* 13.10 (2013), pp. 3910–3917. DOI: 10.1109/JSEN.2013.2258149.

[47] Lac Van Duong and Van Anh Ho. "Large-Scale Vision-Based Tactile Sensing for Robot Links: Design, Modeling, and Evaluation". In: *IEEE Transactions on Robotics* 37.2 (2021), pp. 390–403. DOI: 10.1109/TRO.2020.3031251.

[48] Qiukai Qi and Van Anh Ho. "Wrinkled Soft Sensor With Variable Afferent Morphology: Case of Bending Actuation". In: *IEEE Robotics and Automation Letters* 5.3 (2020), pp. 4102–4109. DOI: https://doi.org/10.1109/LRA.2020.2982867.

[49] Josie Hughes, Luca Scimeca, Perla Maiolino, et al. "Online Morphological Adaptation for Tactile Sensing Augmentation". In: *Frontiers in Robotics and AI* 8 (2021), p. 216. ISSN: 2296-9144. DOI: https://doi.org/10.3389/frobt.2021.665030.

[50] K.J. Quillin. "Kinematic scaling of locomotion by hydrostatic animals: ontogeny of peristaltic crawling by the earthworm lumbricus terrestris". In: *Journal of Experimental Biology* 202.6 (Mar. 1999), pp. 661–674. ISSN: 0022-0949. DOI: https://doi.org/10.1242/jeb.202.6.661.

[51] C McCusker and D M Gardiner. "The Axolotl Model for Regeneration and Aging Research: A Mini-Review". In: *Gerontology* 57.6 (2011), pp. 565–571. ISSN: 0304-324X. DOI: 10.1159/000323761.

[52] Michael Levin, Alexis M. Pietak, and Johanna Bischof. "Planarian regeneration as a model of anatomical homeostasis: Recent progress in biophysical and computational approaches". In: *Seminars in Cell Developmental Biology* 87 (2019). Planarian regeneration, pp. 125–144. ISSN: 1084-9521. DOI: https://doi.org/10.1016/j.semcdb.2018.04.003.

[53] Jessica Mustard and Michael Levin. "Bioelectrical Mechanisms for Programming Growth and Form: Taming Physiological Networks for Soft Body Robotics". In: *Soft Robotics* 1.3 (2014), pp. 169–191. DOI: 10.1089/soro.2014.0011.

[54] Antoine Cully, Jeff Clune, Danesh Tarapore, et al. "Robots that can adapt like animals". In: *Nature* 521.7553 (2015), pp. 503–507. ISSN: 1476-4687. DOI: 10.1038/nature14422. URL: https://doi.org/10.1038/nature14422.

[55] Tan Zhang, Dan Zhang, Madan M. Gupta, et al. "Design of a general resilient robotic system based on axiomatic design theory". In: *2015 IEEE International Conference on Advanced Intelligent Mechatronics (AIM)*. 2015, pp. 71–78. DOI: 10.1109/AIM.2015.7222511.

[56] Zhi-hong Sun, G. S. Yang, Bing Zhang, et al. "On the concept of the resilient machine". In: *2011 6th IEEE Conference on Industrial Electronics and Applications*. 2011, pp. 357–360. DOI: 10.1109/ICIEA.2011.5975608.

[57] Tan Zhang, Dan Zhang, Madan M. Gupta, et al. "Design of a general resilient robotic system based on axiomatic design theory". In: *2015 IEEE International Conference on Advanced Intelligent Mechatronics (AIM)*. 2015, pp. 71–78. DOI: https://doi.org/10.1109/AIM.2015.7222511.

[58] Sylvain Koos, Antoine Cully, and Jean-Baptiste Mouret. "Fast damage recovery in robotics with the T-resilience algorithm". In: *The International Journal of Robotics Research* 32.14 (2013), pp. 1700–1723. DOI: 10.1177/0278364913499192.

[59] Konstantinos Chatzilygeroudis, Vassilis Vassiliades, and Jean-Baptiste Mouret. "Reset-free Trial-and-Error Learning for Robot Damage Recovery". In: *Robotics and Autonomous Systems* 100 (2018), pp. 236–250. ISSN: 0921-8890. DOI: https://doi.org/10.1016/j.robot.2017.11.010. URL: https://www.sciencedirect.com/science/article/pii/S0921889017302440.

[60] Takeshi Kano, Eiki Sato, Tatsuya Ono, et al. "A brittle star-like robot capable of immediately adapting to unexpected physical damage". In: *Royal Society Open Science* 4.12 (2017), p. 171200. DOI: 10.1098/rsos.171200.

[61] Sam Kriegman, Stephanie Walker, Dylan S. Shah, et al. "Automated Shapeshifting for Function Recovery in Damaged Robots". In: *Robotics: Science and Systems XV* (June 2019). DOI: https://doi.org/10.15607/rss.2019.xv.028.

[62] Guanjiao Ren, Weihai Chen, Sakyasingha Dasgupta, et al. "Multiple chaotic central pattern generators with learning for legged locomotion and malfunction compensation". In: *Information Sciences* 294 (2015), pp. 666–682. ISSN: 0020-0255. DOI: https://doi.org/10.1016/j.ins.2014.05.001.

[63] Tan Zhang, Wenjun Zhang, and Madan M. Gupta. "Resilient Robots: Concept, Review, and Future Directions". In: *Robotics* 6.4 (2017). ISSN: 2218-6581. DOI: 10.3390/robotics6040022.

[64] Seppe Terryn, Joost Brancart, Dirk Lefeber, et al. "Self-healing soft pneumatic robots". In: *Science Robotics* 2.9 (2017), eaan4268. DOI: 10.1126/scirobotics.aan4268.

[65] Yuanyuan Chen, Kaiyue Lu, Yuhan Song, et al. "A Skin-Inspired Stretchable, Self-Healing and Electro-Conductive Hydrogel with A Synergistic Triple Network for Wearable Strain Sensors Applied in Human-Motion Detection". In: *Nanomaterials (Basel, Switzerland)* 9.12 (Dec. 2019), p. 1737. ISSN: 2079-4991. DOI: 10.3390/nano9121737.

[66] Abdon Pena-Francesch, Huihun Jung, Melik C Demirel, et al. "Biosynthetic self-healing materials for soft machines". In: *Nature Materials* (2020). ISSN:

1476-4660. DOI: 10.1038/s41563-020-0736-2. URL: https://doi.org/10.1038/s41563-020-0736-2.

[67] M. W. Keller, S. R. White, and N. R. Sottos. "A Self-Healing Poly(Dimethyl Siloxane) Elastomer". In: *Advanced Functional Materials* 17.14 (2007), pp. 2399–2404. DOI: https://doi.org/10.1002/adfm.200700086.

[68] Helmut Hauser, Auke J Ijspeert, Rudolf M Füchslin, et al. "Towards a theoretical foundation for morphological computation with compliant bodies". In: *Biological Cybernetics* 105.5-6 (2011), pp. 355–370. ISSN: 03401200. DOI: https://doi.org/10.1007/s00422-012-0471-0.

[69] Bo Persson. "Wet adhesion with application to tree frog adhesive toe pads and tires". In: *Journal of Physics: Condensed Matter* 19 (Aug. 2007), p. 376110. DOI: https://doi.org/10.1088/0953-8984/19/37/376110.

[70] W Federle, W.J.P Barnes, W Baumgartner, et al. "Wet but not slippery: boundary friction in tree frog adhesive toe pads". In: *Journal of The Royal Society Interface* 3.10 (2006), pp. 689–697. DOI: https://doi.org/10.1098/rsif.2006.0135.

[71] Vincent C. Müller and Matej Hoffmann. "What Is Morphological Computation? On How the Body Contributes to Cognition and Control". In: *Artificial Life* 23.1 (Feb. 2017), pp. 1–24. ISSN: 1064-5462. DOI: https://doi.org/10.1162/ARTL_a_00219.

[72] Hiep Xuan Trinh, Van Anh Ho, and Koji Shibuya. "Theoretical Foundation for Design of Friction-Tunable Soft Finger With Wrinkle's Morphology". In: *IEEE Robotics and Automation Letters* 4.4 (2019), pp. 4027–4034. DOI: https://doi.org/10.1109/LRA.2019.2926960.

[73] Qiukai Qi, Shinichi Hirai, and Van Anh Ho. "Wrinkled Soft Sensor With Variable Afferent Morphology". In: *IEEE Robotics and Automation Letters* 4.2 (2019), pp. 1908–1915. DOI: https://doi.org/10.1109/LRA.2019.2898712.

[74] Martin J Pearson, Ben Mitchinson, J Charles Sullivan, et al. "Biomimetic vibrissal sensing for robots". In: *Philosophical Transactions of the Royal Society B: Biological Sciences* 366.1581 (2011), pp. 3085–3096. ISSN: 14712970. DOI: https://doi.org/10.1098/rstb.2011.0164.

[75] Jenq-Wei Yang, Werner Kilb, Sergei Kirischuk, et al. "Development of the whisker-to-barrel cortex system". In: *Current Opinion in Neurobiology* 53 (2018). Developmental Neuroscience, pp. 29–34. ISSN: 0959-4388. DOI: https://doi.org/10.1016/j.conb.2018.04.023.

[76] Ben Mitchinson, Ehsan Arabzadeh, Mathew E Diamond, et al. "Spike-timing in primary sensory neurons: a model of somatosensory transduction in the rat". In: *Biological Cybernetics* 98.3 (2008), pp. 185–194. ISSN: 1432-0770. DOI: 10.1007/s00422-007-0208-7.

[77] Brian W. Quist and Mitra J. Z. Hartmann. "Mechanical signals at the base of a rat vibrissa: the effect of intrinsic vibrissa curvature and implications for tactile exploration". In: *Journal of Neurophysiology* 107.9 (2012). PMID: 22298834, pp. 2298–2312. DOI: 10.1152/jn.00372.2011.

[78] Joseph H Solomon and Mitra J Hartmann. "Robotic whiskers used to sense features". In: *Nature* 443.7111 (2006), p. 525. ISSN: 1476-4687. DOI: https://doi.org/10.1038/443525a.

[79] P. Melzer and C.B. Smith. "Plasticity of cerebral metabolic whisker maps in adult mice after whisker follicle removal—I. modifications in barrel cortex coincide with reorganization of follicular innervation". In: *Neuroscience* 83.1 (1998), pp. 27–41. ISSN: 0306-4522. DOI: https://doi.org/10.1016/S0306-4522(97)00332-1.

[80] Jianguo G. Gu. "Molecular Mechanisms of the Sense of Touch: An Overview of Mechanical Transduction and Transmission in Merkel Discs of Whisker Hair Follicles and Some Clinical Perspectives". In: *Advances in Pain Research: Mechanisms and Modulation of Chronic Pain*. Ed. by Bai-Chuang Shyu and

Makoto Tominaga. Singapore: Springer Singapore, 2018, pp. 1–12. ISBN: 978-981-13-1756-9. DOI: https://doi.org/10.1007/978-981-13-1756-9_1.

[81] R. Blythe Towal, Brian W. Quist, Venkatesh Gopal, et al. "The Morphology of the Rat Vibrissal Array: A Model for Quantifying Spatiotemporal Patterns of Whisker-Object Contact". In: *PLOS Computational Biology* 7.4 (Apr. 2011), pp. 1–17. DOI: https://doi.org/10.1371/journal.pcbi.1001120.

[82] Julius E. Bernth, Van Anh Ho, and Hongbin Liu. "Morphological computation in haptic sensation and interaction: from nature to robotics". In: *Advanced Robotics* 32.7 (2018), pp. 340–362. DOI: 10.1080/01691864.2018.1447393.

[83] R Andrew Russell. "Object recognition using articulated whisker probes". In: *Int. Symp. on Industrial Robots* (1985), pp. 605–612.

[84] M. Kaneko, N. Kanayama, and T. Tsuji. "Active antenna for contact sensing". In: *IEEE Transactions on Robotics and Automation* 14.2 (1998), pp. 278–291. DOI: https://doi.org/10.1109/70.681246.

[85] DaeEun Kim and Ralf Möller. "Biomimetic whiskers for shape recognition". In: *Robotics and Autonomous Systems* 55.3 (2007), pp. 229–243. ISSN: 0921-8890. DOI: https://doi.org/10.1016/j.robot.2006.08.001.

[86] Mathew Evans, Charles Fox, Nathan Lepora, et al. "The effect of whisker movement on radial distance estimation: a case study in comparative robotics". In: *Frontiers in Neurorobotics* 6 (2013), p. 12. ISSN: 1662-5218. DOI: https://doi.org/10.3389/fnbot.2012.00012.

[87] Hannah Emnett, Matthew M. Graff, and Mitra J Z Hartmann. "A Novel Whisker Sensor Used for 3D Contact Point Determination and Contour Extraction". English (US). In: *Proceedings of Robotics*. Ed. by Hadas Kress-Gazit, Siddhartha Srinivasa, Tom Howard, et al. 2018. ISBN: 978-0992374747. DOI: https://doi.org/10.15607/RSS.2018.XIV.059.

[88] J. Wijaya and R. A. Russell. "Object exploration using whisker sensors". In: 2002.

[89] William Deer and Pauline E. I. Pounds. "Lightweight Whiskers for Contact, Pre-Contact, and Fluid Velocity Sensing". In: *IEEE Robotics and Automation Letters* 4.2 (2019), pp. 1978–1984. DOI: https://doi.org/10.1109/LRA.2019.2899215.

[90] Pablo Valdivia y Alvarado, Vignesh Subramaniam, and Michael Triantafyllou. "Design of a bio-inspired whisker sensor for underwater applications". In: *SENSORS, 2012 IEEE*. 2012, pp. 1–4. DOI: 10.1109/ICSENS.2012.6411517.

[91] Mitra J Hartmann. "Active Sensing Capabilities of the Rat Whisker System". In: *Autonomous Robots* 11.3 (2001), pp. 249–254. ISSN: 1573-7527. DOI: https://doi.org/10.1023/A:1012439023425.

[92] Martin J. Pearson, Anthony G. Pipe, Chris Melhuish, et al. "Whiskerbot: A Robotic Active Touch System Modeled on the Rat Whisker Sensory System". In: *Adaptive Behavior* 15.3 (2007), pp. 223–240. DOI: https://doi.org/10.1177/1059712307082089.

[93] Martin J. Pearson, Ben Mitchinson, Jason Welsby, et al. "SCRATCHbot: Active Tactile Sensing in a Whiskered Mobile Robot". In: *From Animals to Animats 11*. Ed. by Stéphane Doncieux, Benoît Girard, Agnès Guillot, et al. Berlin, Heidelberg: Springer Berlin Heidelberg, 2010, pp. 93–103.

[94] J. Charles Sullivan, Ben Mitchinson, Martin J. Pearson, et al. "Tactile Discrimination Using Active Whisker Sensors". In: *IEEE Sensors Journal* 12.2 (2012), pp. 350–362. DOI: https://doi.org/10.1109/JSEN.2011.2148114.

[95] Giovanni Mirabella, Stefano Battiston, and Mathew E. Diamond. "Integration of Multiple-whisker Inputs in Rat Somatosensory Cortex". In: *Cerebral Cortex* 11.2 (Feb. 2001), pp. 164–170. ISSN: 1047-3211. DOI: https://doi.org/10.1093/cercor/11.2.164.

[96] Takayuki Yamashita, Aurélie Pala, Leticia Pedrido, et al. "Membrane Potential Dynamics of Neocortical Projection Neurons Driving Target-Specific Signals". In: *Neuron* 80.6 (2013), pp. 1477–1490. ISSN: 0896-6273. DOI: https://doi.org/10.1016/j.neuron.2013.10.059.

[97] Mehdi Adibi. "Whisker-Mediated Touch System in Rodents: From Neuron to Behavior". In: *Frontiers in Systems Neuroscience* 13 (2019), p. 40. ISSN: 1662-5137. DOI: https://doi.org/10.3389/fnsys.2019.00040.

[98] V. Rema, Michael Armstrong-James, and Ford F. Ebner. "Experience-Dependent Plasticity Is Impaired in Adult Rat Barrel Cortex after Whiskers Are Unused in Early Postnatal Life". In: *Journal of Neuroscience* 23.1 (2003), pp. 358–366. ISSN: 0270-6474. DOI: https://doi.org/10.1523/JNEUROSCI.23-01-00358.2003.

[99] "What the Whiskers Tell the Brain". In: *Neuroscience* 368 (2018). Barrel Cortex Function, pp. 95–108. ISSN: 0306-4522. DOI: https://doi.org/10.1016/j.neuroscience.2017.08.005.

[100] Facundo Adrián Lucianna, Ana Lía Albarracín, Sonia Mariel Vrech, et al. "The mathematical whisker: A review of numerical models of the rats vibrissa biomechanics". In: *Journal of Biomechanics* 49.10 (2016), pp. 2007–2014. ISSN: 0021-9290. DOI: https://doi.org/10.1016/j.jbiomech.2016.05.019.

[101] Hayley M. Belli, Anne E. T. Yang, Chris S. Bresee, et al. "Variations in vibrissal geometry across the rat mystacial pad: base diameter, medulla, and taper". In: *Journal of Neurophysiology* 117.4 (2017), pp. 1807–1820. DOI: 10.1152/jn.00054.2016.

[102] Brian W. Quist, Rafay A. Faruqi, and Mitra J.Z. Hartmann. "Variation in Young's modulus along the length of a rat vibrissa". In: *Journal of Biomechanics* 44.16 (2011), pp. 2775–2781. ISSN: 0021-9290. DOI: https://doi.org/10.1016/j.jbiomech.2011.08.027.

[103] Joshua Bishop-Moser, Girish Krishnan, Charles Kim, et al. "Design of soft robotic actuators using fluid-filled fiber-reinforced elastomeric enclosures in parallel combinations". In: *2012 IEEE/RSJ International Conference on Intelligent Robots and Systems*. 2012, pp. 4264–4269. DOI: 10.1109/IROS.2012.6385966.

[104] Marcin Szwed, Knarik Bagdasarian, Barak Blumenfeld, et al. "Responses of Trigeminal Ganglion Neurons to the Radial Distance of Contact During Active Vibrissal Touch". In: *Journal of Neurophysiology* 95.2 (2006), pp. 791–802. DOI: 10.1152/jn.00571.2005.

[105] Joseph H. Solomon and Mitra J. Z. Hartmann. "Radial distance determination in the rat vibrissal system and the effects of Weber's law". In: *Philosophical Transactions of the Royal Society B: Biological Sciences* 366.1581 (2011), pp. 3049–3057. DOI: 10.1098/rstb.2011.0166.

[106] Samuel Andrew Hires, Lorenz Pammer, Karel Svoboda, et al. "Tapered whiskers are required for active tactile sensation". In: *eLife* 2 (Nov. 2013). Ed. by Misha Tsodyks, e01350. ISSN: 2050-084X. DOI: 10.7554/eLife.01350.

[107] Lorenz Pammer, Daniel H. O'Connor, S. Andrew Hires, et al. "The Mechanical Variables Underlying Object Localization along the Axis of the Whisker". In: *Journal of Neuroscience* 33.16 (2013), pp. 6726–6741. ISSN: 0270-6474. DOI: 10.1523/JNEUROSCI.4316-12.2013.

[108] Tony Atkins and Marcel Escudier. *A Dictionary of Mechanical Engineering*. Oxford University Press, 2013. ISBN: 9780191752308. DOI: 10.1093/acref/9780199587438.001.0001.

[109] G.P. O'Hara, ARMY ARMAMENT RESEARCH, and DEVELOPMENT CENTER WATERVLIET NY LARGE CALIBER WEAPON SYSTEMS LAB. *Mechanical Properties of Silicone Rubber in a Closed Volume*. Defense Technical Information Center, 1983. URL: https://books.google.co.jp/books?id=XoVgnQAACAAJ.

[110] Christopher M Williams and Eric M Kramer. "The advantages of a tapered whisker". In: *PLoS one* 5.1 (2010), e8806.

[111] Helmut Hauser, Auke J Ijspeert, Rudolf M Füchslin, et al. "The role of feedback in morphological computation with compliant bodies". In: *Biological cybernetics* 106.10 (2012), pp. 595–613.

[112] Mitra J. Z. Hartmann. "A night in the life of a rat: vibrissal mechanics and tactile exploration". In: *Annals of the New York Academy of Sciences* 1225.1 (2011), pp. 110–118. DOI: https://doi.org/10.1111/j.1749-6632.2011.06007.x.

[113] Helmut Hauser, Auke J Ijspeert, Rudolf M Füchslin, et al. "The role of feedback in morphological computation with compliant bodies". In: *Biological Cybernetics* 106.10 (2012), pp. 595–613. ISSN: 03401200. DOI: 10.1007/s00422-012-0516-4.

[114] Ren, Da, Chen, Yiming, Lin, Bojun, et al. "Modelling and Simulation of Vessel Surgery based on Mass-spring". In: *MATEC Web Conf.* 108 (2017), p. 13004. DOI: 10.1051/matecconf/201710813004. URL: https://doi.org/10.1051/matecconf/201710813004.

[115] K.J. Bathe. *Finite Element Procedures*. Prentice Hall, 2006. ISBN: 9780979004902. URL: https://books.google.co.jp/books?id=rWvefGICfO8C.

[116] Ricardo E. Barbosa and Jamshid Ghaboussi. "Discrete finite element method for multiple deformable bodies". In: *Finite Elements in Analysis and Design* 7.2 (1990), pp. 145–158. ISSN: 0168-874X. DOI: https://doi.org/10.1016/0168-874X(90)90006-Z.

[117] Adriana S. Franca and Kamyar Haghighi. "Adaptive Finite Element Analysis of Air Flow Inside Grain Dryers". In: *Drying Technology* 13.1-2 (1995), pp. 125–146. DOI: 10.1080/07373939508916945.

[118] Jan Taler and Paweł Ocłoń. "Finite Element Method in Steady-State and Transient Heat Conduction". In: *Encyclopedia of Thermal Stresses*. Ed. by Richard B. Hetnarski. Dordrecht: Springer Netherlands, 2014, pp. 1604–1633. ISBN: 978-94-007-2739-7. DOI: 10.1007/978-94-007-2739-7_897.

[119] O.C. Zienkiewicz, R.L. Taylor, and P. Nithiarasu. "Chapter 1 - Introduction to the Equations of Fluid Dynamics and the Finite Element Approximation". In: *The Finite Element Method for Fluid Dynamics (Seventh Edition)*. Ed. by O.C.

Zienkiewicz, R.L. Taylor, and P. Nithiarasu. Seventh Edition. Oxford: Butterworth-Heinemann, 2014, pp. 1–29. ISBN: 978-1-85617-635-4. DOI: https://doi.org/10.1016/B978-1-85617-635-4.00001-7.

[120] *Finite Element Modeling: Step 2: Create and assign materials*. URL: https://softroboticstoolkit.com/book/fr-abaqus-step-2.

[121] Peter J. van Dijk and T. H. Noel Ellis. "The Full Breadth of Mendel's Genetics". In: *Genetics* 204.4 (2016), pp. 1327–1336. ISSN: 0016-6731. DOI: 10.1534/genetics.116.196626.

[122] Yongsheng Fang and Jun li. "A Review of Tournament Selection in Genetic Programming". In: Oct. 2010, pp. 181–192. ISBN: 978-3-642-16492-7. DOI: 10.1007/978-3-642-16493-4_19.

[123] Angel Fernando Kuri-Morales and Jesús Gutiérrez-García. "Penalty Function Methods for Constrained Optimization with Genetic Algorithms: A Statistical Analysis". In: *MICAI 2002: Advances in Artificial Intelligence*. Ed. by Carlos A. Coello Coello, Alvaro de Albornoz, Luis Enrique Sucar, et al. 2002, pp. 108–117. ISBN: 978-3-540-46016-9.

[124] Jens Kober, J. Andrew Bagnell, and Jan Peters. "Reinforcement learning in robotics: A survey". In: *The International Journal of Robotics Research* 32.11 (2013), pp. 1238–1274. DOI: 10.1177/0278364913495721.